UNIWERSYTET JAGIELLOŃSKI
W KRAKOWIE

Wydział Biochemii, Biofizyki i Biotechnologii

Zakażenie wirusowe:
internalizacja i transport wewnątrzkomórkowy

Katarzyna Owczarek

Rozprawa doktorska wykonana pod opieką

prof. dr hab. Krzysztofa Pyrcia

w Zakładzie Mikrobiologii na Wydziale Biochemii, Biofizyki i Biotechnologii oraz

w Małopolskim Centrum Biotechnologii Uniwersytetu Jagiellońskiego

Kraków 2019

Wykonane w niniejszej pracy eksperymenty finansowane były w ramach następujących projektów:

- „Internalizacja ludzkich koronawirusów do komórek gospodarza” – projekt finansowany przez Narodowe Centrum Nauki w ramach programu Sonata Bis kierowany przez prof. dr hab. Krzysztofa Pyrcia. 2012/07/E/NZ6/01712.
- „Analiza procesu internalizacji ludzkich wirusów OC43 i Zika w komórkach. Zahamowanie wczesnych etapów infekcji poprzez modulację wewnątrzkomórkowego pH” – projekt finansowany przez Narodowe Centrum Nauki w ramach programu Preludium kierowany przez mgr Katarzynę Owczarek. 2017/25/N/NZ6/01310.

Doktorantka jest również beneficjentem Programu „Jagiellonian Interdisciplinary PhD Programme - Jagiellońskiego Programu Interdyscyplinarnych Studiów Doktoranckich” realizowanego w ramach Projektu „ZintegrUJ – Kompleksowy Program Rozwoju Uniwersytetu Jagiellońskiego” oraz Programu Operacyjnego Wiedza Edukacja Rozwój 2014 – 2020 współfinansowanego ze środków Europejskiego Funduszu Społecznego, nr POWR.03.05.00-00-Z309/17-00.

Doktorantka jest członkiem grupy Virogenetics, która uczestniczy w Europejskim Programie Współpracy w Dziedzinie Badań Naukowo-Technicznych (COST), wspieranym przez Ministerstwo Nauki i Szkolnictwa Wyższego.

W czasie realizacji badań do pracy doktorskiej Wydział Biochemii, Biofizyki i Biotechnologii Uniwersytetu Jagiellońskiego posiadał status Krajowego Naukowego Ośrodka Wiodącego (KNOW) wspieranego przez Ministerstwo Nauki i Szkolnictwa Wyższego.

NARODOWE CENTRUM NAUKI

Ministerstwo Nauki
i Szkolnictwa Wyższego

Krajowy Naukowy
Ośrodek Wiodący

Podziękowania

Składam serdeczne podziękowania:

***Panu prof. dr hab. Krzysztofowi Pyrciowi**,*
Promotorowi mojej pracy, za umożliwienie mi rozwoju naukowego oraz zawodowego,
za przekazaną mi wiedzę i cenne wskazówki, za inspirację, a także za wieloletnią opiekę
oraz wszelką okazaną mi życzliwość i cierpliwość;

*Dziękuję recenzentom: **Pani prof. dr hab. Krystynie Bieńkowskej-Szewczyk***
*oraz **Pani prof. dr hab. Agnieszce Szuster-Ciesielskiej**;*

*Składam podziękowania **Panu prof. dr hab. Janowi Potempie***
za umożliwienie pracy w Zakładzie Mikrobiologii;

*Dziękuję **Panu mgr Arturowi Szczepańskiemu***
za pomoc w realizacji doświadczeń, a także życzliwość i wsparcie;

*Dziękuję **Koleżankom i Kolegom z grupy „Virogenetics" oraz z Zakładu Mikrobiologii WBBiB UJ***
za wsparcie merytoryczne, przyjazną atmosferę oraz owocną współpracę;

*Dziękuję także **mojej kochanej Rodzinie**, a w szczególności **Rodzicom** i **Markowi**, za nieustające*
wsparcie we wszystkich przedsięwzięciach, troskę, obecność i wiarę we mnie każdego dnia;

*Dziękuję **Przyjaciołom** za inspirujące rozmowy i motywację do działania.*

Katarzyna Owczarek

Spis treści

Streszczenie 5

Abstract 7

Wstęp 9

1. Mechanizmy wejścia wirusów do komórek 9

2. Endocytoza 11

2.1. Endocytoza klatrynozależna 11

2.2 Endocytoza kaweolinozależna 12

2.3. Endocytoza niezależna od klatryny i kaweoliny 12

2.4. Wewnątrzkomórkowy transport ładunków 13

3. Ludzki koronawirus OC43 15

4. Wirus Zika 18

Cele badań 21

Streszczenie wyników 22

Wykaz publikacji 24

Bibliografia 25

Załączniki 28

„Early events during human coronavirus OC43 entry to the cell” 29

„Zika virus: mapping and reprogramming the entry” 41

Oświadczenia współautorów 60

Streszczenie

Błona komórkowa stanowi podstawową barierę dla infekcji wirusowej, a obecność konkretnych białek na jej powierzchni determinuje specyficzność tkankową i gatunkową wirusa. Aby ją przekroczyć, wirusy wykształciły liczne mechanizmy, których wykorzystanie zależne jest od budowy wirusa oraz komórki docelowej. Wirusy opłaszczone generalnie ulegają fuzji z błoną komórkową, co skutkuje przeniesieniem nukleoproteiny do wnętrza komórki. Proces ten może nastąpić na powierzchni komórki, jednak bardzo często jest poprzedzony internalizacją, w której wykorzystywane są naturalne mechanizmy komórkowe służące w warunkach fizjologicznych między innymi do odżywiania się, czy odbierania cząsteczek sygnałowych.

Przedmiotem prezentowanych badań są dwa wirusy wywołujące choroby u człowieka. Pierwszy z nich, ludzki koronawirus OC43 (HCoV-OC43, od ang. *human coronavirus OC43*), jest częstą przyczyną chorób górnych i dolnych dróg oddechowych o cięższym przebiegu u dzieci, osób starszych oraz z niedoborem odporności. Drugim wirusem wybranym do badań jest wirus Zika (ZIKV, od ang. *Zika virus*). Choć choroba związana z tym flawiwirusem jest łagodna lub asymptomatyczna, zakażenie może prowadzić do rozwoju zespołu Guillaina-Barrégo (autoimmunologicznego uszkodzenia nerwów) u dorosłych i małogłowia u noworodków. Choć każdy z tych wirusów wykorzystuje inną ścieżkę wejścia, to ostatecznie obydwu udaje się przedostać do wczesnych endosomów, a fuzja ich otoczek z błoną pęcherzyków komórki gospodarza silnie zależy od niskiego pH.

W ramach przeprowadzonych badań opisano drogi wejścia obydwu wirusów do komórki gospodarza. Podczas gdy HCoV-OC43 inicjuje klasyczną, stosunkowo wolną (około 90 min) drogę kaweolinozależną, ZIKV wnika do komórek drogą klatrynozależną i ulega fuzji już po 10-15 min. Zastosowanie mikroskopii konfokalnej umożliwiło obserwację kolokalizacji białek wirusowych z białkami markerowymi poszczególnych przedziałów komórkowych. W efekcie byliśmy w stanie śledzić trasę pojedynczych wirionów w początkowej fazie zakażenia komórki. Znaczenie poszczególnych białek w tym procesie zostało następnie potwierdzone poprzez zahamowanie ich aktywności z wykorzystaniem selektywnych inhibitorów lub poprzez wyciszenie wyrażania poszczególnych białek przy pomocy małych interferujących RNA. W związku z tym, że proces internalizacji obydwu wirusów jest wrażliwy na zmiany pH, inkubacja komórek z czynnikami zwiększającymi wewnątrzkomórkowe pH (bafilomycyna A1 oraz NH_4Cl) również prowadziła do zahamowania infekcji. Bafilomycyna A1 jest inhibitorem pompy protonowej i hamuje obniżanie pH w przedziałach wewnątrzkomórkowych, natomiast chlorek amonu działa buforująco, neutralizując zakwaszenie endosomu. Oba te związki są złotym standardem stosowanym w badaniach nad endocytozą i uważa się, że ich działanie polega na hamowaniu procesu fuzji poprzez zablokowanie zmian strukturalnych indukowanych niskim pH.

W takim scenariuszu w obu przypadkach powinno dochodzić do zatrzymania procesu fuzji, a wirusy powinny wejść na ścieżkę degradacji i zostać usunięte z komórki. Przeprowadzone badania wykazały, że w przypadku bafilomycyny A1 faktycznie realizowany jest ten scenariusz, jednak w obecności chlorku amonu uzyskane wyniki były niezgodne z teorią. Bezsprzecznie wykazaliśmy, że chlorek amonu działa w sposób całkowicie odmienny od opisanego, zmieniając transport wewnątrzkomórkowy i prowadząc do usunięcia wirionów zaraz po wejściu do przedziału endosomalnego poprzez szybki recykling zależny od Rab35. Uzyskane wyniki podważają jeden z paradygmatów w wirusologii i biologii komórki i pozwalają sądzić, że duża część badań dotyczących wczesnych etapów zakażenia wymaga weryfikacji.

Przeprowadzone badania pozwoliły lepiej zrozumieć proces zakażenia wirusami HCoV-OC43 i ZIKV, a w przyszłości mogą przyczynić się do opracowania lepszych strategii terapeutycznych w zakresie opracowania inhibitorów wejścia.

Abstract

Although plasma membrane is the primary barrier to viral infection, its composition and the presence of particular proteins on the cell surface determine the possibility of virus entry and, in consequence, tissue and species specificity of the virus. Enveloped viruses have developed different strategies of fusion with host cell membranes, which allows them to deliver their genetic material to the replication site. Subsequent to binding, some viruses are able to fuse with the host membrane immediately on the cell surface, while others need to be delivered to a precisely defined intracellular location. In the latter case, viruses hijack inward transport machinery, that in physiological conditions serves the cell for nutrition and communication.

The main goal of this study was to identify and characterize the entry pathways of two viruses that pose a significant risk to human health. Human coronavirus OC43 (HCoV-OC43) frequently causes upper and lower respiratory tract disease, which may take a more severe course in children, the elderly and immunocompromised people. Zika virus (ZIKV) is a mosquito-borne flavivirus, that is usually associated with mild infections manifested by a set of unspecific symptoms, such as fever, rash, conjunctivitis, muscle and joint pain, malaise and headache. However, in some cases neurologic complications may occur, leading to the development of Guillain-Barré syndrome in adults and lethal microcephaly in fetuses.

HCoV-OC43 was found to initiate infection *via* relatively slow (~90 min) caveolin-dependent pathway, whereas ZIKV was found to follow clathrin-dependent endocytosis and to undergo fusion as soon as 10-15 min post inoculation. Using confocal microscopy, we were able to observe co-localization between viral proteins and marker proteins of different intracellular compartments, which allowed us to track single virions during the early phase of infection. The results were further verified using *small interfering RNA* to transiently silence the expression of proteins involved in the chosen internalization processes, and also by using selective chemical inhibitors of these pathways.

As far as the internalization process of both viruses is endocytosis-dependent and thus is sensitive to pH changes, incubation of the virus-overlaid cells with pH-increasing agents hampered the infection development. Bafilomycin A1 is a proton pump inhibitor which suppresses the pH decrease in intracellular compartments, whereas NH_4Cl exhibits a simple buffering function and in this way neutralizes the acidification of endosomes.

Both of the compounds are golden standards in the research of endocytosis process; by now, it has been commonly believed that their inhibitory function relies on the blocking of structural changes that in physiological (low pH) conditions induce fusion process. In such a scenario, both agents would inhibit

the fusion between the viral envelope and the host membrane, which would further lead the virus to the degradation pathway. Although such a pattern has been indeed observed in the case of bafilomycin A1-treated cells, the results obtained for NH_4Cl are significantly different. We have demonstrated that NH_4Cl reprograms the endocytic hub so that virions are immediately ejected from endosomal compartment *via* Rab35-driven fast recycling pathway. These data call into question one of the paradigms in virology and cell biology and suggest that much of the research on the early stages of infection requires verification.

The complex research on mechanisms of HCoV-OC43 and ZIKV trafficking presented in this study shed light on the regulation of intracellular transport and helped to understand viral strategies of host cells deception. In a broader perspective, identification of cellular factors indispensable for the early steps of infection is going to contribute to the development of novel antiviral therapies.

Wstęp

Jedną z głównych determinant specyficzności gatunkowej oraz tkankowej jest obecność receptorów komórkowych oraz szlaków pozwalających na transport materiału zakaźnego do miejsca replikacji wewnątrz komórki gospodarza. Kluczową rolę w tym procesie wypadku odgrywa proces przekroczenia bariery błony komórkowej. W przypadku wirusów otoczkowych proces ten jest nieodmiennie związany z fuzją błon, która jest przeprowadzana przez białka fuzyjne znajdujące się na powierzchni wirionu. Ich aktywność jest ściśle regulowana, tak że stają się aktywne wyłącznie w precyzyjnie kontrolowanych warunkach.

Prezentowane w niniejszej pracy badania ukazują strategię wejścia do komórek dwóch patogenów człowieka: ludzkiego koronawirusa OC43 (HCoV-OC43, od ang. ***h**uman **co**rona**v**irus* **OC43**) oraz wirusa Zika (ZIKV, od ang. ***Zik**a **v**irus*). Analiza dróg internalizacji tych wirusów przyczyniła się również do zwiększenia stanu wiedzy w zakresie regulacji procesu endocytozy.

1. Mechanizmy wejścia wirusów do komórek

Pierwszą barierą napotykaną przez wirusy w czasie infekcji jest błona komórkowa. Od jej składu (lipidom – proteom – glikom), ładunku oraz otoczenia zależy podatność danej komórki na zakażenie. Niespecyficzne oddziaływanie pomiędzy glikoproteiną wirusową a cząsteczkami występującymi w dużej ilości na powierzchni komórek eukariotycznych (receptory adhezyjne) pozwala zwiększyć gęstość wirusów na powierzchni błony komórkowej, a w niektórych przypadkach pozwala również na transport wirionów do regionów błony charakteryzujących się wysokim stężeniem receptorów wejścia[1]. Na skutek związania się glikoprotein wirusowych z właściwymi receptorami wejścia dochodzi do indukcji wybranych ścieżek sygnałowych, inicjacji procesu reorganizacji błony komórkowej i internalizacji. Wirusy otoczkowe wykształciły dwie strategie wejścia do komórek:

1. fuzja z błoną komórkową bezpośrednio na powierzchni komórki,
2. fuzja z błoną komórkową w przedziałach wewnątrzkomórkowych, z wykorzystaniem fizjologicznych dróg transportu komórkowego.

Wirusowe białka fuzyjne ze względu na znaczne różnice strukturalne zostały podzielone na trzy klasy. Białka należące do klasy I [takie jak hemaglutynina ortomyksowirusów czy białko S (od ang. ***s**pike*) koronawirusów] występują w formie skierowanych prostopadle do błony trimerów, w których dominującą strukturą drugorzędową jest α−helisa. Peptyd fuzyjny, czyli hydrofobowy region, który w czasie trwania fuzji zatapiany jest w błonie komórki gospodarza, zlokalizowany jest na N-końcu. Białka fuzyjne II klasy tworzą dimery ułożone równolegle do błony. Dominującą strukturą drugorzędową jest w tym wypadku β-harmonijka, a peptyd fuzyjny jest ulokowany w środkowej części sekwencji

aminokwasowej białka. Do tej klasy zalicza się między innymi białko E (od ang. ***e**nvelope*) flawiwirusów oraz E1/E2 togawirusów. Białka fuzyjne zaliczane do klasy III [m.in. białko G (od ang. ***g**lycoprotein*) rabdowirusów i białko gB (od ang. ***g**lycoprotein **B***) herpeswirusów] dzielą wspólne cechy z białkami fuzyjnymi I i II klasy. Podobnie jak białka klasy I, są one trimerami z konserwatywnie zachowaną strukturą α−helisy w centralnej części białka. Ich domeny fuzyjne wykazują natomiast większe podobieństwo do klasy II - są zlokalizowane w obrębie wydłużonych końców β-harmonijki[2].

Białka fuzyjne w swojej aktywnej postaci są niestabilne i łatwo dochodzi do ich inaktywacji. Aby temu zapobiec, wirusowe białka fuzyjne przyjmują początkowo formę nieaktywną. Miejsce fuzji zależy zatem od dostępności czynników aktywujących, takich jak proteazy komórkowe, pH, czy potencjał redoks. Poszczególne przedziały wewnątrzkomórkowe charakteryzuje specyficzny skład lipidowy, który służy wirusom jako „mapa" do precyzyjnego rozpoznania wybranej lokalizacji[3]. W optymalnych warunkach wirusowe białka fuzyjne ulegają aktywacji, co jest związane z drastycznymi zmianami ich konformacji oraz uwolnieniem energii potrzebnej do fuzji otoczki wirusowej z błoną komórki gospodarza[4]. Fuzja pozwala na transport wirusowego materiału genetycznego do cytoplazmy, gdzie dochodzi do jego wyrażania i kolejnych etapów infekcji. Schemat potencjalnych miejsc aktywacji wirusowych białek fuzyjnych przedstawia **Rycina 1**.

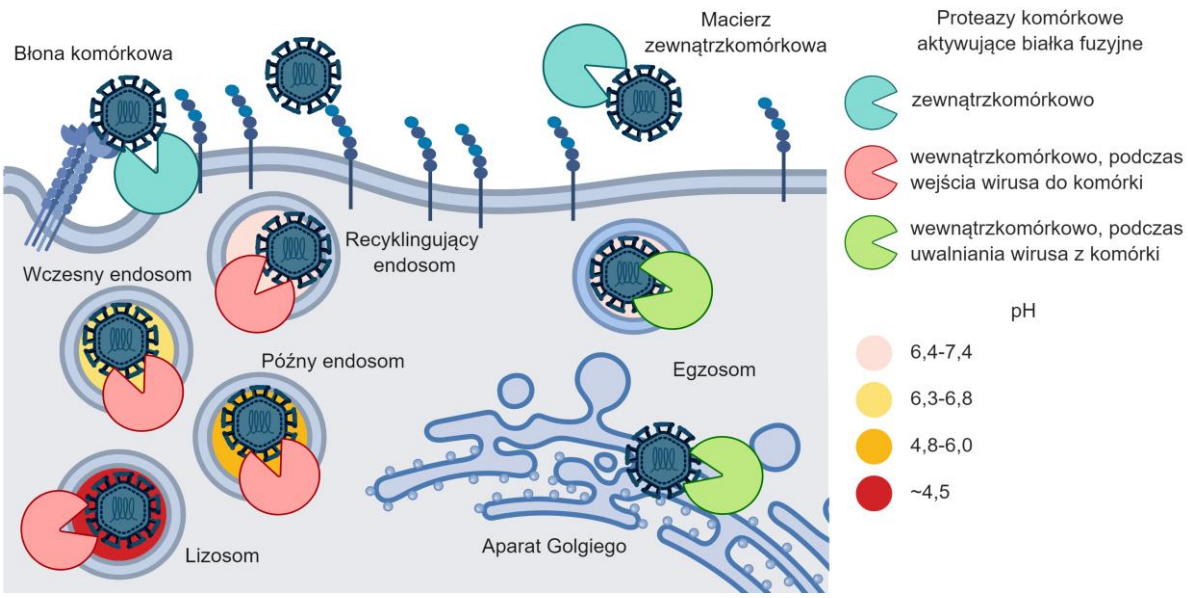

***Rycina 1 Schemat aktywacji wirusowych białek fuzyjnych w komórce gospodarza**. Rycinę utworzono korzystając z narzędzia Biorender.*

2. Endocytoza

Wirusy niezdolne do fuzji z błoną na powierzchni komórki przedostają się do jej wnętrza wykorzystując proces endocytozy. Endocytoza w warunkach fizjologicznych służy eukariontom do internalizacji składników błony komórkowej, związanych z nimi ligandów oraz związków zawieszonych w macierzy zewnątrzkomórkowej. Pełni kluczową rolę w odżywianiu i komunikacji komórek. Aż do wczesnych lat dziewięćdziesiątych jedyną znaną ścieżką endocytozy była droga klatrynozależna. Kiedy zaobserwowano, że jej hamowanie nie prowadzi do całkowitego zablokowania importu komórkowego, rozpoczęto intensywne badania ukierunkowane na poszukiwanie alternatywnych szlaków. Jako pierwszą zidentyfikowano drogę kaweolinozależną. Do dnia dzisiejszego opisano wiele innych wariantów internalizacji, takich jak szybka endocytoza zależna od endofiliny (FEME, od ang. ***F**ast **E**ndophilin-**M**ediated **E**ndocytosis*)[5], CLIC/GEEC (od ang. ***Cl**athrin-**I**ndependent **C**arrier/ **G**PI-anchored **E**nriched **E**ndocytic **C**ompartments*)[6,7], drogi zależne od Arf6[8], flotylliny[9], a także makropinocytoza[10] i entoza[11].

2.1. Endocytoza klatrynozależna

Droga klatrynozależna wykorzystywana jest przez szereg wirusów należących do różnych jednostek taksonomicznych, m.in. przez wirusa Dengi[12], metapneumowirusa[13], enterowirusa 71[14] czy wirusa wścieklizny[15]. Związanie wirusa z receptorem inicjuje skoordynowane działania kompleksu białkowego złożonego z FCHo1/2 (od ang. ***F**er/**C**ip4 **ho**mology domain-only proteins **1** and **2***), Eps15 (od ang. ***Ep**idermal growth factor receptor **s**ubstrate **15***) i intersektyny-1, mające na celu utworzenie płaszcza klatrynowego dookoła cząsteczki wirusa[16]. Pierwszym etapem jest tworzenie się w tym miejscu wgłębienia w błonie komórkowej. FCHo1/2 poprzez domenę F-BAR (od ang. ***B**in/**A**mphiphysin/**R**vs*) wiąże się do 4,5-difosforanu fosfatydyloinozytolu w błonie komórkowej i indukuje jej wygięcie, natomiast poprzez domenę µHD (od ang. ***µ**-**h**omology **d**omain*) wiąże Eps15 oraz intersektynę-1, które z kolei rekrutują białko adaptorowe 2 (AP2, od ang. ***a**daptor **p**rotein 2*) do miejsca nukleacji. Do AP2 przyłączają się jednostki klatryny i w momencie gdy ich stężenie osiągnie poziom krytyczny polimeryzują, tworząc płaszcz wokół powstającego pęcherzyka[17]. Stabilizowana przez ładunek struktura o średnicy ok. 100 nm pogłębia się[18]. Pączkowaniu pęcherzyka towarzyszy tworzenie się szyjki, do której przyciągane jest kolejne białko - amfifizyna. Amfifizyna rekrutuje dynaminę - GTPazę, która polimeryzuje tworząc charakterystyczny pierścieniowy kształt, w którym dwie domeny GTPazowe znajdują się obok siebie[19]. Hydroliza GTP wywołuje zmiany konformacyjne cząsteczek dynaminy, przez co pierścieniowa struktura zaciska się wokół przewężenia przy powierzchni komórki, aby ostatecznie umożliwić fuzję błon i odcięcie pęcherzyka zawierającego ładunek. Następnie pęcherzyk jest transportowany przez cytoszkielet aktynowy lub wzdłuż mikrotubul do wnętrza

komórki. W czasie podróży dojrzewa, traci płaszcz klatrynowy i ulega fuzji z innymi pęcherzykami lub ze stacją sortującą, jaką jest wczesny endosom.

W badaniach nad wykorzystaniem drogi klatrynowej przez wirusy stosuje się komercyjnie dostępne inhibitory, w tym: amantadynę, która stabilizuje dołki klatrynowe i nie dopuszcza do ich pogłębiania[20]; chlorpromazynę[21], przy której kompleks klatryna-AP2 ulega translokacji z powierzchni komórek do endosomów; PitStop, który wiąże się z N-terminalną domeną klatryny, przez co blokuje dynamikę jej oddziaływań[22]. Alternatywnym podejściem jest zahamowanie internalizacji pęcherzyków klatrynowych poprzez inaktywację dynaminy. Do powszechnie stosowanych inhibitorów dynaminy należą MitMAB, który blokuje jej oddziaływanie z fosfolipidami błony komórkowej oraz Dynasore, który hamuje aktywność GTPazy[23].

2.2. Endocytoza kaweolinozależna

Droga kaweolinozależna jest kolejnym rodzajem endocytozy wykorzystywanym przez szereg wirusów, między innymi przez flawiwirusa Japońskiego zapalenia mózgu[24], poliomawirusa SV40 (od ang. ***S**imian **V**irus 40*)[25], czy echowirusa 1[26].

Kaweole to butelkowate zagłębienia w błonie komórkowej o średnicy 50–100 nm zlokalizowane na powierzchni komórki. Ich integralnym elementem jest kaweolina-1, która stabilizuje strukturę bogatą w cholesterol i sfingolipidy[27]. Załadowanie *cargo* do kaweoli indukuje rekrutację dynaminy, która podobnie jak w przypadku drogi klatrynozależnej odcina inwaginację z powierzchni komórki. Utworzony w ten sposób pęcherzyk może wejść na klasyczną drogę endocytozy poprzez fuzję z wczesnym endosomem, albo stworzyć multi-kaweolarny kompleks o neutralnym pH zwany kaweosomem, który nie ulega fuzji z przedziałami o niskim pH[28].

Do hamowania drogi kaweolinozależnej stosuje się związki wiążące cholesterol, które stabilizują kaweole i nie dopuszczają do ich pogłębiania (metylo-β-cyklodekstryna, nystatyna)[29], jak również opisane poprzednio inhibitory dynaminy[23].

2.3. Endocytoza niezależna od klatryny i kaweoliny

Choć w ostatnich latach wykryto szereg dróg endocytozy niezależnych od klatryny i kaweoliny, ich przebieg do tej pory nie został szczegółowo opisany.

FEME jest drogą zależną od endofiliny – białka, które jest również zaangażowane w endocytozę klatrynozależną. Podczas gdy droga klatrynozależna może zachodzić zarówno konstytutywnie, jak i pod wpływem wiązania ligandów do receptorów na powierzchni komórki, FEME jest indukowana tylko w

obecności ligandów. Rekrutacja endofiliny do 3,4,5-trifosforanu inozytolu prowadzi do internalizacji receptorów do drobnych pęcherzyków. Proces ten zależy od dynaminy, Rac, kinazy PAK1 oraz aktyny[5].

CLIC/GEEC tworzą cylindryczne zagłębienia o średnicy ok. 40 nm, bogate w sfingolipidy oraz cholesterol. Ważną rolę w ich internalizacji odgrywa białko GRAF1 (z ang. ***G**TPase **r**egulator **a**ssociated with **f**ocal adhesion kinase-**1***), które jest w nich zakotwiczone poprzez swoje domeny BAR oraz PH (od ang. ***p**leckstrin **h**omology*). Reguluje ono aktywność małych białek G (Cdc42, Arf1), a także oddziałuje z dynaminą. Co ciekawe, funkcja dynaminy w tym procesie pozostaje niewyjaśniona, podobnie jak mechanizm odcinania pęcherzyków z powierzchni komórki[7]. CLIC/GEEC odpowiada za endocytozę fazy płynnej oraz pełni znaczącą rolę w migracji i polaryzacji komórek. Ponadto wiadomym jest, że stanowi drogę wejścia do komórek dla wirusa związanego z adenowirusami 2 (AAV-2, od ang. ***a**deno-**a**ssociated **v**irus **2***)[30].

Tak jak w przypadku CLIC/GEEC, endocytoza zależna od Arf6 wymaga cholesterolu i nie zależy od dynaminy. Ze względu na podobieństwo w zakresie transportowanego *cargo*, wysunięto hipotezę, że jest to jedna i ta sama droga, a różnice w wykorzystaniu Arf6 są charakterystyczne dla różnych typów komórek[31]. Podobne wątpliwości tyczą się drogi zależnej od flotylliny – przypuszcza się, że flotyllina może jedynie pełnić rolę białka adaptorowego dla wybranych ładunków[31].

Ze względu na sposób tworzenia pęcherzyków, na tle alternatywnych ścieżek endocytozy wyróżnia się proces makropinocytozy. Aktywacja ścieżek sygnałowych przez receptory o aktywności kinaz tyrozynowych wywołuje zmiany w cytoszkielecie aktynowym. Ważną rolę w tym procesie pełni mała GTPaza Rac1. W wyniku tych rearanżacji dochodzi do wytworzenia uwypukleń błony komórkowej, które zagarniają *cargo* wraz ze znacznymi objętościami fazy płynnej i zawartymi w niej molekułami. W efekcie powstaje pęcherzyka o średnicy 0,5-10 µm, który jest odcinany z powierzchni komórki przez białka CtBP1/BARS albo przez dynaminę[32]. Makropinocytoza wykorzystywana jest m.in. przez syncytialnego wirusa oddechowego (RSV, od ang. ***r**espiratory **s**yncytial **v**irus*)[33] oraz przez adenowirusa 3[34].

2.4. Wewnątrzkomórkowy transport ładunków

Wewnątrzkomórkowy transport pęcherzyków kierowany jest przez małe GTPazy membranowe należące do rodziny Rab[35]. Wczesne endosomy są adresowane poprzez białka Rab5 i antygen wczesnego endosomu 1 (EEA1, od ang. ***e**arly **e**ndosome **a**ntigen **1***) i charakteryzują się umiarkowanie niskim pH (6,3-6,8)[36]. Zawarte w nich *cargo* ulega wstępnemu sortowaniu i może zostać skierowane do degradacji poprzez ciałko wielopęcherzykowe, późne endosomy i lizosomy, albo wracać na powierzchnię komórki na drodze recyklingu, egzocytozy lub poprzez aparat Golgiego[37,38].

Transport prowadzący do degradacji związany jest ze stopniowym spadkiem pH dzięki aktywności pomp protonowych oraz w wyniku fuzji z kwaśnymi pęcherzykami. W późnych endosomach, adresowanych przez Rab7, pH zwiera się w przedziale 4,8-6,0, natomiast w lizosomach osiąga wartość 4,5[39]. Lizosomy są przedziałem docelowym na tej drodze, służą do przechowywania hydrolaz i innych enzymów proteolitycznych. Ich białkiem markerowym jest białko związane z błoną lizosomu (LAMP1, od ang. ***l****ysosomal* ***a****ssociated* ***m****embrane* ***p****rotein* ***1***)[40].

W przedziałach ukierunkowanych na transport powrotny do błony komórkowej pH utrzymuje się na wyższym poziomie (~6,5). W tym przypadku *cargo* może być adresowane przez Rab35 na drogę szybkiego recyklingu (5 min) lub przez Rab11 na drogę wolnego recyklingu (15-30 min)[36]. Alternatywnie, ładunek może zostać zamknięty w pęcherzyku tworzącym się w świetle ciałka wielopęcherzykowego, który jest adresowany przez Rab27a/b do transportu na powierzchnię komórki i dalej do macierzy zewnątrzkomórkowej w formie egzosomu[41]. Egzosomy mają średnicę 30-100 nm i są wykorzystywane przez wirusy do transportu na zewnątrz komórki[42-44]. Ponadto, *cargo* może przejść do aparatu Golgiego i podążać ścieżką wstecznego transportu przez endosomy adresowane Rab9 lub w sposób niezależny od Rab9, prowadzącą do aparatu Golgiego na przykład z recyklingujących endosomów[45]. Wybór ścieżki transportu retrogradowego jest uzależniony od obecności specyficznych motywów w sekwencji aminokwasowej ładunków znajdujących się w przedziale endosomalnym[46].

Sieć wewnątrzkomórkowego transportu schematycznie podsumowuje **Rycina 2**.

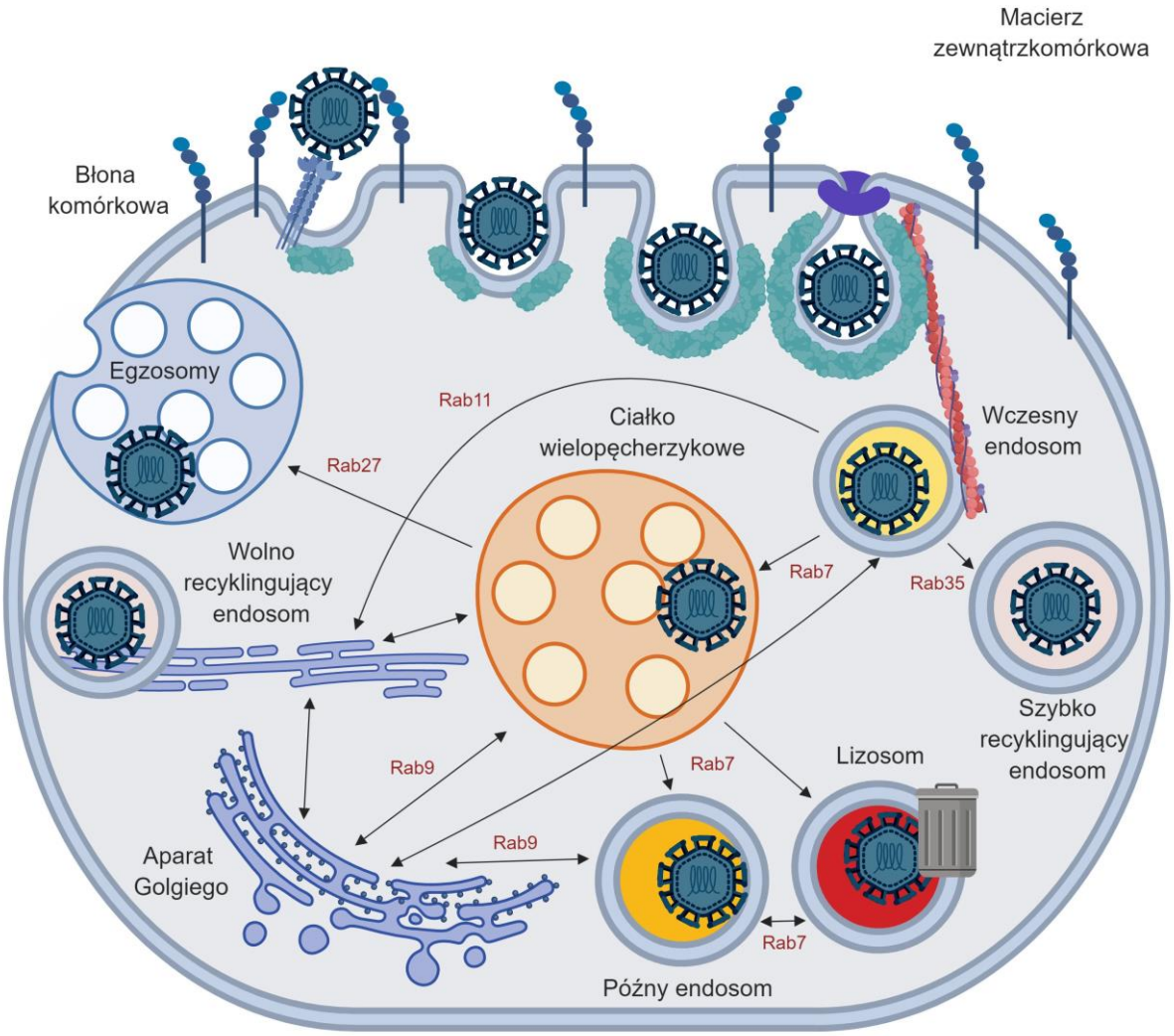

Rycina 2 ***Schemat transportu wewnątrzkomórkowego****. Rycinę utworzono korzystając z narzędzia Biorender.*

Badania przedstawione w niniejszej pracy zostały oparte o obserwację wirionów w kontekście białek markerowych dla wybranych przedziałów wewnątrzkomórkowych przy zastosowaniu mikroskopii konfokalnej. Doświadczenia z powszechnie stosowanymi inhibitorami pozwoliły uzyskać wyniki spójne z analizą mikroskopową, a rola kluczowych białek w procesie wejścia wirusów została potwierdzona poprzez selektywne wyciszenie wyrażania tych białek w komórkach.

Przedmiotem opisywanych badań jest analiza procesu wejścia wirusów do komórek gospodarza oraz ich transportu wewnątrzkomórkowego. Badania przeprowadzono na dwóch wirusach otoczkowych, które wywołują u człowieka objawy chorobowe - HCoV-OC43 oraz ZIKV.

3. Ludzki koronawirus OC43

Na chwilę obecną znanych jest sześć koronawirusów patogennych dla człowieka. HCoV-229E oraz HCoV-OC43 zostały po raz pierwszy opisane w latach sześćdziesiątych dwudziestego wieku i przez prawie czterdzieści lat były uznawane za jedyne koronawirusy zdolne do infekcji człowieka. Szeroko

zakrojone badania nad tą rodziną wirusów rozpoczęły się dopiero w 2002 r., wraz z pojawieniem się wirusa zespołu ciężkiej ostrej niewydolności oddechowej (SARS, od ang. **s**evere **a**cute **r**espiratory **s**yndrome) o wysokiej śmiertelności (wynoszącej średnio 10%, a wśród osób powyżej 64 roku życia nawet powyżej 50%)[47,48]. Wtedy też zidentyfikowano dwa kolejne, jak się okazało szeroko rozpowszechnione wśród ludzi koronawirusy, HCoV-NL63[49] oraz HCoV-HKU1[50], wywołujące infekcje dróg oddechowych. W 2012 r. w wyniku transmisji odzwierzęcej pojawił się nowy koronawirus zakażający ludzi, powodujący bliskowschodni zespół niewydolności oddechowej (MERS, od ang. **M**iddle **E**ast **r**espiratory **s**yndrome), śmiertelny w ~35% przypadków[51,52]. Zdolność do przekraczania granicy między gatunkami oraz wysoki współczynnik śmiertelności odzwierzęcych koronawirusów wskazują na konieczność dalszego prowadzenia intensywnych badań nad przebiegiem procesu zakażenia w celu identyfikacji potencjalnych celów terapeutycznych.

HCoV-OC43 infekuje górne i dolne drogi oddechowe, a nasilenie choroby zależy od wieku oraz ogólnego stanu zdrowia człowieka. Jest najczęściej występującym koronawirusem wśród ludzi, przy czym najwyższa zapadalność przypada na okres zimowo-wiosenny[53,54].

Genom HCoV-OC43 składa się z prawie 31 tys. nukleotydów. W pierwszych dwóch trzecich wirusowego RNA od strony 5’ znajdują się dwie otwarte ramki odczytu 1a i 1ab, które kodują pojedynczą poliproteinę. Powstałe białko (ok. 7 tys. aminokwasów) ulega autoproteolizie, co prowadzi do powstania kilkunastu dojrzałych białek niestrukturalnych niezbędnych dla replikacji wirusa i modulujących mikrośrodowisko zakażenia. Pozostała jedna trzecia genomu koduje białka strukturalne oraz białka dodatkowe: białko niestrukturalne ns2 (od ang. ***n**on**s**tructural protein 2*), esterazę hemaglutyniny (HE, od ang. ***h**emmaglutin **e**sterase*), białko S (od ang. ***s**pike*), białko niestrukturalne ns12.9, białko otoczki E (od ang. ***e**nvelope*), białko błonowe M (od ang. ***m**embrane*) oraz białko kapsydu N (od ang. ***n**ucleocapsid*)[55]. W części 5’ genu kodującego białko N znajdują się jeszcze dwie małe, wewnętrzne ramki odczytu: Ia oraz Ib. Z wyjątkiem białka HE, białka dodatkowe są białkami niestrukturalnymi, a ich funkcje nie zostały do tej pory całkowicie poznane. Białko HE występuje wyłącznie wśród betakoronawirusów. Jego główną funkcją jest aktywność esterazy, która przejawia się przez odcinanie grup acetylowych z kwasów sjalowych. We wczesnych etapach infekcji ta funkcja ułatwia wirusowi związanemu z czynnikami adhezyjnymi przedostanie się do receptora, natomiast w późnych etapach infekcji ułatwia uwalnianie potomnych wirionów z zainfekowanej komórki[56]. S to glikoproteina powierzchniowa, która pośredniczy w procesie wejścia koronawirusów do komórek, a jej struktura determinuje ich specyficzność tkankową. Należy do I klasy białek fuzyjnych. Składa się z krótkiej C-terminalnej endodomeny, domeny transbłonowej oraz dużej N-terminalnej ektodomeny, którą tworzą podjednostki S1 i S2. W obrębie podjednostki S1 znajduje się domena wiążąca receptor, natomiast podjednostka S2 odpowiada za fuzję z błoną komórki gospodarza[57].

Białko E to małe białko otoczkowe, które uczestniczy w tworzeniu wirionów oraz w ich odcinaniu z powierzchni błony. Tworzy kanał jonowy, który najprawdopodobniej warunkuje prawidłowy transport wirionów na powierzchnię komórki[58]. Białko M jest białkiem transbłonowym i stanowi rusztowanie, na którym tworzony jest wirion. Może przyjmować dwie konformacje: kompaktową oraz wydłużoną, przy czym najprawdopodobniej tylko jedna z nich – wydłużona – odpowiada za sztywność i jednorodną krzywiznę błony, a także za inkorporację białka S do tworzących się wirionów[59]. Białko N jest białkiem nukleokapsydu. Wiążę się z RNA i chroni dużą cząsteczkę wirusowego genomu, a także aktywnie uczestniczy w modyfikacji procesów komórkowych oraz w replikacji i transkrypcji wirusa[60].

Proces wejścia HCoV-OC43 do komórek można podzielić na dwa etapy: przyłączanie się do powierzchni komórki oraz internalizację wirionu. W permisywnych dla tego wirusa komórkach ludzkiego nowotworu okrężnicy (HCT-8), rolę czynników adhezyjnych pełnią powszechnie występujące kwasy sjalowe oraz siarczan heparanu. Szczepy kliniczne wykorzystują kwasy sjalowe zarówno w roli receptora adhezyjnego, jak i receptora wejścia[61].

Proces internalizacji HCoV-OC43 drogą kaweolinozależną został przedstawiony w artykule:

Owczarek K, Szczepanski A, Milewska A, Baster Z, Rajfur Z, Sarna M, Pyrc K, **Early events during human coronavirus OC43 entry to the cell**. Sci Rep. 2018;8(1):7124

Zależność od endocytozy zbadano poprzez określenie stopnia kolokalizacji wirionów z EEA1 na wczesnym etapie infekcji komórek HCT-8. W tym celu komórki utrwalone w różnych punktach czasowych od momentu inokulacji wirusem (p.i., od ang. ***p**ost **i**noculation*) poddano barwieniu immunofluorescencyjnemu, specyficznemu względem wirusowego białka N oraz białka EEA1. Preparaty zobrazowano korzystając z mikroskopii konfokalnej, a otrzymane zdjęcia poddano analizie. Zaobserwowano, że w czasie 5 - 20 min od momentu inokulacji HCoV-OC43 wraz z EEA1 znajdowały się w pobliżu błony komórkowej, a następnie (w czasie 40 - 120 min p.i.) tworzyły coraz większe skupiska, które stopniowo przesuwały się do wnętrza komórki. Zależność internalizacji wirusów od procesu endocytozy potwierdzono poprzez dodanie do pożywki hodowlanej związków zwiększających wewnątrzkomórkowe pH: NH_4Cl i bafilomycyny A1. Analiza liczby kopii wirusowego RNA w pożywce 5 dni p.i. ujawniła silne zahamowanie infekcji w obecności tych związków, dowodząc ważnej roli niskiego pH w procesie infekcji HCoV-OC43.

Aby bliżej scharakteryzować proces wejścia wirusa, HCoV-OC43 wybarwiono w kontekście białek markerowych wybranych ścieżek endocytozy. W czasie 5 - 90 min p.i. zaobserwowano silną kolokalizację wirionów z kaweoliną-1. Istotność tej drogi potwierdzono poprzez tymczasowe wyciszenie kaweoliny w komórkach, co spowodowało zatrzymanie wirionów na ich powierzchni.

Podobne obserwacje towarzyszyły zastosowaniu chemicznych inhibitorów tej ścieżki: dodanie nystatyny i metylo-β-cyklodekstryny do pożywki uniemożliwiło wejście wirusów do komórek i doprowadziło do znacznego zahamowania infekcji. Proces wejścia okazał się być zależny również od aktywności dynaminy oraz filamentów aktynowych, co zbadano poprzez zastosowanie powszechnie znanych inhibitorów tych białek.

Co ciekawe, przekierowanie transportu tego wirusa na inną drogę endocytozy jest możliwe, lecz nie prowadzi do efektywnej infekcji. Zaprezentowane badania pokazują, że po zahamowaniu endocytozy kaweolinozależnej za pomocą inhibitorów chemicznych HCoV-OC43 może wnikać do komórek atypową dla siebie drogą makropinocytozy, ale w takim wypadku nie dochodzi do fuzji i zakażenia. Warunki panujące w przedziale wewnątrzkomórkowym, do którego trafia wirus poprzez makropinocytozę nie są odpowiednie dla aktywacji białka fuzyjnego.

4. Wirus Zika

Wirus Zika (ZIKV) należy do rodziny flawirusów. Jest blisko spokrewniony z wirusami wywołującymi między innymi gorączkę Dengi, żółtą febrę, gorączkę Zachodniego Nilu, kleszczowe zapalenie mózgu czy Japońskie zapalenie mózgu. Po raz pierwszy wirus został zidentyfikowany w latach 40. XX wieku w próbkach pobranych od makaków zamieszkujących las Zika w Ugandzie, a następnie u ludzi w latach 50. XX wieku w Ugandzie oraz w Zjednoczonej Republice Tanzanii. Główną drogą transmisji wirusa są komary należące do rodzaju *Aedes*, chociaż wirus może rozprzestrzeniać się także przez kontakty seksualne oraz przez łożysko.[62] Przez wiele lat wirus utrzymywał się na stosunkowo niewielkim terytorium i nie był postrzegany jako zagrożenie medyczne. Z czasem jednak zakażenia zaczęły występować w centralnej i zachodniej Afryce oraz w południowej części Azji. Pierwsza epidemia wywołana ZIKV rozpoczęła się w 2007 roku na wyspie Yap, kolejna na wyspach Polinezji Francuskiej w latach 2013-2014. W 2014 roku (najprawdopodobniej w czasie Mistrzostw Świata w piłce nożnej organizowanych w Brazylii) wirus dotarł do części Ameryki Południowej i Środkowej, gdzie w kolejnym roku wywołał epidemię. Niewiele później obecność ZIKV odnotowano również w Stanach Zjednoczonych[63-68].

Choć infekcje wirusem ZIKA mają zwykle łagodny przebieg i charakteryzują się niespecyficznymi objawami, takimi jak ból głowy, gorączka, zaczerwienione oczy, bóle mięśni i stawów czy wysypka[69], wykazano związek zakażenia z rozwojem zespołu Guillaina-Barrégo (autoimmunologicznego uszkodzenia nerwów) u dorosłych[70] i małogłowia u płodów[71]. Brak dostępnej szczepionki, szybkie tempo rozprzestrzeniania i korelacja z zagrażającymi ludzkiemu życiu zaburzeniami neurologicznymi wskazuje potrzebę prowadzenia intensywnych badań nad infekcją ZIKV.

Genom ZIKV tworzy prawie 11 tys. nukleotydów[72], które kodują pojedynczą ramkę odczytu oflankowaną rejonami nieulegającymi translacji. Po wniknięciu do komórki genomowe RNA wirusa służy bezpośrednio jako matryca dla maszynerii translacyjnej, co prowadzi do powstania poliproteiny, która następnie ulega trawieniu przez proteazy komórkowe oraz autoproteolizie przez proteazę wirusową tworząc trzy białka strukturalne: białko kapsydu C (od ang. ***c****apsid*), prekursor białka błonowego prM (od ang. ***p****recursor* ***m****embrane*) i białko otoczki E (od ang. ***e****nvelope*); oraz siedem białek niestrukturalnych: NS1 (od ang. ***n****on-****s****tructural protein*), NS2A, NS2B, NS3, NS4A, NS4B i NS5. Podobnie jak w przypadku HCoV-OC43, białka niestrukturalne uczestniczą w replikacji wirusa oraz wchodzą w interakcję z czynnikami odpowiedzi immunologicznej komórki gospodarza. Białka strukturalne są natomiast zaangażowane w proces wejścia, składania potomnych wirionów oraz wyjścia z komórki gospodarza. Białko C rekrutuje RNA do formujących się wirionów oraz pozostaje z nim związane aż do momentu infekcji kolejnej komórki. prM jest prekursorem białka błonowego M (od ang. ***m****embrane*) i w czasie transportu przez aparat Golgiego pełni funkcję ochronną dla glikoproteiny E: osłania ją przed ekspozycją na niskie pH, tym samym zapobiegając przedwczesnej aktywacji peptydu fuzyjnego[73].

Proces wejścia ZIKV do komórek drogą klatrynozależną został szczegółowo opisany w artykule

Owczarek K, Chykunova Y, Jassoy C, Maksym B, Rajfur Z, Pyrc K, **Zika virus: mapping and reprogramming the entry**. Cell Commun Signal. 2019;17(1):41

Doświadczenia wykonano w komórkach Vero, w których ZIKV wydajnie replikuje. Przy użyciu mikroskopii konfokalnej zaobserwowano kolokalizację ZIKV z klatryną i EEA1 w okresie 2 - 10 min p.i. Istotność klatryny w procesie wejścia wirusa została potwierdzona poprzez jej tymczasowe wyciszenie, które skutkowało zatrzymaniem wirionów na powierzchni komórek. Traktowanie komórek komercyjnie dostępnymi inhibitorami drogi klatrynozależnej oraz dynaminy (odpowiednio amantadyną i PitStopem oraz Dynasorem i MitMabem) doprowadziło do znacznej redukcji liczby kopii wirusowego RNA w pożywce 3 dni p.i., co dodatkowo potwierdziło zależność wirusa od tej ścieżki endocytozy.

Dzięki możliwości immunofluorescencyjnego wybarwienia dwóch białek strukturalnych wirusa: białka E oraz białka C dokonano analizy procesu fuzji otoczki wirusa z błoną komórki gospodarza. Celem określenia czasu i miejsca fuzji, białka wirusowe zostały wybarwione w kontekście markerów wybranych przedziałów wewnątrzkomórkowych w kilku punktach czasowych między 5 - 20 min p.i. Przez pierwsze 10 min obydwa białka silnie kolokalizowały z markerem późnych endosomów – Rab7. Następnie (w okresie między 10 a 15 min p.i.) ich kolokalizacja z Rab7 zanikła, a białko E zaczęło kolokalizować z Rab11, markerem wolno recyklingujących endosomów. W wyniku fuzji w późnych

endosomach wirusowe RNA i białko C przedostały się do cytoplazmy, natomiast białko E zatopione w błonie pęcherzykowej uległo wolnemu recyklingowi na powierzchnię komórki.

Ponieważ proces fuzji jest silnie zależny od czynników komórkowych, zbadano jaki wpływ na wydajność fuzji ZIKV mają proteazy oraz wewnątrzkomórkowe pH. W celu sprawdzenia roli proteaz przeprowadzono infekcję w obecności camostatu (inhibitora proteaz serynowych), E64 (inhibitora proteaz cysteinowych) oraz CMK (inhibitora furyny), które dodawano na komórki na różnych etapach infekcji. Liczba kopii wirusowego RNA po 3 dniach p.i. została zredukowana względem kontroli tylko w przypadku, gdy CMK był obecny na późnych etapach infekcji, co świadczy o istotnej roli proteazy komórkowej o specyficzności podobnej do furyny w procesie produkcji aktywnych wirionów.

W celu zbadania roli wewnątrzkomórkowego pH w procesie fuzji ZIKV przeprowadzono infekcję w obecności NH_4Cl i bafilomycyny A1. Okazało się, że mechanizm ich działania jest różny: podczas gdy bafilomycyna A1 zahamowała infekcję tylko na jej wczesnym etapie, NH_4Cl ograniczyło ją także na późnych etapach. Jeszcze ciekawszy obraz otrzymano w wyniku analizy mikroskopowej lokalizacji wirusów w obecności tych związków. Choć obydwa zahamowały infekcję w wyniku poniesienia pH w przedziałach wewnątrzkomórkowych stanowiących standardową drogę wejścia tego wirusa, to zaaplikowanie każdego z tych związków skutkowało przekierowaniem wirionów na inną ścieżkę. W obecności bafilomycyny A1 wiriony nie ulegały fuzji w późnych endosomach. Pęcherzyki zawierające wiriony przekształciły się w lizosomy, w których materiał zakaźny uległ proteolizie i inaktywacji, a pozostałości uległy wolnemu recyklingowi na powierzchnię komórki. W obecności NH_4Cl ZIKV ulegała szybkiemu recyklingowi na powierzchnię komórek, przez co również nie doszło do fuzji wirusa z błoną gospodarza.

Zaprezentowane wyniki odkrywają różnice w mechanizmach działania NH_4Cl i bafilomycyny A1 - związków, które do tej pory były stosowane w wirusologii do rozróżnienia czy wirus przenika do cytoplazmy bezpośrednio z powierzchni błony komórkowej, czy jest zależny od endocytozy.

Cele badań

1. Charakterystyka wczesnych etapów replikacji wirusów HCoV-OC43 oraz ZIKV
2. Wyznaczenie czynników komórkowych regulujących proces wejścia tych wirusów do komórek

W szerszym znaczeniu, przeprowadzone badania miały na celu poszerzenie stanu wiedzy w zakresie przebiegu zakażenia oraz mechanizmów transportu wewnątrzkomórkowego, jak również wyznaczenie potencjalnych celów terapeutycznych w zakażeniach HCoV-OC43 oraz ZIKV.

Streszczenie wyników

Wyniki przedstawione w artykule: Owczarek K, Szczepanski A, Milewska A, Baster Z, Rajfur Z, Sarna M, Pyrc K, **Early events during human coronavirus OC43 entry to the cell**. Sci Rep. 2018;8(1):7124

- HCoV-OC43 w celu wejścia do ludzkich komórek nowotworu okrężnicy HCT-8 wykorzystuje proces endocytozy zależnej od kaweoliny;
- Proces wejścia HCoV-OC43 do komórki gospodarza jest zależny od pH;
- Zahamowanie endocytozy zależnej od kaweoliny powoduje zahamowanie wejścia wirusów do komórki gospodarza, a w konsekwencji uniemożliwia rozwój infekcji;
- Proces internalizacji HCoV-OC43 zależy od aktywności dynaminy, która odcina z powierzchni komórki zagłębienia kaweolinowe;
- Ograniczenie dynamiki filamentów aktynowych hamuje infekcję HCoV-OC43;
- W przypadku zahamowania endocytozy kaweolinozależnej HCoV-OC43 może wniknąć do komórek atypową dla siebie drogą makropinocytozy, jednak takie warunki nie pozwalają na fuzję – w konsekwencji nadal nie dochodzi do rozwoju zakażenia.

Wyniki przedstawione w artykule: Owczarek K, Chykunova Y, Jassoy C, Maksym B, Rajfur Z, Pyrc K, **Zika virus: mapping and reprogramming the entry**. Cell Commun Signal. 2019;17(1):41

- ZIKV ulega internalizacji na drodze endocytozy zależnej od klatryny; inhibitory drogi klatrynozależnej oraz tymczasowe wyciszenie klatryny zatrzymują wiriony na powierzchni komórki i w konsekwencji hamują rozwój infekcji;
- Pęcherzyki opłaszczone klatryną są odcinane z powierzchni komórki przez dynaminę;
- Otoczka wirusa ulega fuzji z błoną komórki gospodarza w przedziale późnych endosomów w czasie 10 - 15 min od momentu inokulacji;
- Warunkiem koniecznym do fuzji jest niskie pH w przedziale endosomalnym. W wyniku fuzji wirusowe RNA i białko C przedostają się do cytoplazmy, natomiast białko E zatopione w błonie pęcherzykowej ulega wolnemu recyklingowi na powierzchnię komórki;
- Do wytworzenia aktywnych cząstek wirusowych konieczna jest aktywność proteazy komórkowej o specyficzności podobnej do furyny, która najprawdopodobniej wstępnie aktywuje białko odpowiedzialne za fuzję (białko E);
- Traktowanie komórek bafilomycyną A1 (inhibitorem pompy protonowej) hamuje infekcję ZIKV na jej wczesnym etapie. W takich warunkach wiriony nie ulegają fuzji w późnych endosomach. Pęcherzyki zawierające wiriony przekształcają się w lizosomy, w których materiał zakaźny ulega proteolizie i inaktywacji. Pozostałości ulegają wolnemu recyklingowi na powierzchnię komórki;
- NH_4Cl indukuje szybki recykling ZIKV na powierzchnię komórek, przez co nie dochodzi do fuzji wirusa z błoną gospodarza. Tymczasowe wyciszenie Rab35 (białka markerowego dla szybko recyklingujących endosomów) pozwala zatrzymać wiriony pod powierzchnią komórek traktowanych NH_4Cl;
- NH_4Cl (w przeciwieństwie do bafilomycyny A1) hamuje również późne etapy infekcji. Zahamowanie może wynikać z zaburzenia składania albo transportu potomnych wirionów, a także pośrednio z inaktywacji furyny, która do swojej aktywacji w aparacie Golgiego potrzebuje pH ~6,0.

Wykaz publikacji

1. Milewska A, Kaminski K, Ciejka J, **Kosowicz K**, et al. HTCC: Broad Range Inhibitor of Coronavirus Entry. PLoS One. 2016;11(6):e0156552.
2. **Kosowicz K**, Pyrc K. A method for concentration and purification of human coronavirus HCoV-OC43 using CIM QA monolithic columns. Notka aplikacyjna BIA Separations. 2016.
3. Milewska A, Nowak P, **Owczarek K**, et al. Entry of human coronavirus NL63 to the cell. J Virol. 2017.
4. **Owczarek K**, Szczepanski A, Milewska A, et al. Early events during human coronavirus OC43 entry to the cell. Sci Rep. 2018;8(1):7124.
5. Szczepanski A, **Owczarek K**, Milewska A, et al. Canine respiratory coronavirus employs caveolin-1-mediated pathway for internalization to HRT-18G cells. Vet Res. 2018;49(1):55.
6. Szczepanski A, **Owczarek** K, Bzowska M, et al. Canine Respiratory Coronavirus, Bovine Coronavirus, and Human Coronavirus OC43: Receptors and Attachment Factors. Viruses. 2019;11(4).
7. **Owczarek K**, Chykunova Y, Jassoy C, Maksym B, Rajfur Z, Pyrc K. Zika virus: mapping and reprogramming the entry. Cell Commun Signal. 2019;17(1):41.

Bibliografia

1. Lehmann MJ, Sherer NM, Marks CB, Pypaert M, Mothes W. Actin- and myosin-driven movement of viruses along filopodia precedes their entry into cells. *J Cell Biol.* 2005;170(2):317-325.
2. White JM, Delos SE, Brecher M, Schornberg K. Structures and mechanisms of viral membrane fusion proteins: multiple variations on a common theme. *Crit Rev Biochem Mol Biol.* 2008;43(3):189-219.
3. Zaitseva E, Yang ST, Melikov K, Pourmal S, Chernomordik LV. Dengue virus ensures its fusion in late endosomes using compartment-specific lipids. *PLoS Pathog.* 2010;6(10):e1001131.
4. Harrison SC. Viral membrane fusion. *Nat Struct Mol Biol.* 2008;15(7):690-698.
5. Boucrot E, Ferreira AP, Almeida-Souza L, et al. Endophilin marks and controls a clathrin-independent endocytic pathway. *Nature.* 2015;517(7535):460-465.
6. Sabharanjak S, Sharma P, Parton RG, Mayor S. GPI-anchored proteins are delivered to recycling endosomes via a distinct cdc42-regulated, clathrin-independent pinocytic pathway. *Dev Cell.* 2002;2(4):411-423.
7. Lundmark R, Doherty GJ, Howes MT, et al. The GTPase-activating protein GRAF1 regulates the CLIC/GEEC endocytic pathway. *Curr Biol.* 2008;18(22):1802-1808.
8. Eyster CA, Higginson JD, Huebner R, et al. Discovery of new cargo proteins that enter cells through clathrin-independent endocytosis. *Traffic.* 2009;10(5):590-599.
9. Glebov OO, Bright NA, Nichols BJ. Flotillin-1 defines a clathrin-independent endocytic pathway in mammalian cells. *Nat Cell Biol.* 2006;8(1):46-54.
10. Swanson JA, Watts C. Macropinocytosis. *Trends Cell Biol.* 1995;5(11):424-428.
11. Overholtzer M, Mailleux AA, Mouneimne G, et al. A nonapoptotic cell death process, entosis, that occurs by cell-in-cell invasion. *Cell.* 2007;131(5):966-979.
12. van der Schaar HM, Rust MJ, Chen C, et al. Dissecting the cell entry pathway of dengue virus by single-particle tracking in living cells. *PLoS Pathog.* 2008;4(12):e1000244.
13. Cox RG, Mainou BA, Johnson M, et al. Human Metapneumovirus Is Capable of Entering Cells by Fusion with Endosomal Membranes. *PLoS Pathog.* 2015;11(12):e1005303.
14. Hussain KM, Leong KL, Ng MM, Chu JJ. The essential role of clathrin-mediated endocytosis in the infectious entry of human enterovirus 71. *J Biol Chem.* 2011;286(1):309-321.
15. Xu H, Hao X, Wang S, et al. Real-time Imaging of Rabies Virus Entry into Living Vero cells. *Sci Rep.* 2015;5:11753.
16. Henne WM, Boucrot E, Meinecke M, et al. FCHo proteins are nucleators of clathrin-mediated endocytosis. *Science.* 2010;328(5983):1281-1284.
17. Rappoport JZ, Kemal S, Benmerah A, Simon SM. Dynamics of clathrin and adaptor proteins during endocytosis. *Am J Physiol Cell Physiol.* 2006;291(5):C1072-1081.
18. Traub LM. Regarding the amazing choreography of clathrin coats. *PLoS Biol.* 2011;9(3):e1001037.
19. Takei K, Slepnev VI, Haucke V, De Camilli P. Functional partnership between amphiphysin and dynamin in clathrin-mediated endocytosis. *Nat Cell Biol.* 1999;1(1):33-39.
20. Phonphok Y, Rosenthal KS. Stabilization of clathrin coated vesicles by amantadine, tromantadine and other hydrophobic amines. *FEBS Lett.* 1991;281(1-2):188-190.
21. Vercauteren D, Vandenbroucke RE, Jones AT, et al. The use of inhibitors to study endocytic pathways of gene carriers: optimization and pitfalls. *Mol Ther.* 2010;18(3):561-569.
22. von Kleist L, Stahlschmidt W, Bulut H, et al. Role of the clathrin terminal domain in regulating coated pit dynamics revealed by small molecule inhibition. *Cell.* 2011;146(3):471-484.
23. Harper CB, Popoff MR, McCluskey A, Robinson PJ, Meunier FA. Targeting membrane trafficking in infection prophylaxis: dynamin inhibitors. *Trends Cell Biol.* 2013;23(2):90-101.
24. Xu Q, Cao M, Song H, et al. Caveolin-1-mediated Japanese encephalitis virus entry requires a two-step regulation of actin reorganization. *Future Microbiol.* 2016;11:1227-1248.

25. Norkin LC, Kuksin D. The caveolae-mediated sv40 entry pathway bypasses the golgi complex en route to the endoplasmic reticulum. *Virol J.* 2005;2:38.
26. Marjomäki V, Pietiäinen V, Matilainen H, et al. Internalization of echovirus 1 in caveolae. *J Virol.* 2002;76(4):1856-1865.
27. Nabi IR, Le PU. Caveolae/raft-dependent endocytosis. *J Cell Biol.* 2003;161(4):673-677.
28. Kiss AL, Botos E. Endocytosis via caveolae: alternative pathway with distinct cellular compartments to avoid lysosomal degradation? *J Cell Mol Med.* 2009;13(7):1228-1237.
29. Rothberg KG, Heuser JE, Donzell WC, Ying YS, Glenney JR, Anderson RG. Caveolin, a protein component of caveolae membrane coats. *Cell.* 1992;68(4):673-682.
30. Nonnenmacher M, Weber T. Adeno-associated virus 2 infection requires endocytosis through the CLIC/GEEC pathway. *Cell Host Microbe.* 2011;10(6):563-576.
31. Mayor S, Parton RG, Donaldson JG. Clathrin-independent pathways of endocytosis. *Cold Spring Harb Perspect Biol.* 2014;6(6).
32. Mercer J, Helenius A. Virus entry by macropinocytosis. *Nat Cell Biol.* 2009;11(5):510-520.
33. Krzyzaniak MA, Zumstein MT, Gerez JA, Picotti P, Helenius A. Host cell entry of respiratory syncytial virus involves macropinocytosis followed by proteolytic activation of the F protein. *PLoS Pathog.* 2013;9(4):e1003309.
34. Amstutz B, Gastaldelli M, Kälin S, et al. Subversion of CtBP1-controlled macropinocytosis by human adenovirus serotype 3. *EMBO J.* 2008;27(7):956-969.
35. Novick P, Brennwald P. Friends and family: the role of the Rab GTPases in vesicular traffic. *Cell.* 1993;75(4):597-601.
36. Jovic M, Sharma M, Rahajeng J, Caplan S. The early endosome: a busy sorting station for proteins at the crossroads. *Histol Histopathol.* 2010;25(1):99-112.
37. Huotari J, Helenius A. Endosome maturation. *EMBO J.* 2011;30(17):3481-3500.
38. Maxfield FR, McGraw TE. Endocytic recycling. *Nat Rev Mol Cell Biol.* 2004;5(2):121-132.
39. Maxfield FR, Yamashiro DJ. Endosome acidification and the pathways of receptor-mediated endocytosis. *Adv Exp Med Biol.* 1987;225:189-198.
40. Eskelinen EL. Roles of LAMP-1 and LAMP-2 in lysosome biogenesis and autophagy. *Mol Aspects Med.* 2006;27(5-6):495-502.
41. Ostrowski M, Carmo NB, Krumeich S, et al. Rab27a and Rab27b control different steps of the exosome secretion pathway. *Nat Cell Biol.* 2010;12(1):19-30; sup pp 11-13.
42. Bukong TN, Momen-Heravi F, Kodys K, Bala S, Szabo G. Exosomes from hepatitis C infected patients transmit HCV infection and contain replication competent viral RNA in complex with Ago2-miR122-HSP90. *PLoS Pathog.* 2014;10(10):e1004424.
43. Fraile-Ramos A, Cepeda V, Elstak E, van der Sluijs P. Rab27a is required for human cytomegalovirus assembly. *PLoS One.* 2010;5(12):e15318.
44. Gerber PP, Cabrini M, Jancic C, et al. Rab27a controls HIV-1 assembly by regulating plasma membrane levels of phosphatidylinositol 4,5-bisphosphate. *J Cell Biol.* 2015;209(3):435-452.
45. Lombardi D, Soldati T, Riederer MA, Goda Y, Zerial M, Pfeffer SR. Rab9 functions in transport between late endosomes and the trans Golgi network. *EMBO J.* 1993;12(2):677-682.
46. Lieu ZZ, Gleeson PA. Endosome-to-Golgi transport pathways in physiological processes. *Histol Histopathol.* 2011;26(3):395-408.
47. Ksiazek TG, Erdman D, Goldsmith CS, et al. A novel coronavirus associated with severe acute respiratory syndrome. *N Engl J Med.* 2003;348(20):1953-1966.
48. Du L, He Y, Zhou Y, Liu S, Zheng BJ, Jiang S. The spike protein of SARS-CoV--a target for vaccine and therapeutic development. *Nat Rev Microbiol.* 2009;7(3):226-236.
49. van der Hoek L, Pyrc K, Jebbink MF, et al. Identification of a new human coronavirus. *Nat Med.* 2004;10(4):368-373.
50. Woo PC, Lau SK, Chu CM, et al. Characterization and complete genome sequence of a novel coronavirus, coronavirus HKU1, from patients with pneumonia. *J Virol.* 2005;79(2):884-895.

51. Zaki AM, van Boheemen S, Bestebroer TM, Osterhaus AD, Fouchier RA. Isolation of a novel coronavirus from a man with pneumonia in Saudi Arabia. *N Engl J Med.* 2012;367(19):1814-1820.
52. Alsolamy S, Arabi YM. Infection with Middle East respiratory syndrome coronavirus. *Can J Respir Ther.* 2015;51(4):102.
53. Gaunt ER, Hardie A, Claas EC, Simmonds P, Templeton KE. Epidemiology and clinical presentations of the four human coronaviruses 229E, HKU1, NL63, and OC43 detected over 3 years using a novel multiplex real-time PCR method. *J Clin Microbiol.* 2010;48(8):2940-2947.
54. Vabret A, Mourez T, Gouarin S, Petitjean J, Freymuth F. An outbreak of coronavirus OC43 respiratory infection in Normandy, France. *Clin Infect Dis.* 2003;36(8):985-989.
55. Vijgen L, Keyaerts E, Moës E, et al. Complete genomic sequence of human coronavirus OC43: molecular clock analysis suggests a relatively recent zoonotic coronavirus transmission event. *J Virol.* 2005;79(3):1595-1604.
56. Desforges M, Desjardins J, Zhang C, Talbot PJ. The acetyl-esterase activity of the hemagglutinin-esterase protein of human coronavirus OC43 strongly enhances the production of infectious virus. *J Virol.* 2013;87(6):3097-3107.
57. Li F. Structure, Function, and Evolution of Coronavirus Spike Proteins. *Annu Rev Virol.* 2016;3(1):237-261.
58. Ruch TR, Machamer CE. The coronavirus E protein: assembly and beyond. *Viruses.* 2012;4(3):363-382.
59. Neuman BW, Kiss G, Kunding AH, et al. A structural analysis of M protein in coronavirus assembly and morphology. *J Struct Biol.* 2011;174(1):11-22.
60. Fehr AR, Perlman S. Coronaviruses: an overview of their replication and pathogenesis. *Methods Mol Biol.* 2015;1282:1-23.
61. Szczepanski A, Owczarek K, Bzowska M, et al. Canine Respiratory Coronavirus, Bovine Coronavirus, and Human Coronavirus OC43: Receptors and Attachment Factors. *Viruses.* 2019;11(4).
62. Sharma A, Lal SK. Zika Virus: Transmission, Detection, Control, and Prevention. *Front Microbiol.* 2017;8:110.
63. Duffy MR, Chen TH, Hancock WT, et al. Zika virus outbreak on Yap Island, Federated States of Micronesia. *N Engl J Med.* 2009;360(24):2536-2543.
64. Hayes EB. Zika virus outside Africa. *Emerg Infect Dis.* 2009;15(9):1347-1350.
65. Musso D, Nilles EJ, Cao-Lormeau VM. Rapid spread of emerging Zika virus in the Pacific area. *Clin Microbiol Infect.* 2014;20(10):O595-596.
66. Zanluca C, Melo VC, Mosimann AL, Santos GI, Santos CN, Luz K. First report of autochthonous transmission of Zika virus in Brazil. *Mem Inst Oswaldo Cruz.* 2015;110(4):569-572.
67. DICK GW, KITCHEN SF, HADDOW AJ. Zika virus. I. Isolations and serological specificity. *Trans R Soc Trop Med Hyg.* 1952;46(5):509-520.
68. Marini G, Guzzetta G, Rosà R, Merler S. First outbreak of Zika virus in the continental United States: a modelling analysis. *Euro Surveill.* 2017;22(37).
69. Petersen LR, Jamieson DJ, Honein MA. Zika Virus. *N Engl J Med.* 2016;375(3):294-295.
70. Parra B, Lizarazo J, Jiménez-Arango JA, et al. Guillain-Barré Syndrome Associated with Zika Virus Infection in Colombia. *N Engl J Med.* 2016;375(16):1513-1523.
71. Mlakar J, Korva M, Tul N, et al. Zika Virus Associated with Microcephaly. *N Engl J Med.* 2016;374(10):951-958.
72. Wongsurawat T, Jenjaroenpun P, Athipanyasilp N, et al. Genome Sequences of Zika Virus Strains Recovered from Amniotic Fluid, Placenta, and Fetal Brain of a Microcephaly Patient in Thailand, 2017. *Microbiol Resour Announc.* 2018;7(11).
73. Sirohi D, Kuhn RJ. Zika Virus Structure, Maturation, and Receptors. *J Infect Dis.* 2017;216(suppl_10):S935-S944.

Załączniki

SCIENTIFIC REPORTS

OPEN

Early events during human coronavirus OC43 entry to the cell

Katarzyna Owczarek[1,2], Artur Szczepanski[1,2], Aleksandra Milewska[1,2], Zbigniew Baster[3], Zenon Rajfur[3], Michal Sarna[2,4] & Krzysztof Pyrc[1,2]

Received: 8 December 2017
Accepted: 25 April 2018
Published online: 08 May 2018

The *Coronaviridae* family clusters a number of large RNA viruses, which share several structural and functional features. However, members of this family recognize different cellular receptors and exploit different entry routes, what affects their species specificity and virulence. The aim of this study was to determine how human coronavirus OC43 enters the susceptible cell. Using confocal microscopy and molecular biology tools we visualized early events during infection. We found that the virus employs caveolin-1 dependent endocytosis for the entry and the scission of virus-containing vesicles from the cell surface is dynamin-dependent. Furthermore, the vesicle internalization process requires actin cytoskeleton rearrangements. With our research we strove to broaden the understanding of the infection process, which in future may be beneficial for the development of a potential therapeutics.

There are currently six human coronaviruses described. The well-known human coronaviruses (HCoV) 229E and OC43 were described in 1960's and for almost 40 years were considered to be the only representatives of *Coronaviridae* infecting humans. Emergence of Severe Acute Respiratory Syndrome–associated coronavirus (SARS-CoV) in 2002, followed by identification of HCoV-NL63 and HCoV-HKU1 revealed that these viruses are far more common and clinically relevant than previously expected. Further, emergence of the Middle East respiratory syndrome coronavirus (MERS-CoV) in 2012 proved that these pathogens frequently cross the species border and may pose a significant healthcare risk.

HCoV-OC43 infection has been associated with respiratory tract illnesses of varying severity[1]. The virus is considered to be the most common human coronavirus worldwide, with highest incidence during winter and spring months[1,2]. Due to genomic sequence similarities between HCoV-OC43, bovine coronavirus (BCoV) and, to a lesser extent, canine respiratory coronavirus, which cause the disease in respective animals, it has been assumed that zoonotic transmission to humans occurred relatively recently. The most recent common ancestor of HCoV-OC43 and BCoV has been dated to the end of 19th century[3] and the evolutionary rate was estimated to be 4×10^{-4} nucleotide changes per site per year[3].

The coronavirus entry to the cell is a complex process, which requires a series of cellular factors. First, the virus binds to the attachment receptor. This interaction results in an increased cell surface density of virus particles and (or) facilitates interaction with the fusion receptor. To make an example, HCoV-OC43 and bovine coronavirus bind to N-acetyl-9-O-acetylneuraminic acid[4], HCoV-HKU1 binds to O-acetylated sialic acids[5], while HCoV-NL63 and SARS-CoV bind to heparan sulfate proteoglycans[6,7]. In some cases this step seems to be redundant[8], while in others depletion of the adhesion receptor results in lack of interaction between the virus and the cell and consequently severe decrease in virus infectivity[6,9,10]. Nonetheless, the presence of the adhesion factor is not sufficient to make the cell permissive. Coronaviruses utilize a broad variety of fusion receptors. Most of the alphacoronaviruses use aminopeptidase N (CD13) for cell entry, with the exception of HCoV-NL63, which similarly to SARS-CoV employs human angiotensin-converting enzyme 2[11]. HCoV-OC43 was reported to utilize HLA class I molecule or sialic acids[12,13], MERS-CoV - dipeptidyl peptidase 4 (DPP4 or CD26)[14], whereas the receptor for HCoV-HKU1 remains unknown[5]. Recognition of different receptors implies not only different cellular tropism, but also different internalization routes. It is worth to mention, however, that recent reports also stress the importance of other cellular factors for virus tissue specificity, including tissue-specific proteases[15–18].

[1]Microbiology Department, Faculty of Biochemistry, Biophysics and Biotechnology, Jagiellonian University, Gronostajowa 7, 30-387, Krakow, Poland. [2]Virogenetics Laboratory of Virology, Malopolska Centre of Biotechnology, Jagiellonian University, Gronostajowa 7a, 30-387, Krakow, Poland. [3]Institute of Physics, Faculty of Physics, Astronomy and Applied Computer Sciences, Jagiellonian University, Lojasiewicza 11, 30-348, Krakow, Poland. [4]Department of Biophysics, Faculty of Biochemistry, Biophysics and Biotechnology, Jagiellonian University, Gronostajowa 7, 30-387, Krakow, Poland. Correspondence and requests for materials should be addressed to K.P. (email: k.a.pyrc@uj.edu.pl)

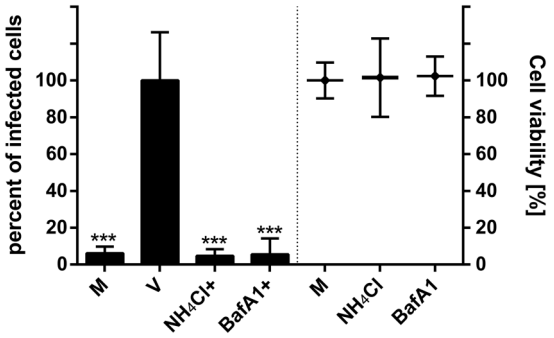

Figure 1. Inhibition of endosomal acidification with NH_4Cl or bafilomycin A1 inhibits HCoV-OC43 infection in HCT-8 cell line. The infection efficiency determined with flow cytometry is expressed as the percentage of HCoV-OC43 infected cells, compared to the untreated control, and is presented on the left side of the graph. Right part of the graph shows the cell viability, as determined with an XTT assay. *NH_4Cl* −50 mM NH_4Cl; *BafA1* −2.5 nM bafilomycin A1; *control* – PBS; *M* – mock infected cells; *V* or + − HCoV-OC43 infected cells. The data is presented as the mean of a triplicate for each sample ± SD. To determine the significance of differences between compared groups, Single-Factor Analysis of Variance (ANOVA) was applied. ***P values < 0.05 were considered significant.

The interaction with the receptor is only the beginning. The binding may induce fusion with cellular membranes, but in most of the cases this event is preceded by virus internalization *via* the endocytic route. The most common, and the best described route is clathrin-dependent endocytosis. This path is used by representatives of wide range of viral families (e.g., human enterovirus 71[19], human metapneumovirus[20], rabies virus[21] and others). Upon receptor recognition, a viral particle is docked into a clathrin-coated pit. Its' formation is initialized by concerted action of a protein complex that consists of FCHo1/2, Eps15 and intersectin-1. FCHo1/2 induces curvature of the plasma membrane and through Eps15 recruits Adaptor Protein 2 (AP2) to the nucleation site[22]. AP2 assembles clathrin units and once their concentration reaches a critical level, they polymerize to form a lattice on the membrane[23]. The structure deepens, stabilized by the cargo[24]. Budding of the vesicle is accompanied by a tubular neck formation, to which amphiphysin protein is attracted. It recruits dynamin, which polymerizes in a GTP dependent mode to finally cut off the cargo-containing vesicle from the cell surface[25,26].

Another well-described path is caveolin-1 mediated endocytosis. Caveolae are flask-shaped cholesterol- and sphingolipid-rich smooth membrane invaginations stabilized with caveolin-1[27]. Loading of the caveolae with cargo results in recruitment of dynamin-2[28], which cuts off the invagination, forming a neutral-pH vesicle called caveosome. The vesicle can be either transferred into Golgi complex, endoplasmic reticulum (ER) or progress to early endosomes[27]. Recently, besides these two canonical pathways, numerous alternative routes have been described, including entosis, flotillin-dependent entry, FEME, and IL2Rβ-like mechanisms.

The aim of this study was to map the entry of HCoV-OC43 to susceptible cell. At first, we confirmed that the virus binds to the cells and is internalized *via* endocytosis. Subsequently, we have shown that HCoV-OC43 particle after binding to the cell surface migrates to caveolae and is trafficked to endosomes by caveolin-mediated and dynamin-dependent route. Virus internalization requires unwinding of the actin cortex, yet actin filaments are not required for the entry.

Results

HCoV-OC43 enters HCT-8 the cell via endosomes. First, we determined whether the virus requires endocytosis, or the virus-cell fusion may occur on the cell surface. HCT-8 cells were pre-incubated with NH_4Cl and subsequently incubated with the virus in the presence of NH_4Cl, which prevents acidification of endosomes during maturation. Afterwards, media was refreshed to remove unbound virus particles. Infection was carried on for 3 days and its course was monitored with flow cytometry. As shown in Fig. 1, addition of NH_4Cl early during the infection resulted in reduction of the number of virus-positive cells. Similarly, another inhibitor of endocytic compartment acidification, vacuolar-type ATPase inhibitor, bafilomycin A1, limited the number of infected cells (Fig. 1).

In order to confirm our observation, we evaluated co-localization of virus particles with early endosome marker EEA1. HCT-8 cells were overlaid with HCoV-OC43 and incubated at 4 °C to synchronize entry of viral particles. Next, cultures were warmed up to 32 °C to enable intracellular transport and virus internalization. Subsequently, cultures were fixed, permeabilized and stained with specific antibodies to visualize viral proteins and EEA1 5-20 min post-inoculation (p.i). virus particles co-localized with EEA1, but remained in a close proximity to the cellular membrane (Fig. 2A,B). After that time virions started to gradually accumulate in larger, less abundant clusters (Fig. 2C–F) to eventually enter the cell.

HCoV-OC43 particles migrate to the caveolin-1-rich invaginations. To determine which endocytic route is employed, co-localization of virions with markers of different pathways was tested. Clearly, 5–90 min p.i. the virus co-localized with caveolin-1 (Fig. 3A–D). Prolonged co-localization is consistent with the reported

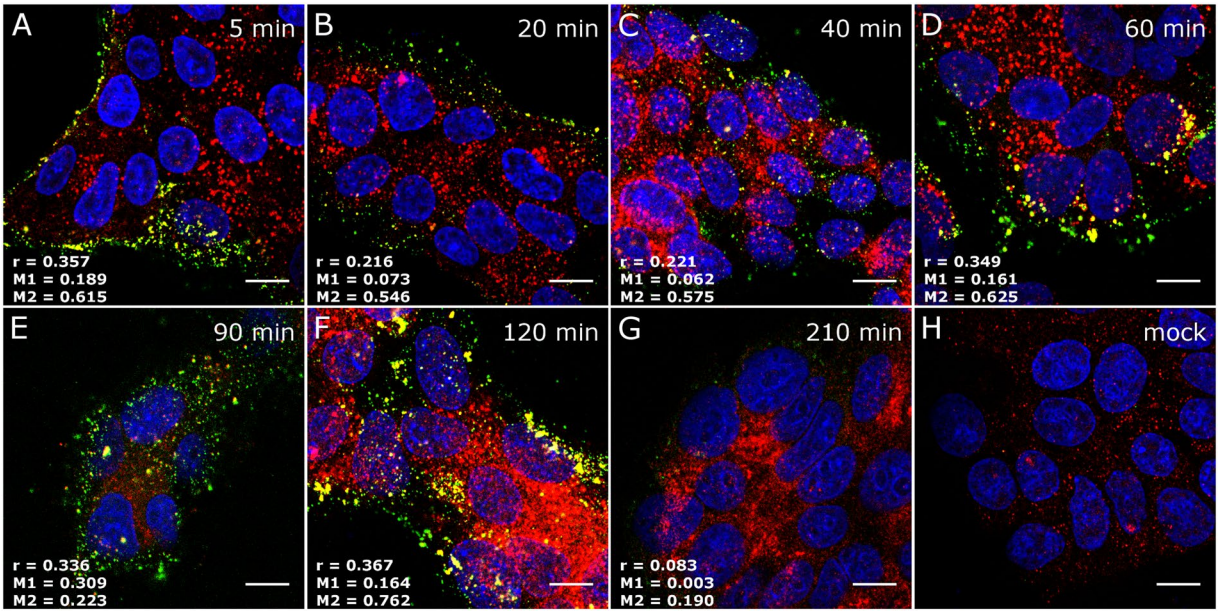

Figure 2. Co-localization of HCoV-OC43 with early endosomes' marker EEA1. Co-localization of EEA1 with HCoV-OC43 in HCT-8 cells at different time points post infection was studied with confocal microscopy. Respective time points are indicated in the upper right corners. (**A**) HCoV-OC43-infected cells fixed 5 min p.i.; (**B**) 20 min p.i.; (**C**) 40 min p.i.; (**D**) 60 min p.i.; (**E**) 90 min p.i.; (**F**) 120 min p.i.; (**G**) 210 min p.i.; (**H**) mock-infected cells, stained with isotype control antibodies. The virus is visualized in green, EEA1 is shown in red, and nuclei are presented in blue. Scale bar = 10 μm. Co-localization parameters: r – Pearson's coefficient; M1 - Manders' coefficient M1 (EEA1 overlapping with the virus); M2 - Manders' coefficient M2 (the virus overlapping with EEA1). The experiment was conducted at least thrice and representative images are presented.

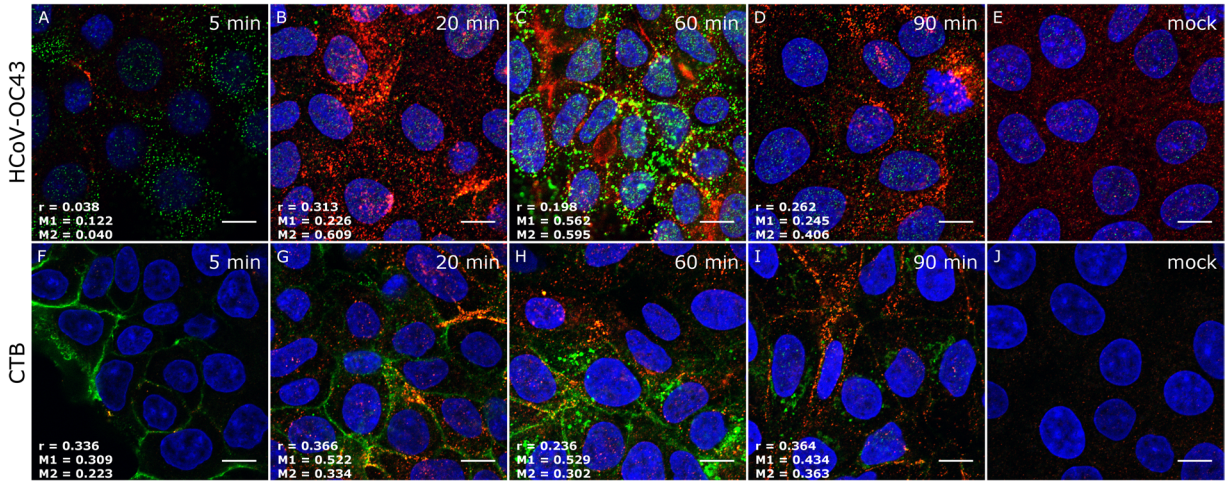

Figure 3. Co-localization of HCoV-OC43 with caveolin-1. Entry of HCoV-OC43 or cholera toxin B (CTB) was studied with confocal microscopy. Respective time points are indicated in the upper right corners. (**A**) HCoV-OC43-infected cells fixed 5 min p.i.; (**B**) 20 min p.i.; (**C**) 60 min p.i.; (**D**) 90 min p.i.; (**E**) mock-infected control cells; (**F**) CTB-overlaid cells fixed 5 min post-inoculation; (**G**) 20 min post-inoculation; (**H**) 60 min post-inoculation; (**I**) 90 min post-inoculation; (**J**) not-overlaid control cells. The virus and CTB are visualized in green, caveolin-1 is shown in red, and nuclei are presented in blue. Scale bar = 10 μm. Co-localization parameters: r – Pearson's coefficient; M1 - Manders' coefficient M1 (caveolin-1 overlapping with the virus); M2 - Manders' coefficient M2 (the virus overlapping with caveolin-1). The experiment was conducted at least thrice, and representative images are presented.

kinetics of caveolae transport[29,30]. No co-localization with clathrin was noted (Supplementary Fig. 2). In order to validate this observation, cholera toxin B (CTB) conjugated with fluorescein isothiocyanate (FITC) was used as a positive control for caveolin-1 dependent entry[31,32] (Fig. 3F–I).

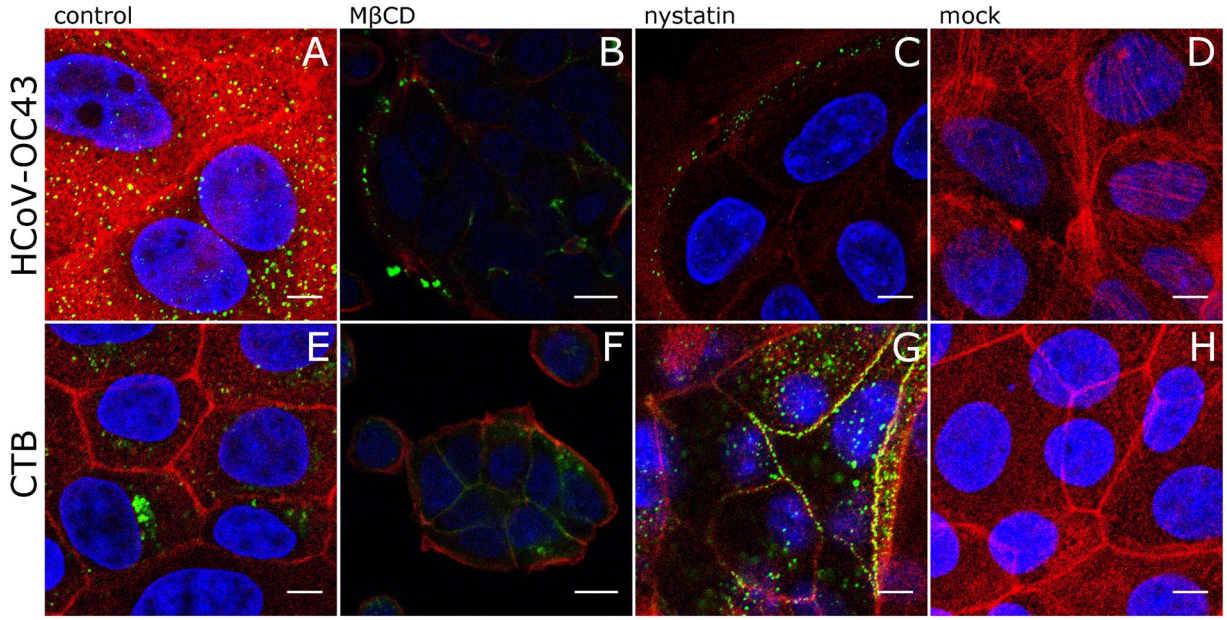

Figure 4. Disruption of caveolae with MβCD and nystatin hampers HCoV-OC43 entry. Confocal analysis of HCoV-OC43 or cholera toxin (CTB) entry to HCT-8 cells in the presence of cholesterol-sequestring agents was conducted. Following 1 h pretreatment with nystatin (100 μg/ml) or MβCD (100 μM), the cells were infected with HCoV-OC43 or overlaid with FITC-conjugated CTB (green). Actin cytoskeleton was stained to show the cell boundaries (red). Nuclei are shown in blue. (**A**) HCoV-OC43-infected inhibitor-untreated cells; (**B**) HCoV-OC43-infected MβCD-treated cells; (**C**) HCoV-OC43-infected nystatin-treated cells; (**D**) mock infected, inhibitor-untreated cells; (**E**) CTB inoculated, inhibitor-untreated cells; (**F**) CTB inoculated, MβCD-treated cells; (**G**) CTB inoculated, nystatin-treated cells; (**H**) mock inoculated, inhibitor-untreated cells. *mock* – mock inoculated cells; *control* – HCoV-OC43/CTB inoculated cells, in the absence of inhibitors. Scale bar = 10 μm. The experiment was conducted at least thrice and representative images are presented.

Disruption of caveolae hampers HCoV-OC43 entry. In order to ensure that HCoV-OC43 enters the cell using caveolae, specific inhibitors of this endosomal pathway were used. Caveolae are formed in membrane clusters, where caveolin-1 is accompanied by cholesterol and sphingolipids. Consequently, the caveolin-mediated entry is sensitive to cholesterol-binding or depleting agents such as nystatin or methyl-β-cyclodextrin (MβCD). HCT-8 cells were pre-incubated with the compounds and overlaid with the virus. Following the incubation, cells were fixed, permeabilized and immunostained for HCoV-OC43 and actin, and virus entry was evaluated using confocal microscopy. As shown in Fig. 4, incubation with MβCD and nystatin (Fig. 4B,C) resulted in significant retention of virus on the cell surface, further proving that caveolae are required for virus internalization. Cholera toxin was used as a reference (Fig. 4F,G), as it was previously reported to enter the cell *via* caveosomes[31,32]. The MβCD-mediated inhibition of HCoV-OC43 entry (Fig. 4B) was more effective than CTB (Fig. 4F). To ensure that the observed effect is specific, we silenced expression of caveolin-1 in HCT-8 cells using siRNAs delivered in two consecutive transfections. Scrambled siRNAs were used as controls. Twenty-four hours after the second transfection, cells were incubated with HCoV-OC43 for 1 h. Subsequently, cells were fixed, permeabilized and immunostained to visualize the virus. In the cells transfected with caveolin-1 specific siRNAs protein levels were reduced by almost 80%, as assessed by Western blot, while scrambled siRNAs didn't influence the protein level. β-tubulin was used as a reference household gene (Fig. 5A; the original image of the membrane is provided in Supplementary Fig. 1). Virus internalization to cells depleted of caveolin-1 was evaluated by confocal microscopy. As shown in Fig. 5, viral particles were retained on the cell surface in cells depleted of caveolin-1 (Fig. 5C), while no such effect was observed in control cells (Fig. 5B,D,E).

Caveolae are required for HCoV-OC43 infection. To test whether caveolin-mediated endocytosis is the major route of entry, cells were pre-incubated with MβCD or nystatin for 1 h and subsequently infected in the presence of inhibitors for 3 h. Subsequently, medium was discarded to remove unbound virus particles and fresh medium was applied. Infection was carried on for 3 days and its course was monitored with flow cytometry. Obtained results clearly show that MβCD and nystatin (Fig. 6) significantly affected virus infection in HCT-8 cells. In order to ensure that the observed effect does not result from cytotoxicity of inhibitors, cell viability was tested with XTT assay (Fig. 6).

HCoV-OC43 entry is dynamin-dependent. To determine whether HCoV-OC43 entry process is dynamin-mediated, two different dynamin inhibitors were used: MiTMAB, which interacts with the lipid binding (PH) domain of dynamin and dynasore that non-competitively inhibits GTPase activity of dynamin[33]. Obtained results show that dynamin activity is required for effective HCoV-OC43 entry to the target cell (Fig. 7).

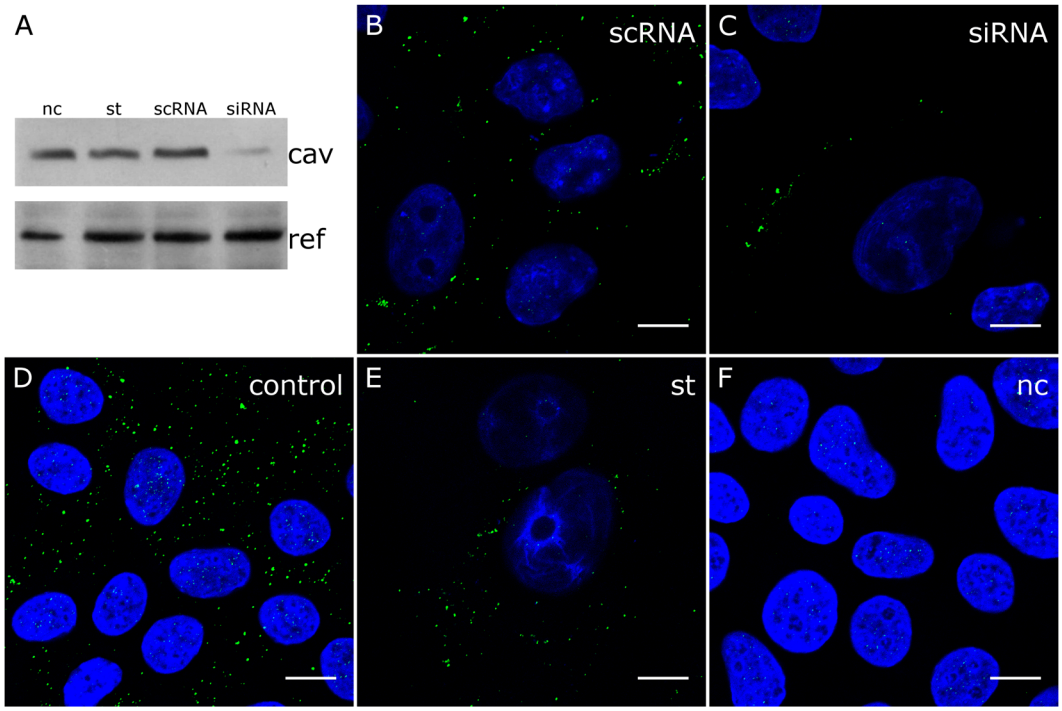

Figure 5. Inhibition of HCoV-OC43 entry to the caveolin-1 depleted cells. (**A**) Western blot analysis of the efficiency of siRNA-dependent caveolin-1 silencing (caveolin-1 expression in HCT-8 cells compared to β-tubulin expression in these cells). Confocal analysis of HCoV-OC43 localization 1 h p.i. in HCT-8 cells. *scRNA* (**B**) HCoV-OC43-infected, scrambled siRNA transfected cells; *siRNA* (**C**) HCoV-OC43-infected, caveolin-1-specific siRNA transfected cells; *control* (**D**) HCoV-OC43-infected, non-transfected cells; *st* (**E**) HCoV-OC43-infected, sham-transfected cells; *nc* (**F**) mock-infected, non-transfected cells. HCoV-OC43 is visualized in green and nuclei are shown in blue. Scale bar = 10 μm. The experiment was conducted at least twice, and representative images are presented.

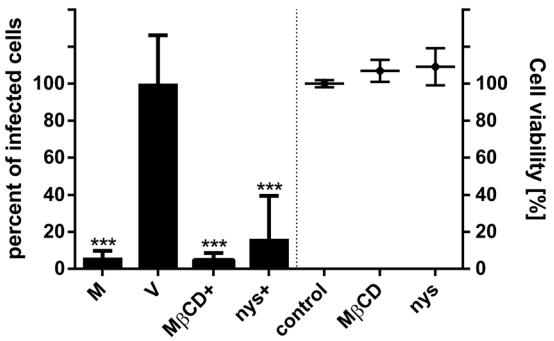

Figure 6. Inhibition of HCoV-OC43 infection in HCT-8 cells by MβCD and nystatin. HCT-8 cells pre-treated with cholesterol-sequestering agents were infected with HCoV-OC43 and analysed by flow cytometry 3 days p.i. The infection efficiency determined with flow cytometry is expressed as the percentage of HCoV-OC43 infected cells, compared to the untreated control, and is presented on the left side of the graph. Right part of the graph shows the cell viability, as determined with an XTT assay. *MβCD* −5 mM MβCD treated cells; *nys* −10 μg/ml nystatin treated cells; *control* − PBS treated cells; *M* – mock infected cells; *V* or + − HCoV-OC43 infected cells. The data is presented as the mean of a triplicate for each sample ± SD. To determine the significance of differences between compared groups, Single-Factor Analysis of Variance (ANOVA) was applied. ***P values < 0.05 were considered significant.

HCoV-OC43 requires actin for successful entry. In order to study the role of cytoskeleton during virus entry, we used two compounds known to affect actin cytoskeleton. Briefly, HCT-8 cells were pre-treated with jasplakinolide or cytochalasin D, inoculated with HCoV-OC43 or dextran and further incubated in conditions allowing for intracellular transport (32 °C). Subsequently, cultures were fixed, permeabilized and stained with specific antibodies to visualize virus particles and actin cytoskeleton. Confocal imaging revealed that stabilization of actin cortex by jasplakinolide results in inhibition of HCoV-OC43 virus entry and dextran internalization

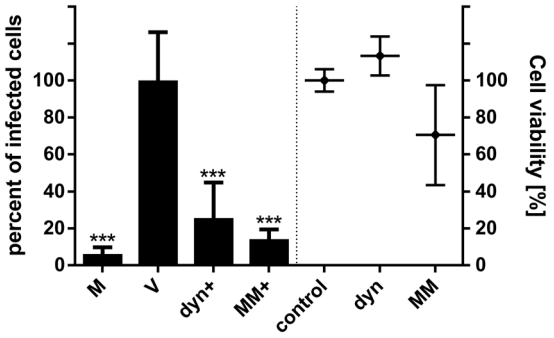

Figure 7. Inhibition of dynamin blocks HCoV-OC43 infection. HCT-8 cells were pre-treated with dynamin inhibitors, infected with HCoV-OC43 and analysed by means of flow cytometry 3 days p.i. The infection efficiency determined with flow cytometry is expressed as the percentage of HCoV-OC43 infected cells, compared to the untreated control, and is presented on the left side of the graph. Right part of the graph shows the cell viability, as determined with an XTT assay. *dyn* −40 μM dynasore; *MM* −10 μM MiTMAB; *control* – PBS treated cells; *M* −mock infected cells; *V* or + − HCoV-OC43 infected cells. The data is presented as the mean of a triplicate for each sample ± SD. To determine the significance of differences between compared groups, Single-Factor Analysis of Variance (ANOVA) was applied. ***P values < 0.05 were considered significant.

(Fig. 8C,G). This may suggest that actin is important for vesicle formation, and the virus enters the cell by macropinocytosis. However, analysis of cells pre-treated with cytochalasin D revealed that depolymerization of actin filaments did not inhibit virus entry, but drastically modulated virus localization (Fig. 8B). Virus particle localized to non-structured actin deposits in the cell's cytoplasm. On the other hand, dextran internalization was hampered (Fig. 8F). Both inhibitors drastically limited virus infection rate, as shown by flow cytometry (Fig. 9). No inhibition of virus entry or infection was observed for wortmannin, PI3K inhibitor known to hamper macropinocytosis (Supplementary Fig. 3).

Re-directing HCoV-OC43 entry. Considering that micropinocytosis may be PI3K independent[34], we made an effort to ensure that the virus does not use this pathway for entry. Briefly, we used dextran (70 kDa) as a cargo reported to enter the cell by micropinocytosis and we tested its co-localization with HCoV-OC43 virions during the virus entry[35]. As shown in Supplementary Fig. 4, strong co-localization of HCoV-OC43 with dextran was observed 5–210 min p.i. At the same time we observed vast decrease in HCoV-OC43 co-localization with EEA1 (early endosome's marker), what suggested that in the presence of dextran the virus is internalized by a different pathway. This triggered another question, whether the dextran-induced micropinocytosis may initiate productive infection. To address this question, cells were infected with HCoV-OC43 in the presence of dextran and nystatin or MiTMAB or NH_4Cl. Infection was carried on for 3 days and its course was monitored with flow cytometry. Obtained results (Fig. 10) clearly show that although the virus effectively enters the cell by macropinocytosis, it is not able to reach the replication site and to start productive infection. Inhibition of caveolin-dependent endocytosis in the presence of dextran did not block virus nor dextran internalization, but it blocked virus replication.

Discussion

HCoV-OC43 remains incessantly one of the most important etiological factors for respiratory tract diseases in humans[1,2,36]. Considering lack of effective vaccine or therapeutics, and zoonotic potential of animal coronaviruses, understanding of the virus' biology seems to be of importance.

The mode of entry remains unknown for a number of betacoronaviruses. One of the HCoV-OC43's cousins, mouse hepatitis virus type 2 (MHV-2), undergoes clathrin-mediated endocytosis independent of Eps15[37], while for SARS-CoV various pathways have been reported[38–40]. The internalization routes for the other three human betacoronaviruses, HCoV-OC43, HCoV-HKU1 and MERS-CoV, have not been described thus far. In this work we delineated early steps of HCoV-OC43 infection in human cells.

First, we aimed to map the events subsequent to virus-receptor interaction. For that we checked whether the virus is able to fuse with cellular membrane on the cell surface or it requires prior internalization. It is generally believed that during internalization additional stimuli is provided due to acidification of the microenvironment and in some cases pH-dependent activation of proteases. Consequently, viruses sensitive to inhibitors preventing pH decrease are believed to require endocytosis for entry. We showed that bafilomycin A1 and ammonium chloride strongly inhibit virus replication (Fig. 1). One may, however, question whether during prolonged incubation only virus entry is affected. To ensure validity of our observation, subcellular localization of viruses entering the cell was tested and its co-localization with endosomal markers was verified. Obtained results confirmed that virions entering the cell co-localize with EEA1 molecule (Fig. 2), which is an established marker of early endosomes.

Knowing that HCoV-OC43 enters the cell by endocytic route, we made an effort to delineate the mechanism of this process. For that, we tested whether virus co-localizes with common endocytic markers. Performed research revealed that interaction between the virus and the cell triggers recruitment of caveolin-1 and subsequent caveolae assembly (Fig. 3). Assembly of these structures depends on membrane content and flexibility, and we investigated the influence of compounds modifying cholesterol content/availability on HCoV-OC43 entry.

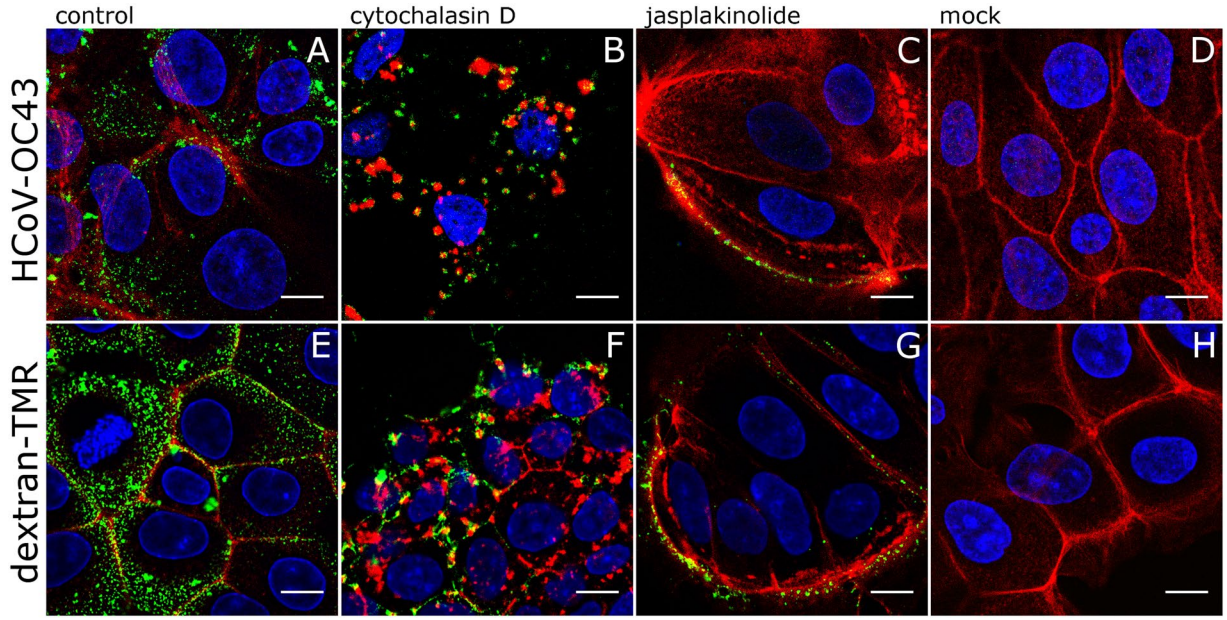

Figure 8. Inhibition of HCoV-OC43 infection in HCT-8 cells by compounds interfering with the actin cytoskeleton. HCoV-OC43 or dextran entry to the cell was studied using confocal microscopy. Following 1 h incubation of cells with inhibitors, cells were inoculated with HCoV-OC43 (**A**–**C**) or fluorescently labelled dextran (**E**–**G**) and incubated for 1 h. HCoV-OC43 and dextran are shown in green, actin cytoskeleton is presented in red. Nuclei are shown in blue. control HCoV-OC43/dextran-TMR inoculated inhibitor-untreated cells; *cytD* (**B,F**) HCoV-OC43/dextran-TMR inoculated, 2 μM cytochalazine D-treated cells; *jasp* (**C,G**) HCoV-OC43/dextran-TMR inoculated, 150 nM jasplakinolide-treated cells; *mock* (**D,H**) mock-inoculated inhibitor-untreated cells. Scale bar = 10 μm. The experiment was conducted at least thrice, and representative images are presented.

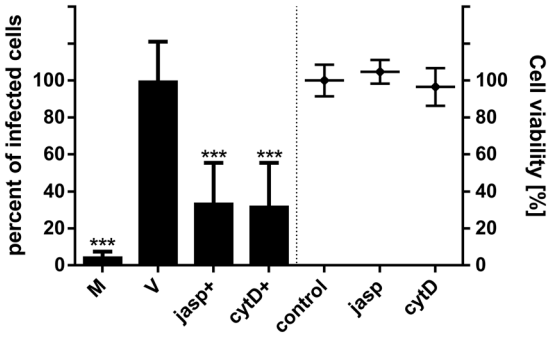

Figure 9. Inhibition of HCoV-OC43 infection of HCT-8 cells by agents interfering with the actin cytoskeleton. HCT-8 cells were pre-treated with actin inhibitors, infected with HCoV-OC43 and analysed by means of flow cytometry 3 days p.i. The infection efficiency determined with flow cytometry is expressed as the percentage of HCoV-OC43 infected cells, compared to the untreated control, and is presented on the left side of the graph. Right part of the graph shows the cell viability, as determined with an XTT assay. *jasp* −150 nM jasplakinolide; *cytD* −2 μM cytochalazine D; *control* – DMSO; *M* – mock infected cells; *V* or + − HCoV-OC43 infected cells. The data is presented as the mean of a triplicate for each sample ± SD. To determine the significance of differences between compared groups, Single-Factor Analysis of Variance (ANOVA) was applied. ***P values < 0.05 were considered significant.

Consistently, nystatin or MβCD pretreatment caused retention of the virus on the cell surface (Fig. 4). Both inhibitors blocked HCoV-OC43 infection, proving the relevance of this pathway for virus replication (Fig. 6). It is, however, known that chemical inhibitors may show non-specific effects[41–43]. In order to ensure that observed effect is not an artifact, caveolin-1 was depleted in HCT-8 cells using RNAi technology (Fig. 5). All experiments consistently showed that HCoV-OC43 entry is caveolin-1 dependent.

The vesicle and its cargo were tracked during trafficking to the replication site. First, we have shown that newly formed caveolae carrying HCoV-OC43 virions are cut off the cell surface membrane by dynamin (Fig. 7).

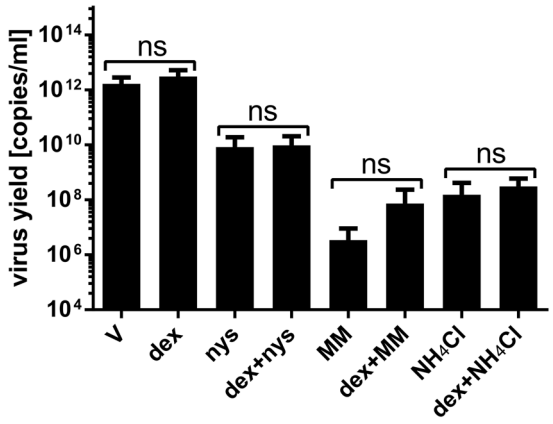

Figure 10. Macropinocytosis – stimulating agents re-direct virus trafficking in the cell. HCT-8 cells pre-treated with caveolin-1 and dynamin inhibitors were infected with HCoV-OC43 in presence or absence of dextran and viral yield was assessed by RT-qPCR 5 days p.i. *nys* −10 μg/ml nystatin; *MM* −10 μM MiTMAB; *NH_4Cl* −50 mM NH_4Cl; *V* – non-treated HCoV-OC43 infected cells; *dex* – dextran-TMR. The data is presented as the mean of a triplicate for each sample ± SD. To determine the significance of differences between compared groups, Single-Factor Analysis of Variance (ANOVA) was applied. ***P values < 0.05 were considered significant; ns – not significant.

Dynamin, a ring-like shaped GTPase driving vesicle scission, has been extensively studied in the context of clathrin-dependent endocytosis[44–46], but it was also demonstrated to participate in caveolae trimming[47,48].

Next, the role of cytoskeleton in virus transport was studied. Interestingly, modification of the actin dynamics affected virus entry, but actin was not essential for virus internalization. Disruption of the actin filaments did not result in inhibition of virus entry, but virions co-localized in the cytoplasm with unstructured actin deposits, suggesting interaction between virus-carrying vesicles and actin filaments (Fig. 8B). On the other hand, stabilization of actin cytoskeleton resulted in retention of virions on cell surface, but we believe that it may be linked with the physical barrier formed by stabilized actin cortex (Fig. 8C). Obtained results are consistent with literature data[49,50].

Further, we have tested the co-localization of HCoV-OC43 with dextrans, which were previously reported to enter the cell by macropinocytosis[35]. To our surprise we recorded co-localization of these two cargoes (Supplementary Fig. 4). Subsequent examination revealed that in the presence of dextrans, which are also known inducers of macropinocytosis, the virus is switching the internalization route to macropinocytosis (Supplementary Fig. 4). It seems, however, that virus internalization by this route does not allow for effective entry and replication (Fig. 10). One may hypothesize that during micropinocytosis the pH in the vesicle is not decreased and the virus – cell fusion does not occur. In such a scenario, viruses are recycled to the cell surface or degraded intracellularly. Interestingly, it was shown for MHV and SARS-CoV that endocytosis may play a role in cell-to-cell spread and micropinocytosis[51], but one may assume that it may differ between these species.

Our study on the early steps of HCoV-OC43 replication cycle was performed in HCT-8 cell line, which constitutes a conventional and accepted model for research on this coronavirus[52,53]. One may, however, question whether more natural system as human airway epithelium (HAE) culture wouldn't be more appropriate. Unfortunately, the HAE culture does not support replication of the strain replicating *in vitro* and therefore it was not possible to compare these two models. This is a direct consequence of cell culture adaptation, as recently reported for laboratory strains of HCoV-OC43, HCoV-229E and HCoV-HKU1[54]. It was suggested that the presence of TMPRSS2 protease on the cell surface modifies the entry route allowing it to bypass the classical endocytic entry[55]. Similar conclusions were also drawn by others[56–58], but we recently provided an alternative explanation for HCoV-NL63 virus[59].

In conclusion, our results allow for understanding of the first steps of HCoV-OC43 infection. We have shown that following interaction with a receptor protein on the cell surface the virus enters the cell *via* caveolae and is transported along actin cytoskeleton. Interestingly, we have shown that even though there are alternative entry pathways for the virus, such event does not lead to the productive infection.

Materials and Methods

Cells and virus. HCT-8 cells (ATCC: CCL-244 Human ileocecal colorectal adenocarcinoma) were cultured in Dulbecco-modified Eagle's medium (DMEM, Thermo Scientific) supplemented with 3% fetal bovine serum (FBS, Thermo Scientific), 100 U/ml penicillin, and 100 μg/ml streptomycin and 5 μg/ml ciprofloxacin. Cells were maintained in a 5% CO_2 incubator at 37 °C.

HCoV-OC43 (ATCC: VR-1558) was propagated in HCT-8 cells in DMEM supplemented with 2% FBS, 100 U/ml penicillin, and 100 μg/ml streptomycin. Cells were lysed 5 days after infection by 2 freeze & thaw cycles and virus was titrated according to the Reed & Muench formula[60]. As a control, mock-infected HCT-8 cells were used. Virus and mock aliquots were stored at −80 °C.

Inhibitors. Methyl-β-cyclodextrin (MβCD), nystatin (nys), bafilomycin A1 (bafA), cytochalasin D (cytD) and wortmannin (wort) were purchased from Sigma Aldrich. Dynasore (dyn) and MiTMAB (MM) were purchased from Abcam, jasplakinolide (jasp) from Merck, NH_4Cl from Bioshop. All stock solutions were prepared either in DMSO (jasp) or PBS (MβCD, nys, BafA1, cytD, wort, dyn, MM and NH_4Cl) and stored at 4 °C or −20 °C, according to the manufacturer's recommendations.

Virus titration. The titration assay was performed as described previously by Reed and Muench[60]. Briefly, confluent HCT-8 cells were cultured in 96-well plates. Serial five-fold dilutions of virus stock were prepared in DMEM supplemented with 2% FBS, 100 U/ml penicillin, and 100 μg/ml streptomycin, and 100 μl of the diluted virus was added into each well. The cells were incubated at 32 °C under 5% CO_2 for 5 days and the cytopathic effect occurrence was scored using an inverted microscope. The number of wells with obvious cytopathic effect was counted and the $TCID_{50}$ values were calculated according to the Reed–Muench formula.

Co-localization assay. HCT-8 cells were seeded in the complete medium onto glass slides in 6-well plates. After 2 days cell culture medium was replaced with serum-free DMEM supplemented with 100 U/ml penicillin and 100 μg/ml streptomycin two hours prior to the experiment. Next, cells in each well were treated with 100 μl of HCoV-OC43 stock (or mock) and incubated for 1 h at 4 °C to synchronize viral particles entry from the cell surface. CTB conjugated to FITC (Sigma), diluted to the final concentration 40 μg/ml in DMEM supplemented with 2% FBS, 100 U/ml penicillin, and 100 μg/ml streptomycin, was used as a positive control for caveolin-dependent entry pathway.

Subsequently, cultures were transferred to 32 °C. At indicated in each experiment p.i. times, the cells were washed twice with PBS, fixed in cold 4% paraformaldehyde for at least 20 min at room temperature and immunostained for HCoV-OC43, caveolin-1 or EEA1.

Immunofluorescence assay. The fixed cells were washed twice with PBS and permeabilized with 0.5% Triton X-100 for 13 min at room temperature. Afterwards, samples were blocked overnight at 4 °C in 5% bovine serum albumin (BSA) in PBS and incubated for 2 h at room temperature with primary anti-HCoV-OC43 antibodies (MAB9012, Merck) diluted 1:1000 in 3% BSA in PBS. Subsequently, samples were incubated for 1 h with Alexa Fluor 488 labeled goat anti-mouse IgG (Thermo Fisher Scientific) diluted 1:400 in 3% BSA in PBS. To visualize host cell proteins, the cells were blocked again overnight at 4 °C with 10% FBS in PBS, incubated for 2 h at room temperature with primary antibodies (Caveolin-1 N-20 Antibody, sc-894, Santa Cruz Biotechnology; Clathrin HC Antibody (C-20), sc-6579, Santa Cruz Biotechnology; EEA1 H-300 Antibody, sc-33585, Santa Cruz Biotechnology) diluted 1:100 in 2.5% FBS in PBS, and finally with Atto 633 labeled goat anti-rabbit IgG (Thermo Fisher Scientific) or Alexa Fluor 546 goat anti-rabbit (Thermo Fisher Scientific) diluted 1:200 in 2.5% FBS in PBS.

In experiments showing localization of virions in the cell actin cytoskeleton was visualized. Briefly, after HCoV-OC43 labelling, cells were stained with Atto 633-phalloidin (Thermo Fisher Scientific) diluted 1:50 in PBS for 1 h at room temperature. Nuclei were stained with DAPI (Thermo Fisher Scientific) diluted 1:10 000 in PBS.

After immunostaining in all the cases cells were washed with 0.5% TWEEN-20 in PBS. Finally, stained cultures were mounted on glass slides in ProLong Diamond antifade medium (Thermo Fisher Scientific) and stored at 4 °C.

Visualization of HCoV-OC43 entry inhibition. Cells were seeded on glass slides in 6-well plates and cultured at 37 °C for 48 h. After that time media were removed and cells were incubated in DMEM with 2% FBS, 100 U/ml penicillin and 100 μg/ml streptomycin supplemented with endocytosis inhibitors at 37 °C for 1 h. Subsequently, media were removed and HCoV-OC43 stock was overlaid on the cells in the presence or absence of inhibitors and cultures were incubated at 32 °C for 1 h. Unbound virus particles were removed by rinsing the cells twice in PBS. Cells were with cold 4% paraformaldehyde for at least 20 min at room temperature and immunostained for HCoV-OC43 and actin.

siRNA silencing. Pooled siRNAs targeting caveolin-1 (sc-44202) and scrambled siRNAs (sc-44237) were purchased from Santa Cruz Biotechnology. HCT-8 cells, cultured on glass slides in a 6-well plate for 1 day (80% confluent), were transfected with siRNA using Lipofectamine RNAiMAX (Thermo Fisher Scientific) according to the manufacturer's instructions. The final amount of siRNA added to each well was 25 pmol. The procedure was repeated 24 h later to improve the silencing effect and further reduce caveolin-1 protein level in the transfected cells. HCoV-OC43 infection (with the viral stock of $TCID_{50} = 2\ 300\ 000$/ml) was carried out 24 h later at 32 °C for 1 h, cells were fixed and immunostained for HCoV-OC43, caveolin-1 and actin as described above. Concomitantly, on the infection day, caveolin-1 protein levels in test samples, mock-transfected and non-transfected cells were compared with Western blotting. β-tubulin was used as the control. Proteins were isolated using RIPA Buffer supplemented with 0.5 M EDTA and 1× proteinase inhibitor.

Western blot analysis. Cell lysates were mixed 1:1 with 2 × SDS-PAGE sample buffer and incubated for 5 min at 95 °C. Afterwards, they were separated by SDS-PAGE electrophoresis and subsequently electrotransferred onto nitrocelulose membrane (Amersham). Membranes were blocked with 5% BSA (Bioshop) in Tris-Buffered Saline with Tween 20 (TBST). Membranes were incubated with primary antibodies (Caveolin-1 N-20 Antibody (sc-894, Santa Cruz Biotechnology) diluted 1:1000 in 2.5% BSA in TBST and β-tubulin Antibody (sc-134234, Santa Cruz Biotechnology) diluted 1:2000 in 2.5% BSA in TBST for 2 h and washed in TBST. Subsequently, membrane was incubated with HRP-labeled anti-rabbit IgG antibody (A0545, Sigma) diluted 1:20 000 in 1% BSA in TBST) for 1 h and finally the signal was developed using the ECL system (Amersham).

Inhibition of HCoV-OC43 replication by endocytosis inhibitors. Cells were seeded in 96-well plates and cultured at 37 °C for 48 h. After that time media were removed and cells were incubated in DMEM with 2% FBS, 100 U/ml penicillin and 100 μg/ml streptomycin supplemented with endocytosis inhibitors at 37 °C for 1 h. Subsequently, media were removed and HCoV-OC43 stock ($TCID_{50} = 800$/ml) was overlaid on the cells in the presence or absence of inhibitors and cultures were incubated at 32 °C for 3 h. Unbound virus particles were removed by rinsing the cells thrice in PBS. The infected cells were further cultured in DMEM supplemented with 2% FBS, 100 U/ml penicillin, and 100 μg/ml streptomycin in the presence of inhibitors at 32 °C for 5 days. Finally, inhibitors' cytotoxicity was inspected with XTT assay in mock-infected cells and viral RNA was isolated from cell culture medium. HCoV-OC43 yield was quantified by RT-qPCR.

Flow cytometry (FACS) analysis. Three days post infection cells were harvested by trypsinization and pelleted in sterile PBS. After fixation in 4% paraformaldehyde, cells were blocked and immunostained for HCoV-OC43 as described above. Washed, resuspended in PBS cells were analyzed by flow cytometry (FACSCalibur, Becton Dickinson). Cell Quest software (Becton Dickinson) was used for data analysis. The infection rate was calculated relatively to untreated, HCoV-OC43 infected cells.

Quantitative real time PCR. Virus detection and quantification was performed by reverse transcription reaction followed by quantitative real-time PCR (RT-qPCR). Viral nucleic acids were isolated from cell culture supernatants using Viral DNA/RNA Kit (A&A Biotechnology), according to the manufacturer's protocol. Reverse transcription was carried out with High Capacity cDNA Reverse Transcription Kit (Thermo Fisher Scientific), according to the manufacturer's protocol. Serially diluted pTZ57R/T plasmid carrying DNA HCoV-OC43 N gene served as standards. Concentration of the linearized form of the standard was assessed using a spectrophotometer and gel electrophoresis.

Subsequently, PCR was performed using KAPA PROBE FAST qPCR Master Mix (Kapa Biosystem), specific probe (TGA CAT TGT CGA TCG GGA CCC AAG TA) labeled with FAM (6-carboxyfluorescein) and TAMRA (6-carboxytetramethylrhodamine), and primers specific for HCoV-OC43 (forward: 5-AGC AAC CAG GCT GAT GTC AAT ACC-3, reverse: 5-AGC AGA CCT TCC TGA GCC TTC AAT-3). Rox was used as a reference dye. The amplification program was set at 50 °C for 2 min, 92 °C for 10 min, 40 cycles of 92 °C for 15 s, and 60 °C for 1 min.

Cell viability assay (XTT assay). HCT-8 cells were cultured on 96-well plates, as described above. Cell viability was examined using the XTT Cell Viability Assay (Biological Industries), according to the manufacturer's protocol. Briefly, the medium was discarded and 70 μl of DMEM supplemented with 2% FBS, 100 U/ml penicillin, and 100 μg/ml streptomycin and 30 μl of the activated XTT solution was added to each well. After 2 h incubation at 37 °C, the medium was transferred onto a new 96-well plate and signal quantified at $\lambda = 490$ nm using the colorimeter (FlexStation Multi-Mode Microplate Reader, Molecular Devices). Experiments were performed at least 3 times. The obtained results were normalized to the control samples, where cell viability was set to 100%.

Fluorescence and confocal microscopy. The fluorescent images were taken under a ZEISS LSM 710 (release version 8.1) confocal microscope with 40× oil immersion objective and acquired with ZEN 2012 SP1 (black edition, version 8.1.0.484) software. Stacks acquisition parameters were as follows: frame size 1024 × 1024, step size 0.15 μm, pixel size 0.06696 × 0.06696 μm. For image processing ImageJ FIJI (National Institutes of Health, Bethesda, Maryland, USA) version was used.

Statistical analyses. All the experiments were performed at least 3 times. The data is presented as the mean of a triplicate for each sample ± SD. To determine the significance of differences between compared groups, Single-Factor Analysis of Variance (ANOVA) was applied. P values < 0.05 were considered significant.

Data availability. All data generated or analysed during this study are included in this published article.

References

1. Vabret, A., Mourez, T., Gouarin, S., Petitjean, J. & Freymuth, F. An outbreak of coronavirus OC43 respiratory infection in Normandy, France. *Clin Infect Dis* **36**, 985–989, https://doi.org/10.1086/374222 (2003).
2. Gaunt, E. R., Hardie, A., Claas, E. C., Simmonds, P. & Templeton, K. E. Epidemiology and clinical presentations of the four human coronaviruses 229E, HKU1, NL63, and OC43 detected over 3 years using a novel multiplex real-time PCR method. *J Clin Microbiol* **48**, 2940–2947, https://doi.org/10.1128/JCM.00636-10 (2010).
3. Vijgen, L. *et al*. Complete genomic sequence of human coronavirus OC43: molecular clock analysis suggests a relatively recent zoonotic coronavirus transmission event. *J Virol* **79**, 1595–1604, https://doi.org/10.1128/JVI.79.3.1595-1604.2005 (2005).
4. Vlasak, R., Luytjes, W., Spaan, W. & Palese, P. Human and bovine coronaviruses recognize sialic acid-containing receptors similar to those of influenza C viruses. *Proc Natl Acad Sci USA* **85**, 4526–4529 (1988).
5. Huang, X. *et al*. Human Coronavirus HKU1 Spike Protein Uses O-Acetylated Sialic Acid as an Attachment Receptor Determinant and Employs Hemagglutinin-Esterase Protein as a Receptor-Destroying Enzyme. *J Virol* **89**, 7202–7213, https://doi.org/10.1128/JVI.00854-15 (2015).
6. Milewska, A. *et al*. Human coronavirus NL63 utilizes heparan sulfate proteoglycans for attachment to target cells. *J Virol* **88**, 13221–13230, https://doi.org/10.1128/JVI.02078-14 (2014).
7. Lang, J. *et al*. Inhibition of SARS pseudovirus cell entry by lactoferrin binding to heparan sulfate proteoglycans. *PLoS One* **6**, e23710, https://doi.org/10.1371/journal.pone.0023710 (2011).
8. Kroschewski, H., Allison, S. L., Heinz, F. X. & Mandl, C. W. Role of heparan sulfate for attachment and entry of tick-borne encephalitis virus. *Virology* **308**, 92–100 (2003).
9. Connell, B. J. & Lortat-Jacob, H. Human immunodeficiency virus and heparan sulfate: from attachment to entry inhibition. *Front Immunol* **4**, 385, https://doi.org/10.3389/fimmu.2013.00385 (2013).
10. Plochmann, K. *et al*. Heparan sulfate is an attachment factor for foamy virus entry. *J Virol* **86**, 10028–10035, https://doi.org/10.1128/JVI.00051-12 (2012).
11. Li, W. *et al*. Angiotensin-converting enzyme 2 is a functional receptor for the SARS coronavirus. *Nature* **426**, 450–454, https://doi.org/10.1038/nature02145 (2003).

12. Collins, A. R. HLA class I antigen serves as a receptor for human coronavirus OC43. *Immunol Invest* **22**, 95–103 (1993).
13. Krempl, C., Schultze, B. & Herrler, G. Analysis of cellular receptors for human coronavirus OC43. *Adv Exp Med Biol* **380**, 371–374 (1995).
14. Raj, V. S. *et al*. Dipeptidyl peptidase 4 is a functional receptor for the emerging human coronavirus-EMC. *Nature* **495**, 251–254, https://doi.org/10.1038/nature12005 (2013).
15. Kido, H., Okumura, Y., Yamada, H., Le, T. Q. & Yano, M. Proteases essential for human influenza virus entry into cells and their inhibitors as potential therapeutic agents. *Curr Pharm Des* **13**, 405–414 (2007).
16. Krzyzaniak, M. A., Zumstein, M. T., Gerez, J. A., Picotti, P. & Helenius, A. Host cell entry of respiratory syncytial virus involves macropinocytosis followed by proteolytic activation of the F protein. *PLoS Pathog* **9**, e1003309, https://doi.org/10.1371/journal.ppat.1003309 (2013).
17. Simmons, G. *et al*. Different host cell proteases activate the SARS-coronavirus spike-protein for cell-cell and virus-cell fusion. *Virology* **413**, 265–274, https://doi.org/10.1016/j.virol.2011.02.020 (2011).
18. Millet, J. K. & Whittaker, G. R. Host cell entry of Middle East respiratory syndrome coronavirus after two-step, furin-mediated activation of the spike protein. *Proc Natl Acad Sci USA* **111**, 15214–15219, https://doi.org/10.1073/pnas.1407087111 (2014).
19. Hussain, K. M., Leong, K. L., Ng, M. M. & Chu, J. J. The essential role of clathrin-mediated endocytosis in the infectious entry of human enterovirus 71. *J Biol Chem* **286**, 309–321, https://doi.org/10.1074/jbc.M110.168468 (2011).
20. Cox, R. G. *et al*. Human Metapneumovirus Is Capable of Entering Cells by Fusion with Endosomal Membranes. *PLoS Pathog* **11**, e1005303, https://doi.org/10.1371/journal.ppat.1005303 (2015).
21. Xu, H. *et al*. Real-time Imaging of Rabies Virus Entry into Living Vero cells. *Sci Rep* **5**, 11753, https://doi.org/10.1038/srep11753 (2015).
22. Henne, W. M. *et al*. FCHo proteins are nucleators of clathrin-mediated endocytosis. *Science* **328**, 1281–1284, https://doi.org/10.1126/science.1188462 (2010).
23. Rappoport, J. Z., Kemal, S., Benmerah, A. & Simon, S. M. Dynamics of clathrin and adaptor proteins during endocytosis. *Am J Physiol Cell Physiol* **291**, C1072–1081, https://doi.org/10.1152/ajpcell.00160.2006 (2006).
24. Ehrlich, M. *et al*. Endocytosis by random initiation and stabilization of clathrin-coated pits. *Cell* **118**, 591–605, https://doi.org/10.1016/j.cell.2004.08.017 (2004).
25. Cocucci, E., Gaudin, R. & Kirchhausen, T. Dynamin recruitment and membrane scission at the neck of a clathrin-coated pit. *Mol Biol Cell* **25**, 3595–3609, https://doi.org/10.1091/mbc.E14-07-1240 (2014).
26. Takei, K., Slepnev, V. I., Haucke, V. & De Camilli, P. Functional partnership between amphiphysin and dynamin in clathrin-mediated endocytosis. *Nat Cell Biol* **1**, 33–39, https://doi.org/10.1038/9004 (1999).
27. Nabi, I. R. & Le, P. U. Caveolae/raft-dependent endocytosis. *J Cell Biol* **161**, 673–677, https://doi.org/10.1083/jcb.200302028 (2003).
28. Pelkmans, L., Püntener, D. & Helenius, A. Local actin polymerization and dynamin recruitment in SV40-induced internalization of caveolae. *Science* **296**, 535–539, https://doi.org/10.1126/science.1069784 (2002).
29. Marjomäki, V. *et al*. Internalization of echovirus 1 in caveolae. *J Virol* **76**, 1856–1865 (2002).
30. Pelkmans, L., Kartenbeck, J. & Helenius, A. Caveolar endocytosis of simian virus 40 reveals a new two-step vesicular-transport pathway to the ER. *Nat Cell Biol* **3**, 473–483, https://doi.org/10.1038/35074539 (2001).
31. Montesano, R., Roth, J., Robert, A. & Orci, L. Non-coated membrane invaginations are involved in binding and internalization of cholera and tetanus toxins. *Nature* **296**, 651–653 (1982).
32. Pelkmans, L. & Helenius, A. Endocytosis via caveolae. *Traffic* **3**, 311–320 (2002).
33. Harper, C. B., Popoff, M. R., McCluskey, A., Robinson, P. J. & Meunier, F. A. Targeting membrane trafficking in infection prophylaxis: dynamin inhibitors. *Trends Cell Biol* **23**, 90–101, https://doi.org/10.1016/j.tcb.2012.10.007 (2013).
34. Araki, N., Hatae, T., Furukawa, A. & Swanson, J. A. Phosphoinositide-3-kinase-independent contractile activities associated with Fcgamma-receptor-mediated phagocytosis and macropinocytosis in macrophages. *J Cell Sci* **116**, 247–257 (2003).
35. Li, L. *et al*. The effect of the size of fluorescent dextran on its endocytic pathway. *Cell Biol Int* **39**, 531–539, https://doi.org/10.1002/cbin.10424 (2015).
36. Al-Ayed, M. S., Asaad, A. M., Qureshi, M. A. & Ameen, M. S. Viral etiology of respiratory infections in children in southwestern Saudi Arabia using multiplex reverse-transcriptase polymerase chain reaction. *Saudi Med J* **35**, 1348–1353 (2014).
37. Pu, Y. & Zhang, X. Mouse hepatitis virus type 2 enters cells through a clathrin-mediated endocytic pathway independent of Eps15. *J Virol* **82**, 8112–8123, https://doi.org/10.1128/JVI.00837-08 (2008).
38. Qinfen, Z. *et al*. The life cycle of SARS coronavirus in Vero E6 cells. *J Med Virol* **73**, 332–337, https://doi.org/10.1002/jmv.20095 (2004).
39. Inoue, Y. *et al*. Clathrin-dependent entry of severe acute respiratory syndrome coronavirus into target cells expressing ACE2 with the cytoplasmic tail deleted. *J Virol* **81**, 8722–8729, https://doi.org/10.1128/JVI.00253-07 (2007).
40. Lu, Y., Liu, D. X. & Tam, J. P. Lipid rafts are involved in SARS-CoV entry into Vero E6 cells. *Biochem Biophys Res Commun* **369**, 344–349, https://doi.org/10.1016/j.bbrc.2008.02.023 (2008).
41. Ares, G. R. & Ortiz, P. A. Dynamin2, clathrin, and lipid rafts mediate endocytosis of the apical Na/K/2Cl cotransporter NKCC2 in thick ascending limbs. *J Biol Chem* **287**, 37824–37834, https://doi.org/10.1074/jbc.M112.386425 (2012).
42. Subtil, A. *et al*. Acute cholesterol depletion inhibits clathrin-coated pit budding. *Proc Natl Acad Sci USA* **96**, 6775–6780 (1999).
43. Dutta, D. & Donaldson, J. G. Search for inhibitors of endocytosis: Intended specificity and unintended consequences. *Cell Logist* **2**, 203–208, https://doi.org/10.4161/cl.23967 (2012).
44. Kosaka, T. & Ikeda, K. Possible temperature-dependent blockage of synaptic vesicle recycling induced by a single gene mutation in Drosophila. *J Neurobiol* **14**, 207–225, https://doi.org/10.1002/neu.480140305 (1983).
45. Chen, M. S. *et al*. Multiple forms of dynamin are encoded by shibire, a Drosophila gene involved in endocytosis. *Nature* **351**, 583–586, https://doi.org/10.1038/351583a0 (1991).
46. van der Bliek, A. M. & Meyerowitz, E. M. Dynamin-like protein encoded by the Drosophila shibire gene associated with vesicular traffic. *Nature* **351**, 411–414, https://doi.org/10.1038/351411a0 (1991).
47. Henley, J. R., Krueger, E. W., Oswald, B. J. & McNiven, M. A. Dynamin-mediated internalization of caveolae. *J Cell Biol* **141**, 85–99 (1998).
48. Oh, P., McIntosh, D. P. & Schnitzer, J. E. Dynamin at the neck of caveolae mediates their budding to form transport vesicles by GTP-driven fission from the plasma membrane of endothelium. *J Cell Biol* **141**, 101–114 (1998).
49. Parton, R. G., Joggerst, B. & Simons, K. Regulated internalization of caveolae. *J Cell Biol* **127**, 1199–1215 (1994).
50. Xu, Q. *et al*. Caveolin-1-mediated Japanese encephalitis virus entry requires a two-step regulation of actin reorganization. *Future Microbiol* **11**, 1227–1248, https://doi.org/10.2217/fmb-2016-0002 (2016).
51. Freeman, M. C., Peek, C. T., Becker, M. M., Smith, E. C. & Denison, M. R. Coronaviruses induce entry-independent, continuous macropinocytosis. *MBio* **5**, e01340–01314, https://doi.org/10.1128/mBio.01340-14 (2014).
52. Lai, F. W., Stephenson, K. B., Mahony, J. & Lichty, B. D. Human coronavirus OC43 nucleocapsid protein binds microRNA 9 and potentiates NF-κB activation. *J Virol* **88**, 54–65, https://doi.org/10.1128/JVI.02678-13 (2014).
53. Gorse, G. J., O'Connor, T. Z., Hall, S. L., Vitale, J. N. & Nichol, K. L. Human coronavirus and acute respiratory illness in older adults with chronic obstructive pulmonary disease. *J Infect Dis* **199**, 847–857, https://doi.org/10.1086/597122 (2009).
54. Shirato, K., Kanou, K., Kawase, M. & Matsuyama, S. Clinical Isolates of Human Coronavirus 229E Bypass the Endosome for Cell Entry. *J Virol* **91**, https://doi.org/10.1128/JVI.01387-16 (2017).

55. Shirato, K., Kawase, M. & Matsuyama, S. Wild-type human coronaviruses prefer cell-surface TMPRSS2 to endosomal cathepsins for cell entry. *Virology*, https://doi.org/10.1016/j.virol.2017.11.012 (2017).
56. Shen, L. W., Mao, H. J., Wu, Y. L., Tanaka, Y. & Zhang, W. TMPRSS2: A potential target for treatment of influenza virus and coronavirus infections. *Biochimie* **142**, 1–10, https://doi.org/10.1016/j.biochi.2017.07.016 (2017).
57. Earnest, J. T. *et al*. The tetraspanin CD9 facilitates MERS-coronavirus entry by scaffolding host cell receptors and proteases. *PLoS Pathog* **13**, e1006546, https://doi.org/10.1371/journal.ppat.1006546 (2017).
58. Reinke, L. M. *et al*. Different residues in the SARS-CoV spike protein determine cleavage and activation by the host cell protease TMPRSS2. *PLoS One* **12**, e0179177, https://doi.org/10.1371/journal.pone.0179177 (2017).
59. Milewska, A. *et al*. Entry of human coronavirus NL63 to the cell. *J Virol*, https://doi.org/10.1128/JVI.01933-17 (2017).
60. Reed, L. J. & Muench, H. A Simple Method Of Estimating Fifty Per Cent Endpoints12. *American Journal of Epidemiology* **27**, 493–497, https://doi.org/10.1093/oxfordjournals.aje.a118408 (1938).

Acknowledgements

This work was supported by the grant from the National Science Center UMO-2012/07/E/NZ6/01712 to KP. KP would like to acknowledge networking contribution by the COST Action CM1407 "Challenging organic syntheses inspired by nature - from natural products chemistry to drug discovery". The Faculty of Biochemistry, Biophysics and Biotechnology of the Jagiellonian University is a beneficiary of the structural funds from the European Union (grant No: POIG.02.01.00-12-475 064/08 – "Molecular biotechnology for health"). Faculty of Biochemistry, Biophysics and Biotechnology of the Jagiellonian University is a partner of the Leading National Research Center supported by the Ministry of Science and Higher Education of the Republic of Poland. The funders had no role in study design, data collection and analysis, decision to publish, or preparation of the manuscript.

Author Contributions

K.O. conducted the experiments. A.S. and A.M. participated in method development for the study. Z.B., Z.R., M.S. participated in confocal imaging. K.O. and K.P. designed the study, analyzed the results and wrote the manuscript. All authors reviewed the manuscript.

Additional Information

Supplementary information accompanies this paper at https://doi.org/10.1038/s41598-018-25640-0.

Competing Interests: The authors declare no competing interests.

Publisher's note: Springer Nature remains neutral with regard to jurisdictional claims in published maps and institutional affiliations.

Cell Communication and Signaling

RESEARCH Open Access

Zika virus: mapping and reprogramming the entry

Katarzyna Owczarek[1,2], Yuliya Chykunova[2], Christian Jassoy[3], Beata Maksym[4], Zenon Rajfur[5] and Krzysztof Pyrc[1*]

Abstract

Background: The *flaviviridae* family comprises single-stranded RNA viruses that enter cells via clathrin-mediated pH-dependent endocytosis. Although the initial events of the virus entry have been already identified, data regarding intracellular virus trafficking and delivery to the replication site are limited. The purpose of this study was to map the transport route of Zika virus and to identify the fusion site within the endosomal compartment.

Methods: Tracking of viral particles in the cell was carried out with confocal microscopy. Immunostaining of two structural proteins of Zika virus enabled precise mapping of the route of the ribonucleocapsid and the envelope and, consequently, mapping the fusion site in the endosomal compartment. The results were verified using RNAi silencing and chemical inhibitors.

Results: After endocytic internalization, Zika virus is trafficked through the endosomal compartment to fuse in late endosomes. Inhibition of endosome acidification using bafilomycin A1 hampers the infection, as the fusion is inhibited; instead, the virus is transported to late compartments where it undergoes proteolytic degradation. The degradation products are ejected from the cell via slow recycling vesicles. Surprisingly, NH_4Cl, which is also believed to block endosome acidification, shows a very different mode of action. In the presence of this basic compound, the endocytic hub is reprogrammed. Zika virus-containing vesicles never reach the late stage, but are rapidly trafficked to the plasma membrane via a fast recycling pathway after the clathrin-mediated endocytosis.
Further, we also noted that, similarly as other members of the *flaviviridae* family, Zika virus undergoes furin- or furin-like-dependent activation during late steps of infection, while serine or cysteine proteases are not required for Zika virus maturation or entry.

Conclusions: Zika virus fusion occurs in late endosomes and is pH-dependent. These results broaden our understanding of Zika virus intracellular trafficking and may in future allow for development of novel treatment strategies. Further, we identified a novel mode of action for agents commonly used in studies of virus entry.

Keywords: ZIKV, Trafficking, Ammonium chloride, Bafilomycin A1, Endocytosis, Recycling, Furin

Plain English summary

Zika virus is a mosquito-borne pathogen, which infects humans. Here, we present how Zika virus hijacks intracellular transport machinery to be delivered to the replication site. Tracking of single virions revealed that they follow clathrin-mediated endocytosis to fuse within late endosomes. Interestingly, we noted that two compounds commonly used to block endocytosis –bafilomycin A1 and NH_4Cl - have a very different activity than previously anticipated. Bafilomycin A1 disables viral fusion by alteration of the endosome pH, while NH_4Cl completely rewires the endosomal hub.

Background

Zika virus (ZIKV) is a (+)ssRNA mosquito-borne flavivirus that infects humans [1]. Although it originates from Africa, it hit the spotlight almost 60 years after its first discovery, due to massive outbreaks in Micronesia, the South Pacific Islands, and South America [2–5]. It is estimated that, since identification of the first case in South America in May 2015, the total number of human cases on this continent has reached 1,300,000 [6]. The rapid spread and neuropathologic complications

* Correspondence: k.a.pyrc@uj.edu.pl
[1]Virogenetics Laboratory of Virology, Malopolska Centre of Biotechnology, Jagiellonian University, Gronostajowa,7a 2.25, 30–387 Krakow, Poland
Full list of author information is available at the end of the article

associated with ZIKV infection (microcephaly in newborns and Guillain-Barré syndrome in adults [7–9]), indicate an urgent need for research into the biology of the pathogen.

The initial events of ZIKV entry have been identified [10–12]; but data regarding its fate thereafter are limited. Upon attachment to a permissive cell, ZIKV crosses the plasma membrane via clathrin- and mucolipin-2-dependent endocytosis, accompanied by formation of LY6E tubules [13, 14]. The dependence of ZIKV on endocytosis has been confirmed in a variety of cell models [15].

Clathrin-mediated endocytosis (CME) is initiated by activation of receptor proteins, followed by recruitment of the AP2 adaptor complex, which induces assembly of the clathrin coat and formation of membrane niches of~ 100 nm [16]. As the invagination deepens, dynamin (GTPase), oligomerizes around the bud neck, cleaves it from the cell surface, and creates an intracellular vesicle [17, 18], which at first is translocated through the actin cortex and then trafficked along microtubules [19]. As the vesicle travels across the cell, it matures. First, the clathrin coat is removed; the uncoated vesicles may then fuse with each other or be delivered to the first (and major) sorting station, i.e., early endosomes. Vesicle trafficking is directed by small membrane GTPases belonging to the Rab family [20]. Early endosomes are characterized by the presence of early endosome antigen 1 (EEA1) and Rab5 proteins. During vesicle maturation, the pH gradually decreases due to the activity of proton pumps and fusion with other acidic vesicles. Early endosomes are moderately acidic (pH ~ 6.3–6.8) [21], and their cargo can be sorted either for degradation via multivesicular bodies and late endosomes to lysosomes, or for recycling to the cell surface, exosomes, or the *trans*-Golgi network [22, 23]. Transport along the degradative pathway is associated with a gradual decrease in pH (from 6.0 to 4.8 in Rab7-positive late endosomes and further to 4.5 in lysosomes [24]). Lysosomes act as a storage site for hydrolases and other proteolytic enzymes; they are the final destination on this pathway. In recycling endosomes, the pH is maintained at ~6.5 and vesicles may be targeted to the outer membrane by Rab35 via fast recycling endosomes (~ 5 min), or by Rab11 via slow recycling endosomes (15–30 min) [21]. Alternatively, cargo may be transported from multivesicular bodies to intraluminal vesicles, which may recycle to the cell surface via a Rab27a/b-mediated pathway, leading to release of cargo-loaded exosomes [25] (30–100 nm, often used by viruses during assembly and egress [26, 27]). Finally, at any point, cargos may enter the *trans*-Golgi network and follow the retrograde transport pathway guided by Rab9 [28].

The microenvironment within the vesicle during its travel is precisely controlled, and viruses usually fuse with the vesicular membrane at a certain time, i.e., when the pH, membrane composition, and activity of cellular proteases are optimal for fusion [22]. Virus dependence on an acidic environment is often treated as a requirement for endocytosis prior to fusion. Consequently, agents such as ammonium chloride (NH_4Cl) or bafilomycin A1 (Baf A1), which increase intravesicular pH, are used to determine whether certain viruses are able to fuse to the cell surface or whether endocytic internalization is required.

Here, we complement and expand the knowledge about cell entry and intracellular trafficking of ZIKV. Tracking of single virions using confocal microscopy and separate labeling of the viral capsid and envelope proteins revealed that virions that enter cells via CME travel to late endosomal compartments and subsequently fuse with the membrane. Blocking endosome acidification using Baf A1 inhibited virus – cell fusion, leading to trafficking of virus either along the degradative pathway to the lysosomal compartments or its slow recycling to the cell surface. Similar results were expected for NH_4Cl-treated cells; however, in this case, virions localized to the cell surface, suggesting a very different mechanism of action. Surprisingly, it appeared that NH_4Cl "rewired" the endosomal hub and altered virus trafficking within the endocytic labyrinth.

Materials and methods

Virus and cells

African green monkey kidney (Vero) cells (ATCC number: CCL-81; RRID:CVCL_0059) were maintained at 37 °C under 5% CO_2 in standard medium [Dulbecco-modified Eagle's medium (DMEM, Thermofisher Scientific, Poland, Poland) supplemented with 3% heat-inactivated fetal bovine serum (FBS, Thermofisher Scientific, Poland), 100 U/ml penicillin and 100 μg/ml streptomycin (Immuniq, Poland)] with addition of 5 μg/ml ciprofloxacin.

ZIKV H/PF/2013 strain acquired from European Virus Archive [29] was propagated in Vero cells under standard medium. After 3 days of infection at 37 °C, virus-containing medium was collected and titrated. As a control, mock-infected Vero cells were subjected to the same procedure. Virus and mock aliquots were stored at − 80 °C. Virus titration was performed on confluent Vero cells on a 96-well plate, according to the Reed–Muench method [30].

Inhibitors

Amantadine (1-adamantylaminean, AMTD; Sigma Aldrich, Poland) was used at 400 μM as clathrin-coated pit stabilizing agent [31]. Bafilomycin A1 [(3Z,5E,7R,8S,9S,11E,13E,15S,16R)-8-hydroxy-16-[(1S,2R,3S)-2-hydroxy-1-methyl-3-[(2R,4R,5S,6R)-tetrahydro-2,4-dihydroxy-5-methyl-6-(1-methylethyl)-2H-pyran-2-yl]butyl]-3,15-dimethoxy-5,7,9,11-tetramethyloxacyclohexadeca-3,5,11,13-tetraen-2-one, Baf A1; Sigma Aldrich, Poland] was used at 100 nM as a vacuolar type H^+-ATPase inhibitor that hampers endosome acidification [32]. Camostat [4-[[4-[(aminoiminomethyl)amino]

benzoyl]oxy] benzeneacetic acid 2-(dimethylamino)-2-oxoethyl ester methanesulfonate, cam; Sigma Aldrich, Poland] was used at 100 μM as a serine protease inhibitor [33]. Decanoyl-arg-val-lys-arg-chloromethylketone (CMK; Sigma Aldrich, Poland) was used at 50 μM as furin inhibitor [34]. Dynasore [3-hydroxynaphthalene-2-carboxylic acid (3,4-dihydroxybenzylidene) hydrazide, Dyn; Abcam, UK] was used at 100 μM as an inhibitor of the GTPase activity of dynamin [35]. Trans-epoxysuccinyl-L-leucylamido (4-guanidino) butane, L-trans-3-Carboxyoxiran-2-carbonyl-L-leucylagmatine, N-(trans-epoxysuccinyl)-L-leucine 4-guanidinobutylamide (E64; Sigma Aldrich, Poland) was used at 100 μM as a cysteine protease inhibitor [33]. MitMAB (tetradecyltrimethylammonium bromide, MM; Abcam, UK) was used at 20 μM as an inhibitor that targets dynamin-phospholipid interaction [36]. NH_4Cl (Bioshop, Poland) was used at 50 mM as an intracellular alkalizing agent [37, 38]. PitStop 2 [N-[5-[4-bromobenzylidene]-4-oxo-4,5-dihydro-1,3-thiazol-2-yl] naphthalene-1-sulfonamide, PtS; Abcam, UK] was used at 50 μM as an inhibitor of ligand association with clathrin's amino terminal domain [39].

Immunostaining

Vero cells were seeded on glass slides in a cell culture plate and cultured in standard medium for two days at 37 °C. Upon experimental procedure, the cells were fixed with ice-cold 4% formaldehyde in PBS for 20 min at room temperature, washed with PBS and permeabilized with 0.5% TWEEN-20 for 10 min at room temperature. Afterwards, non-specific binding sites were blocked overnight at 4 °C with 5% BSA and slides were incubated for 2 h at room temperature with primary anti-ZIKV antibodies (specific to envelope protein (Merck Millipore, Poland) or capsid protein (kind gift from prof. Jassoy, Institut für Virologie, Leipzig, Germany) diluted 1:100 in 3% BSA in PBS. To visualize host cell proteins, slides were incubated with primary antibodies against clathrin, EEA1, Rab7, LAMP1, Rab11, Rab27 and Rab35 [goat anti-clathrin HC (RRID:AB_2083170), rabbit anti-EEA1 (RRID:AB_2277714) and rabbit anti-Rab7 (RRID:AB_2175483) polyclonal antibodies from Santa Cruz Biotechnology, Poland, rabbit anti-Rab11A (RRID:AB_2173458) polyclonal antibody from Proteintech, UK, rabbit anti-Rab27A monoclonal antibodies from Cell Signaling Technology, Poland, rabbit anti-Rab35 polyclonal antibody from Novus Biologicals, Poland, rabbit anti-LAMP1 (RRID:AB_2134611) polyclonal antibody from Thermofisher Scientific, Poland] diluted 1:100 in 3% BSA in PBS, together with anti-ZIKV antibodies. Next, the cells were incubated for another 1 h with Alexa Fluor 488-labeled goat anti-mouse IgG (RRID:AB_2534069, Thermofisher Scientific, Poland) or Alexa Fluor 488-labeled rabbit anti-mouse IgG (RRID:AB_2534106, Thermofisher Scientific, Poland) diluted 1:200 in 3% BSA in PBS. For staining of host cell

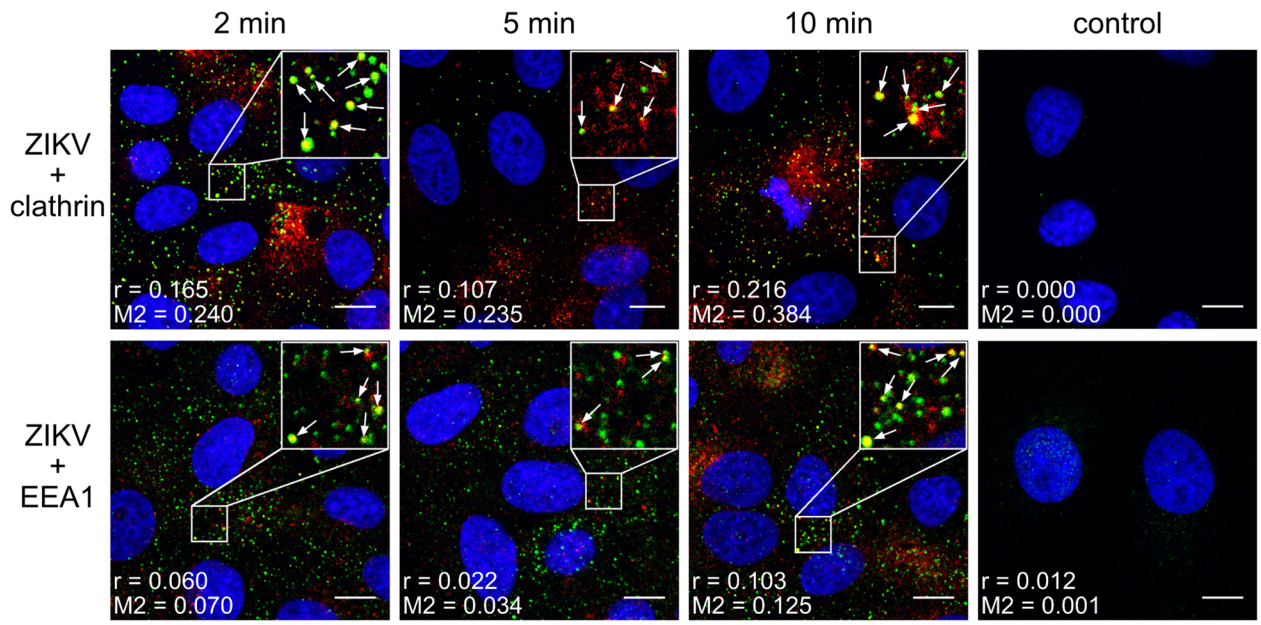

Fig. 1 Co-localization between ZIKV and clathrin-dependent endocytosis markers. Confocal images of Vero cells showing co-localization of ZIKV envelope protein and clathrin (upper) or EEA1 (lower) at different time points p.i. Respective time points are indicated at the top of each column. Control denotes mock-infected cells, stained with anti-ZIKV envelope antibodies and rabbit isotype antibodies (control for staining of cellular proteins). The virus is visualized in green, clathrin and EEA1 are shown in red, and nuclei are presented in blue. Scale bar = 10 μm. Co-localization parameters: r – Pearson's coefficient; M2 - Manders' coefficient M2 (the virus overlapping with clathrin/EEA1)

proteins also Alexa Fluor 546 goat anti-rabbit secondary antibodies (RRID:AB_2534077, Thermofisher Scientific, Poland) or Alexa Fluor 546 donkey anti-goat secondary antibodies (RRID:AB_2534103, Thermofisher Scientific, Poland) diluted 1:200 were added to the mix. In experiments focused on siRNA silencing and inhibitors' influence on virus internalization, the cell surface was labelled by Atto 633-phalloidin (Thermofisher Scientific, Poland) diluted 1:50 in PBS for 1 h at room temperature. Nuclei were stained with DAPI (RRID:AB_2629482, Thermofisher Scientific, Poland) diluted 1:10000 in PBS. At the end of immunostaining procedure slides were thoroughly washed with 0.5% TWEEN-20 in PBS. Stained slides were mounted in ProLong Diamond antifade medium (Thermofisher Scientific, Poland) and stored at 4 °C.

Staining of living cells

Vero cells were seeded on 35 mm glass bottom dishes and cultured in standard medium for two days at 37 °C. Afterwards, the cells were washed with PBS and incubated in standard medium containing 50 nM LysoTracker™ Red DND-99 (Thermofisher Scientific, Poland) for 90 min at 37 °C to visualize acidic organelles. Next, the medium was discarded, and cells were overlaid with BafA1/NH_4Cl-containing or control standard medium and observed for 30 min with a fluorescence microscope. The first images ("0 min") were acquired in < 1 min upon treatment of the cells with the two above mentioned agents.

Fluorescence and confocal microscopy

Images of living cells were acquired using EVOS FL Imaging System (Thermofisher Scientific, Poland) with 60× oil immersion lens. Images of fixed cells were taken under a ZEISS LSM 710 (version 8.1) confocal microscope with 40× oil immersion lens and ZEN 2012 SP1 (black edition, version 8.1.0.484). Image processing was performed with ImageJ FIJI (RRID:SCR_002285,

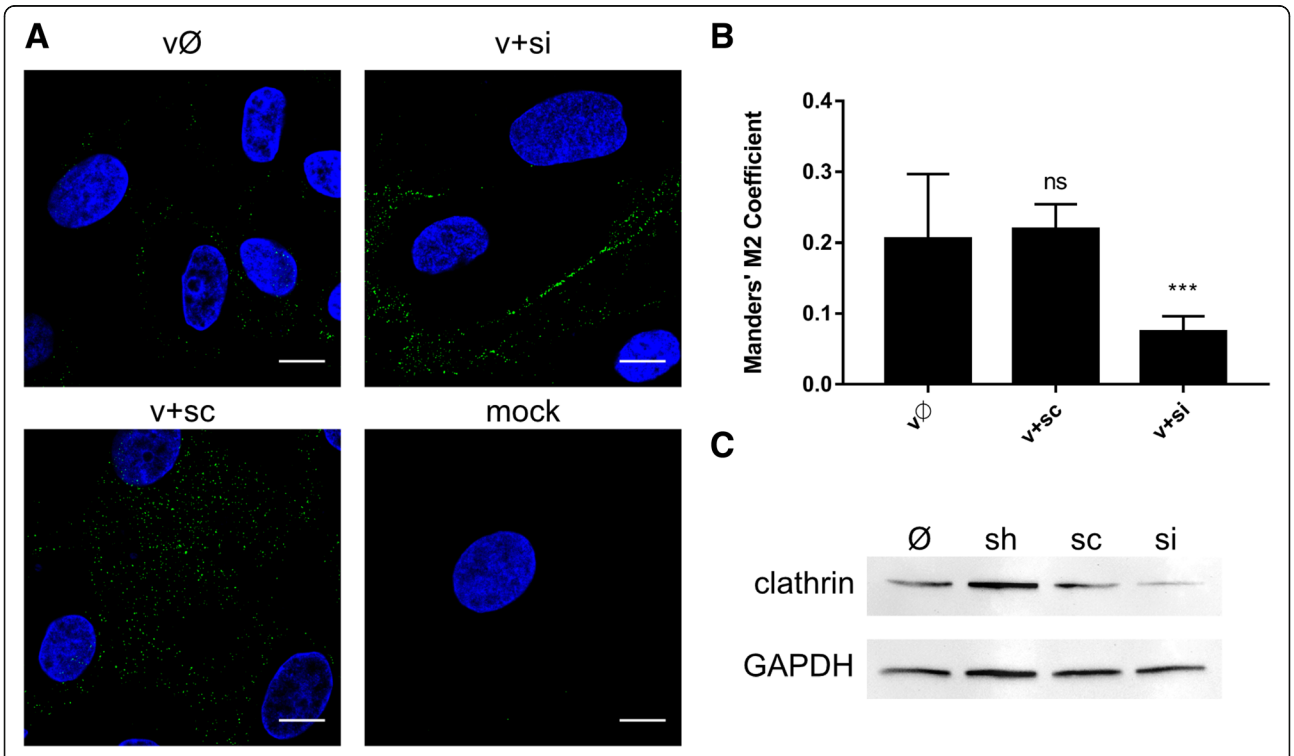

Fig. 2 Inhibition of ZIKV entry to clathrin-depleted cells. (**a**) Confocal analysis of ZIKV localization 10 min p.i. in Vero cells. vØ – ZIKV-infected, non-transfected cells; v + si – ZIKV-infected, clathrin-specific siRNA transfected cells; v + sc – ZIKV-infected, scrambled siRNA transfected cells; v + sh – ZIKV-infected, sham transfected cells; mock – mock-infected, non-transfected cells. ZIKV envelope protein is visualized in green and nuclei are shown in blue. Scale bar = 10 μm. (**b**) Co-localization between ZIKV envelope and clathrin presented as Manders' coefficient M2 for control and clathrin-depleted Vero cells inoculated with ZIKV. The data is presented as mean ± SD. To determine the significance of differences between compared groups, single-factor analysis of variance (ANOVA) was applied. *P* values < 0.05 were considered significant. One asterisk (*) identifies adjusted P values between 0.01 and 0.05, two asterisks (**) identify adjusted *P* values between 0.01 and 0.001, three asterisks (***) identify adjusted *P* values between 0.001 and 0.0001. (**c**) Western blot analysis of the efficiency of siRNA-dependent clathrin silencing (clathrin expression in Vero cells compared to GAPDH expression in these cells). M – BlueStar prestained protein marker; Ø – normal non-transfected Vero cells

National Institutes of Health, Bethesda, Maryland, USA). Co-localization parameters (Pearson's and Manders' coefficients) were calculated using JaCop plugin [40].

Flow cytometry

Vero cells were seeded in a 6-well cell culture plate and cultured in standard medium for two days at 37 °C. Upon experiment, the cells were fixed, permeabilized, blocked and immunostained with primary antibodies specific to viral envelope protein (Merck Millipore, Poland) and secondary rabbit anti-mouse antibodies labeled with Alexa Fluor 488 (RRID:AB_2534106, Thermofisher Scientific, Poland), as indicated in *Immunostaining* section. Proportion of ZIKV-infected cells (corresponding to the median fluorescence of the analyzed cells population) was evaluated with flow cytometry using FACSCalibur (RRID:SCR_000401, Becton Dickinson, Poland). Cell Quest software (RRID:SCR_014489, Becton Dickinson, Poland) was used for data processing and analysis.

Cell viability

Cells were seeded on 96-well plates and cultured in standard medium for two days at 37 °C. Afterwards, the cells were washed with PBS, overlaid with standard medium supplemented with inhibitor or control and further incubated for 3 days at 37 °C. Cell viability was examined using XTT Cell Viability Assay (Biological Industries, Poland), according to the manufacturer's protocol. Briefly, the medium was discarded and 50 μl of fresh standard medium with 50 μl of the activated XTT solution was added to each well. After 2 h incubation at 37 °C, the supernatant was transferred onto a new, transparent 96-well plate and signal from formazan derivative of tetrazolium dye was read at λ = 490 nm using colorimeter (Tecan i-control Infinite 200 Microplate Reader, 1.5.14.0). The obtained results were further normalized to the control, where cell viability was set to 100%.

Virus yield

Virus detection and quantification was performed using reverse transcription (RT) followed by quantitative real-time PCR (qPCR). Viral RNA was isolated from cell culture supernatant 3 days post-infection (p.i.) using Viral DNA / RNA Kit (A&A Biotechnology, Poland), while reverse transcription was carried out with High Capacity cDNA Reverse Transcription Kit (Thermofisher Scientific, Poland), according to manufacturers' protocols. To assess virus yield, DNA standards were subjected to qPCR along with the cDNA acquired from the isolated samples. qPCR was performed using KAPA PROBE FAST qPCR Master Mix (Kapa Biosystem, Poland), ZIKV-specific primers (5′-TTG GTC ATG

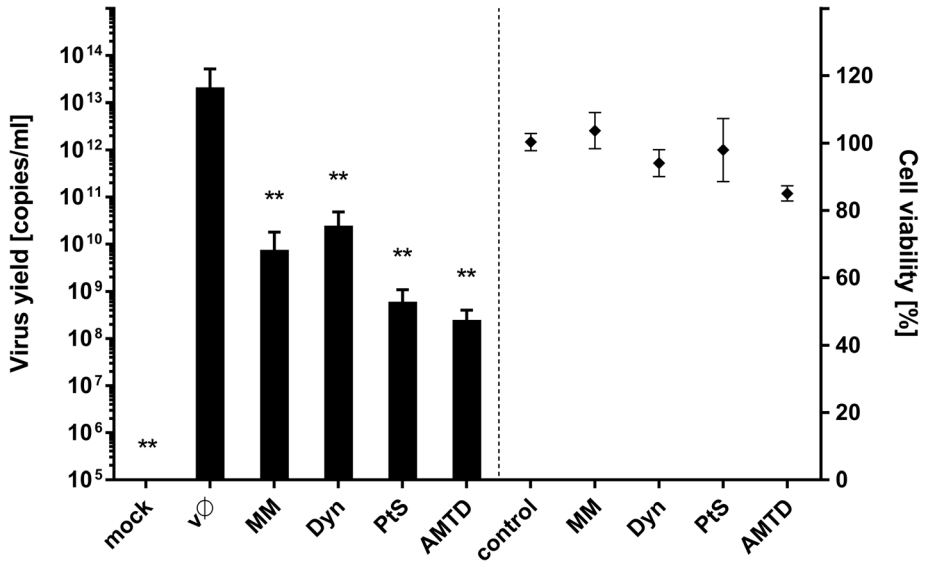

Fig. 3 Inhibition of ZIKV infection in Vero cells by chemical agents blocking clathrin-mediated endocytosis. Vero cells pre-treated with CME inhibitors were infected with ZIKV and viral yield was assessed 3 days p.i. Virus yield (RT-qPCR) is presented on the left side of the graph, while on the right side toxicity of the compounds is visualized (XTT assay). mock – mock-infected cells; vØ – ZIKV-infected cells; AMTD – 400 μM amantadine, Dyn – 100 μM dynasore, MM – 20 μM MitMab, PtS – 50 μM PitStop; control – inhibitor-untreated, non-infected cells. The data is presented as mean ± SD. To determine the significance of differences between compared groups, single-factor analysis of variance (ANOVA) was applied. *P* values < 0.05 were considered significant. One asterisk (*) identifies adjusted P values between 0.01 and 0.05, two asterisks (**) identify adjusted P values between 0.01 and 0.001, three asterisks (***) identify adjusted P values between 0.001 and 0.0001

ATA CTG CTG ATT GC-3′ and 5′-CCT TCC ACA AAG TCC CTA TTG C-3′) and probe (5′-CGG CAT ACA GCA TCA GGT GCA TAG GAG-3′) labelled with FAM (6-carboxyfluorescein) and TAMRA (6-carboxytetramethylrhodamine). Rox was used as a reference dye. The signal was recorded and analysed using 7500 Fast Real-Time PCR System (Thermofisher Scientific, Poland).

siRNA silencing

Control (scrambled) siRNA (sc-44,237) and pooled siRNAs targeting heavy chain of clathrin (sc-35,067) were obtained from Santa Cruz Biotechnology, Poland. siRNA specific to simian Rab35 mRNA (GenBank sequence ID: XM008004920.1) was designed and synthesized by Thermofisher Scientific, Poland.

Vero cells cultured for 1 day in antibiotic- and serum-depleted standard medium on a 6-well plate were transfected with appropriate siRNAs using Lipofectamine RNAiMAX (Thermofisher Scientific, Poland). The procedure was performed according to the manufacturer's instructions and repeated 24 h later to enhance the silencing effect. The efficiency of the procedure was assessed by Western blotting 24 h later (at the same time as microscopic studies on virus subcellular localization).

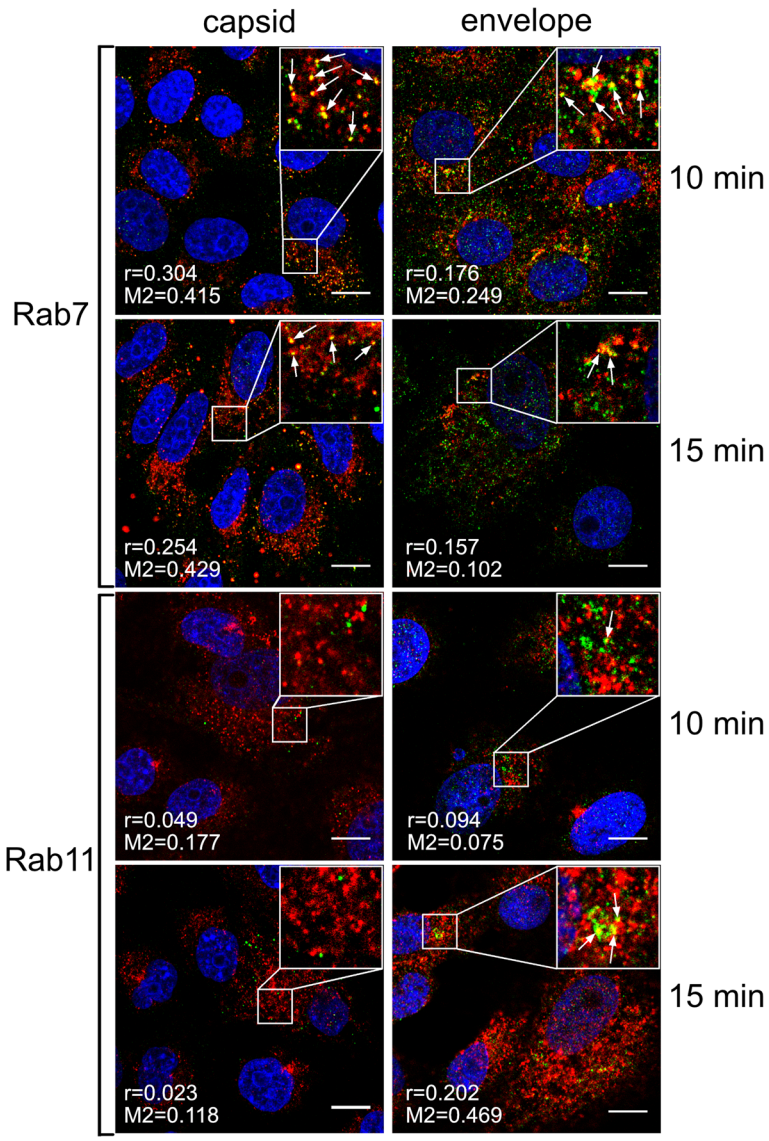

Fig. 4 Co-localization of ZIKV with Rab7 and Rab11 marker proteins 10–15 min p.i.

Western blot analysis

Cells were harvested in RIPA buffer (1 h, 4 °C; Thermofisher Scientific, Poland) supplemented with 0.5 M EDTA and protease inhibitors cocktail (cOmplete Tablets, Roche, Poland)]. Protein concentration was assessed with Pierce BCA Protein Assay Kit (Thermofisher Scientific, Poland), according to manufacturer's protocol. Samples containing equal amounts of proteins were mixed with SDS-PAGE Sample Buffer (0.5 M Tris, pH 6.8, 10% SDS, 50 mg/ml DTT), denatured for 10 min at 95 °C and separated by SDS-PAGE electrophoresis. Subsequently, proteins were electrotransferred onto a PVDF membrane (1.5 h, 100 V; Amersham, Poland). The non-specific binding sites on the membrane were blocked for 1 h at room temperature with 10% milk (Bioshop) in Tris-buffered saline supplemented with 0.25% TWEEN-20 (Bioshop, Poland) (TBST) and incubated with primary antibodies specific to clathrin or Rab35 [rabbit anti-clathrin heavy chain polyclonal antibody, RRID:AB_10695306, Cell Signaling Technology, Poland; rabbit anti-Rab35 polyclonal antibody, Novus Biologicals, Poland] diluted 1:500 or 1:1000 (for clathrin and Rab35, respectively) in 3% BSA in TBST overnight at 4 °C and additionally for 1 h at room temperature; or with primary antibodies specific to GAPDH (rabbit anti-GAPDH antibodies, RRID:AB_561053, Cell Signaling Technology, Poland) diluted 1:5000 in 3% BSA in TBST for 1 h at room temperature. After being washed in TBST, the membrane was incubated with HRP-labelled anti-rabbit IgG antibody (RRID:AB_257896, Sigma Aldrich, Poland) diluted 1:20,000 in 3% BSA in TBST for 1 h at room temperature. Finally, the proteins were visualized with chemiluminescence, using the ECL system (Amersham, Poland).

Co-localization assay

Vero cells were seeded in standard medium on glass slides in 12-well plates. After 2 days, 2 h prior to infection, cell culture medium was replaced with serum-depleted standard medium. Next, cells were cooled down to 4 °C, overlaid with 100 µl of non-diluted ZIKV stock ($TCID_{50}$ ranging from 1000,000 to 10,000,000/ml, which approximately corresponds to MOI = 1.75–17.5 and 7×10^5–7×10^6 PFU/ml) and incubated for 30 min at 4 °C to synchronize cargo particles entry from the cell surface. Subsequently, after incubation at 37 °C (exact times indicated for each experiment) the cells were fixed, permeabilized, blocked and immunostained for viral and cellular proteins, as indicated in *Immunostaining* section.

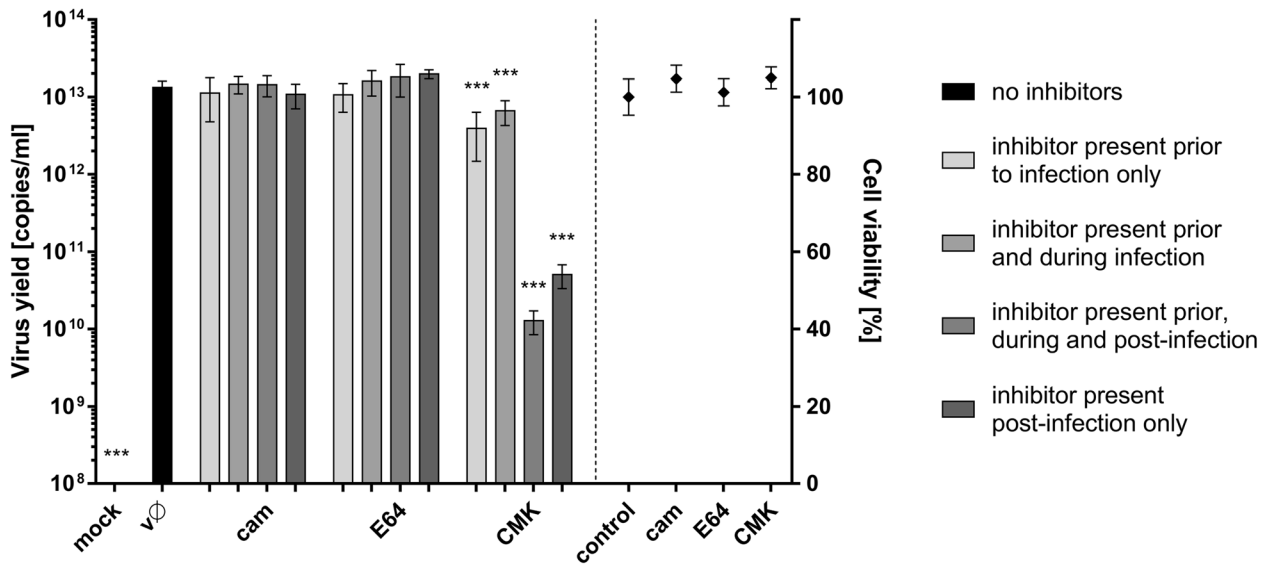

Fig. 5 Cellular proteases and ZIKV. Vero cells were treated with proteases inhibitors (as outlined in the figure) and virus yield 3 days p.i. was assessed using RT-qPCR (left side of the graph); cytotoxity of inhibitors is presented on the right side of the graph (XTT assay). mock – mock infected cells; vØ – ZIKV- infected cells; cam – 100 µM serine protease inhibitor camostat; E64–100 µM cysteine protease inhibitor E64; CMK – 50 µM furin inhibitor CMK; control – inhibitor-untreated, non-infected cells. The data is presented as mean ± SD. To determine the significance of differences between compared groups, single-factor analysis of variance (ANOVA) was applied. P values < 0.05 were considered significant. One asterisk (*) identifies adjusted P values between 0.01 and 0.05, two asterisks (**) identify adjusted P values between 0.01 and 0.001, three asterisks (***) identify adjusted *P* values between 0.001 and 0.0001

Virus inhibition assays

For visualization of virus subcellular localization during experiments with agents interfering with virus trafficking, Vero cells were cultured in standard medium on glass slides in 12-well plates for 2 days and pre-treated with a particular inhibitor 1 h prior to infection. Afterwards, the cells were cooled down to 4 °C, overlaid with 100 μl of non-diluted ZIKV stock ($TCID_{50}$ ranging from 1000,000 to 10,000,000/ml, which approximately corresponds to MOI = 1.75–17.5 and 7×10^5–7×10^6 PFU/ml) in the presence of inhibitory agents and incubated for another 30 min at 4 °C to synchronize cargo internalization. Subsequently, the virus-overlaid cells were warmed up to 37 °C. At indicated for each experiment time points, cells were washed with PBS, fixed, permeabilized, blocked and immunostained for viral and actin cytoskeleton proteins as indicated in *Immunostaining* section. Identical procedure was carried out for visualization of virus particles in cells depleted of certain proteins with siRNAs.

To test the influence of compounds on virus adhesion, Vero cells cultured in standard medium in a 6-well plate for 2 days were cooled down to 4 °C, overlaid with 100 μl of ice-cold non-diluted ZIKV stock ($TCID_{50}$ ranging from 1000,000 to 10,000,000/ml, which approximately corresponds to MOI = 1.75–17.5 and 7×10^5–7×10^6 PFU/ml) and incubated for another 2 h at 4 °C. Further, cells were rinsed twice with ice-cold PBS. The cells were fixed, permeabilized, blocked, immunostained and analyzed with flow cytometry, as described in *Flow cytometry* section.

For assessment of the inhibitors' influence on viral replication, Vero cells were cultured in standard

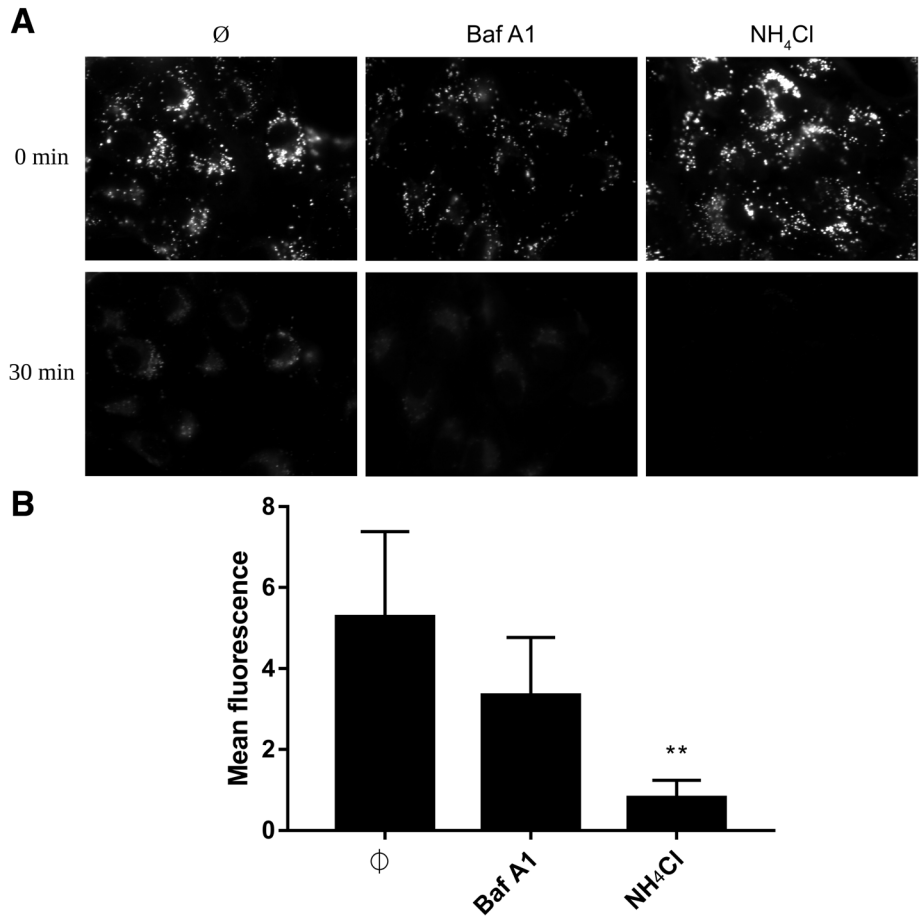

Fig. 6 Endosome acidification in living cells treated with Baf A1 and NH_4Cl. Vero cells were incubated with LysoTracker™ Red DND-99 for 90 min at 37 °C and overlaid with BafA1, NH_4Cl or control medium (Ø) and signal was recorded for 30 min with a fluorescence microscope. (**a**) Images acquired at the beginning (0 min) and by the end (30 min) of incubation. (**b**) Mean fluorescence of the LysoTracker™ Red DND-99 based on the set of xy images collected every 10 s in a 30 min period. The data is presented as mean ± SD. To determine the significance of differences between compared groups, single-factor analysis of variance (ANOVA) was applied. *P* values < 0.05 were considered significant. One asterisk (*) identifies adjusted P values between 0.01 and 0.05, two asterisks (**) identify adjusted P values between 0.01 and 0.001, three asterisks (***) identify adjusted P values between 0.001 and 0.0001

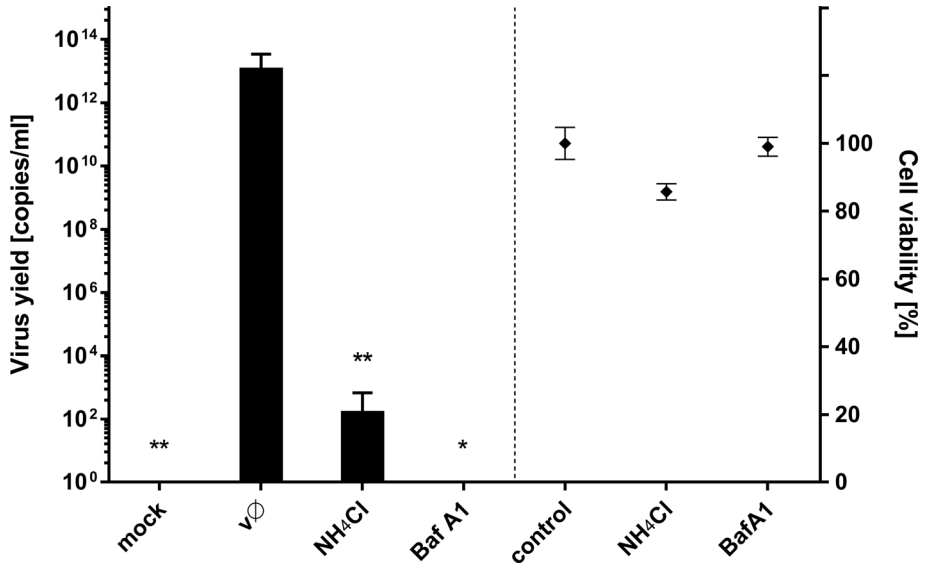

Fig. 7 Baf A1 and NH_4Cl inhibit ZIKV infection. Vero cells pre-treated with intracellular agents hampering endosome acidification were infected with ZIKV and viral yield was assessed at 3 days p.i. RT-qPCR results are presented on the left side of the graph. Right side of the graph shows viability of cells, as determined by an XTT assay. Mock – mock infected cells; vØ – ZIKV- infected cells; NH_4Cl – 50 mM NH_4Cl; BafA1–100 nM bafilomycin A1; control – inhibitor-untreated, non-infected cells. The data is presented as mean ± SD. To determine the significance of differences between compared groups, single-factor analysis of variance (ANOVA) was applied. P values < 0.05 were considered significant. One asterisk (*) identifies adjusted P values between 0.01 and 0.05, two asterisks (**) identify adjusted P values between 0.01 and 0.001, three asterisks (***) identify adjusted P values between 0.001 and 0.0001

medium in 96-well plates for 2 days and pre-treated with a selected agent 1 h prior to infection. Virus at $TCID_{50}$ of 800/ml (which approximately corresponds to MOI = 0.0014 and 550 PFU/ml) was overlaid on the cells in the presence of inhibitors and samples were incubated for 2 h at 37 °C. Wells were washed thrice with PBS and incubated at 37 °C in standard medium supplemented with inhibitors. 3 days p.i. culture supernatants were collected, viral RNA was isolated and its yield was quantified with RT-qPCR. Whether the procedure was modified, it is described in the results section.

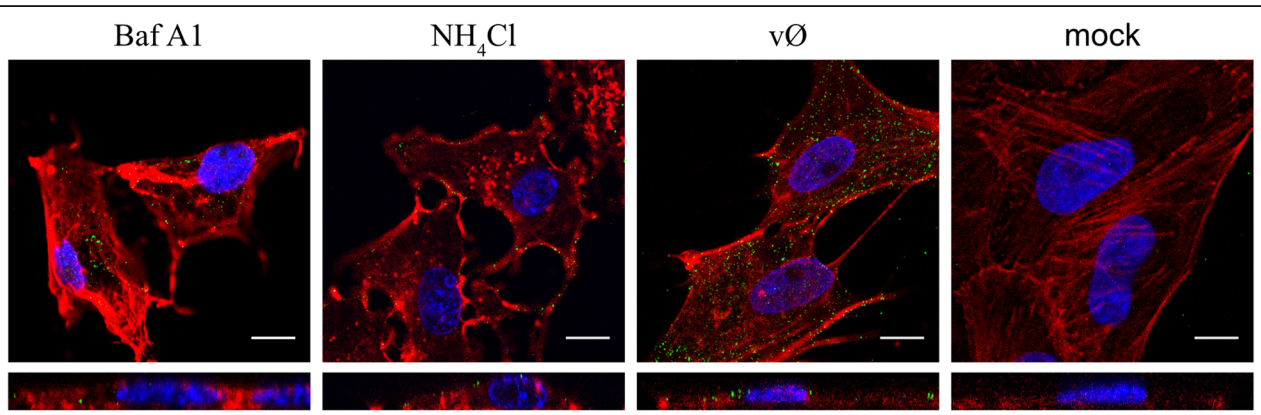

Fig. 8 Increased number of virions trapped in the endosomal hub in cells treated with Baf A1, but not NH_4Cl. Confocal analysis of ZIKV entry to Vero cells in the presence of intracellular agents hampering endosome acidification. Following 1 h pre-treatment with 100 nM Baf A1 or 50 mM NH_4Cl the cells were infected with ZIKV and fixed 40 min p.i. Baf A1 - ZIKV-infected Baf A1-treated cells; NH_4Cl - ZIKV-infected NH_4Cl -treated cells; vØ - ZIKV-infected inhibitor-untreated cells; mock – mock-infected, inhibitor-untreated cells. ZIKV envelope protein is visualized in green, actin cytoskeleton stained in red to show the cell boundaries and nuclei are shown in blue. Scale bar = 10 μm. Upper panel – *xy* projections; bottom panel – *xz* projections

Statistical analyses

Each experiment was performed at least twice in triplicate. Chart bars represent mean ± SD. The significance of differences between compared groups was determined by Single-Factor Analysis of Variance (ANOVA); p values < 0.05 were considered significant.

Results

ZIKV enters Vero cells via clathrin-dependent endocytosis

First, we asked whether ZIKV enters Vero cells via CME, as reported for other in vitro systems. We examined co-localization of virions and cellular proteins (clathrin, caveolin, endophilin, EEA1) at several time points post-infection (p.i.). Co-localization of ZIKV with clathrin was observed at 2–10 min p.i. and coincided with co-localization of virus with the early endosomal marker EEA1 (Fig. 1). No co-localization with caveolin or endophilin was observed (data not shown).

As co-localization rates were not very high (Pearson's coefficient ranging from 0.103 to 0.216 and Manders' coefficients up to 0.384), we carried out a complementary study to validate the results. Subcellular localization of ZIKV in Vero cells in which clathrin expression was transiently silenced was examined. In this model virions were retained on the surface of clathrin-depleted cells even at 10 min p.i.; by contrast, control cells showed normal expression of clathrin and were permissive for ZIKV entry (Fig. 2).

To prove that clathrin-dependent endocytosis is the main route of ZIKV internalization in Vero cells, we

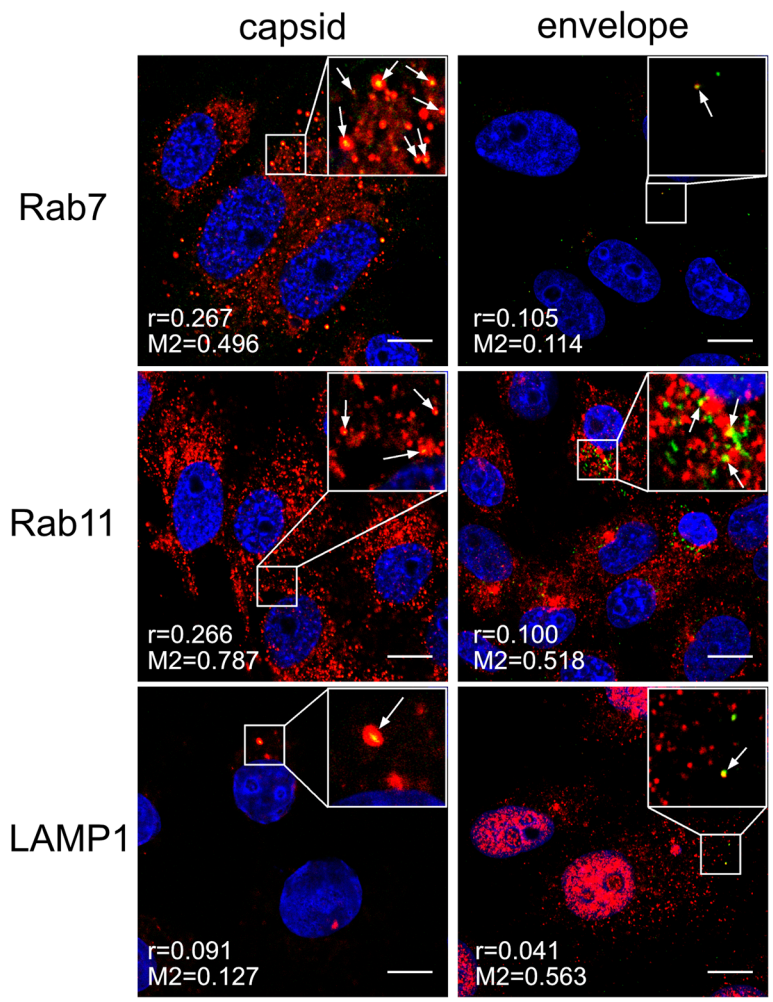

Fig. 9 Baf A1 blocks virus-cell fusion. Co-localization between ZIKV and subcellular marker proteins in Baf A1-treated Vero cells 15 min p.i. Confocal images of 100 nM Baf A1-treated ZIKV-infected Vero cells presenting co-localization between ZIKV capsid or envelope proteins and Rab7, Rab11 and LAMP1 at 15 min p.i.. Rab7 – late endosomes marker protein, Rab11 – slow recycling endosomes marker protein, LAMP1 – lysosomes marker protein. ZIKV proteins are visualized in green, cellular proteins in red and nuclei are shown in blue. Co-localization coefficients for the representative presentations are indicated in the bottom left corners of the respective images; r – Pearson's coefficient; M2 - Manders' coefficient M2 (the virus overlapping with Rab7/Rab11/LAMP1). Scale bar = 10 μm

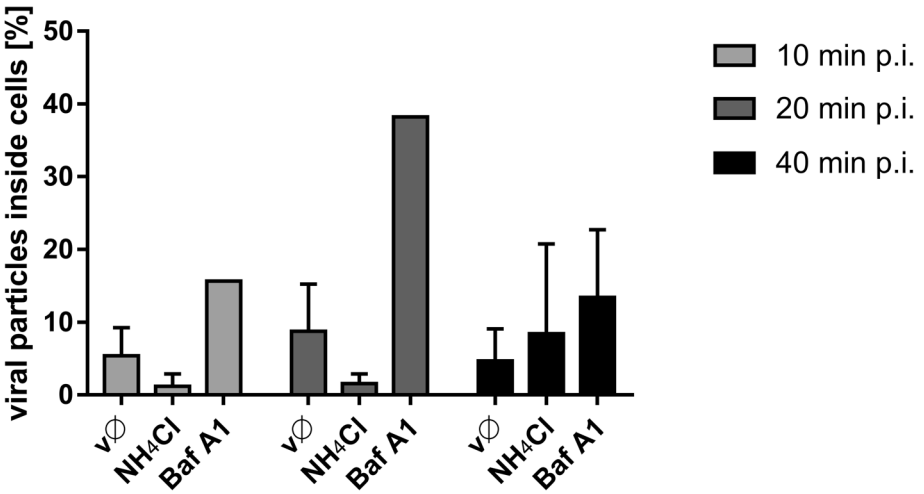

Fig. 10 Intracellular ZIKV virions in cells treated with Baf A1 or NH_4Cl. Ratio of ZIKV particles present inside cells and total number of ZIKV particles, assessed from confocal images of Vero cells infected with ZIKV in the absence (vØ) or presence of 100 nM Baf A1 (Baf A1) or 50 mM NH_4Cl (NH_4Cl). The data is presented as the mean ± SD

examined the effects of CME inhibitors on virus replication. We selected compounds to target multiple steps of the vesicle formation process. These included PitStop (PtS), which inhibits association between ligands with the terminal domain of clathrin [39]; amantadine (AMTD), which stabilizes clathrin-coated pits [31]; MitMAB (MM), which targets the dynamin-phospholipid interaction [36]; and dynasore (Dyn), which inhibits the GTPase activity of dynamin and therefore impairs loss of loaded vesicle from the cell surface [35]. We assessed the impact of each inhibitor on ZIKV infection by measuring the viral yield

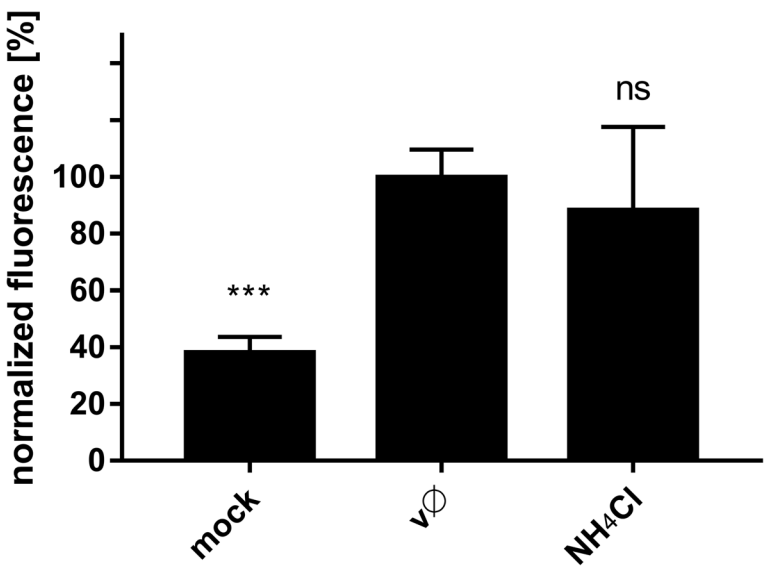

Fig. 11 Influence of NH_4Cl on ZIKV adhesion to the host cells. Flow cytometry analysis of viral adhesion to cells in the presence of NH_4Cl was carried out. Vero cells pre-treated with 50 mM NH_4Cl were overlaid with ZIKV stock and following 2 h incubation at 4 °C, they were fixed and ZIKV was immunostained with Alexa Fluor 488. Graph shows median fluorescence normalized to control, which corresponds to the proportion of ZIKV-positive cells in total cells population. vØ – inhibitor-untreated cells overlaid with ZIKV; NH_4Cl –NH_4Cl-treated cells overlaid with ZIKV; mock – mock-overlaid inhibitor-untreated cells. The data is presented as mean ± SD. To determine the significance of differences between compared groups, single-factor analysis of variance (ANOVA) was applied. *P* values < 0.05 were considered significant. One asterisk (*) identifies adjusted P values between 0.01 and 0.05, two asterisks (**) identify adjusted P values between 0.01 and 0.001, three asterisks (***) identify adjusted P values between 0.001 and 0.0001

released from infected cells into the medium at 3 days p.i. All compounds reduced the ZIKV yield significantly (Fig. 3), suggesting that ZIKV enters the Vero cells via the clathrin-dependent route, as reported for human cells [10].

ZIKV fusion occurs in late endosomal compartment

Once in the endosomal hub, ZIKV has a plethora of pathways by which it can reach the site of fusion with the host cell membrane. Conditions within endosomal compartments differ with respect to lipid/protein content and pH. To find out how the virus is trafficked to reach the site of fusion, using confocal microscopy we tracked two ZIKV structural proteins, the capsid protein (virus core) and the membrane-bound envelope protein. Co-localization of both viral proteins with cellular proteins (Rab7 in late endosomes, Rab11 in slow recycling endosomes, and LAMP1 in lysosomes) was analyzed at 5–20 min p.i. (full set of images is available in Additional file 1: Figure S1 and Additional file 2: Figure S2). The most evident co-localization of the ZIKV capsid was found with Rab7, peaking at 10–15 min p.i. (Fig. 4). However, the envelope protein showed increased co-localization with both Rab7 and Rab11-positive structures at 15 min p.i. (Fig. 4), suggesting that slowly recycling endosomes may carry viral proteins to the cell surface upon delivery of RNA to the cytoplasm from late endosomes. Finally, no co-localization with LAMP1 was found (Additional file 1: Figure S1 and Additional file 2: Figure S2).

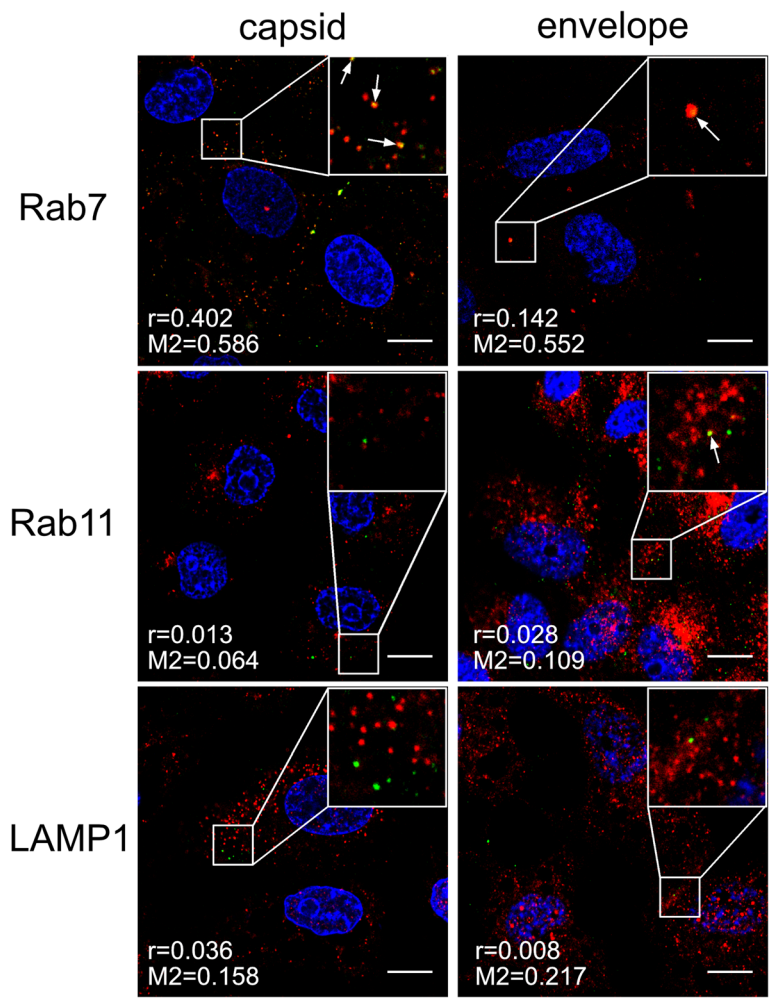

Fig. 12 Co-localization between ZIKV and subcellular marker proteins in NH_4Cl-treated Vero cells 20 min p.i. Confocal images of 50 mM NH_4Cl ZIKV-infected Vero cells presenting co-localization between ZIKV capsid or envelope protein and Rab7, Rab11 and LAMP1 at 20 min p.i.. Rab7 – late endosomes marker protein, Rab11 – slow recycling endosomes marker protein, LAMP1 – lysosomes marker protein. ZIKV proteins are visualized in green, cellular proteins in red and nuclei are shown in blue. Co-localization coefficients for the representative presentations are indicated in the bottom left corners of the respective images; r – Pearson's coefficient; M2 - Manders' coefficient M2 (the virus overlapping with Rab7/Rab11/LAMP1). Scale bar = 10 μm

Role of cellular proteases during ZIKV infection

Upon identification of the fusion site, we next identified host factors taking part in this process. Virus escape from the endosomal compartment usually occurs upon activation of viral fusion proteins, which may be triggered by environmental conditions or/and host proteases [41]. Therefore, we examined the importance of different host cell proteases. Vero cells were treated either with a furin inhibitor (decanoyl-arg-val-lys-arg-chloromethylketone [CMK]), a serine protease inhibitor (camostat [cam]), or a cysteine protease inhibitor (E64) under four different conditions: (1) 1 h prior to infection; (2) 1 h prior to infection and for 2 h during infection; (3) 1 h prior to infection

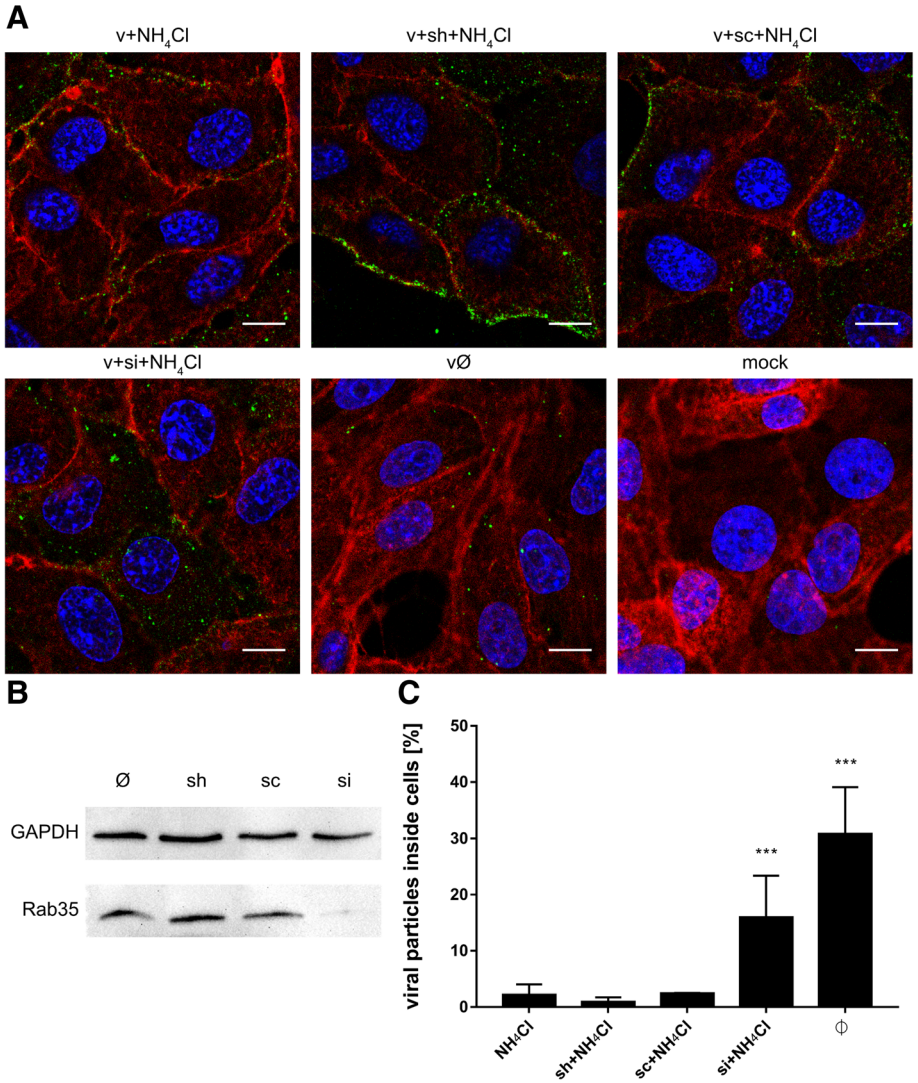

Fig. 13 Subcellular localization of ZIKV in Rab35-depleted cells upon NH_4Cl treatment. (**a**) Confocal analysis of ZIKV localization 1 h p.i. in NH_4Cl-treated Vero cells. ZIKV envelope protein is visualized in green, actin cytoskeleton stained in red to show the cell boundaries and nuclei are shown in blue. Scale bar = 10 μm. (**b**) Western blot analysis of the efficiency of siRNA-dependent Rab35 silencing (Rab35 expression in Vero cells compared to GAPDH expression in these cells). M – BlueStar prestained protein marker; Ø – normal non-transfected Vero cells. (**c**) Graph representing the percent of ZIKV particles present inside cells related to the total number of ZIKV particles, assessed from confocal images of siRNA-transfected and all control Vero cells infected with ZIKV H/PF/2013 in the presence of 50 mM NH_4Cl. v + NH_4Cl - ZIKV-infected, NH_4Cl-treated, non-transfected cells; v + sh + NH_4Cl - ZIKV-infected, NH_4Cl-treated, sham transfected cells; v + sc + NH_4Cl - ZIKV-infected, NH_4Cl-treated, scrambled siRNA transfected cells; v + si + NH_4Cl - ZIKV-infected, NH_4Cl-treated, Rab35-specific siRNA transfected cells; vØ - ZIKV-infected, NH_4Cl-untreated, non-transfected cells; mock - mock-infected, NH_4Cl-untreated, non-transfected cells. The data is presented as the mean ± SD. To determine the significance of differences between compared groups, single-factor analysis of variance (ANOVA) was applied. P values < 0.05 were considered significant. One asterisk (*) identifies adjusted P values between 0.01 and 0.05, two asterisks (**) identify adjusted P values between 0.01 and 0.001, three asterisks (***) identify adjusted P values between 0.001 and 0.0001

and for 72 h p.i.; and (4) 2 h p.i. to 72 h p.i.. Culture supernatants were collected at 72 h p.i., and viral RNA was isolated and quantified by RT-qPCR. As shown in Fig. 5, infection was not affected by serine and cysteine protease inhibitors; however, the furin inhibitor led to a significant decrease in virus yield when administered p.i., suggesting that furin or furin-like enzymes play an important role during ZIKV replication, assembly or egress.

Agents that increase endosomal pH hamper ZIKV entry and infection

We know that for some flaviviruses cell entry is sensitive to pH changes; therefore, we used two compounds that increase intravesicular pH (Fig. 6) to check the pH dependence of ZIKV entry. Vero cells were treated with NH_4Cl or Baf A1 1 h prior to infection. Next, cells were infected with ZIKV in the presence of NH_4Cl or Baf A1 for 3 days at 37 °C. RT-qPCR analysis revealed strong inhibition of infection (Fig. 7). Next, we used confocal microscopy to test whether the compounds indeed inhibit virus entry. Cells were treated with either of the inhibitors for 1 h and then incubated with ZIKV for 40 min in the presence of the inhibitors. Confocal microscopy revealed that viral particles in Baf A1-treated cells were visible in the cytoplasm, probably trapped in the endosomal hub and unable to undergo fusion (Fig. 8). Interestingly, we observed a different intracellular virus distribution in cells treated with NH_4Cl. Only a small number of ZIKV virions was visible in the cytoplasm, while ZIKV particles localized mainly to the cell surface.

Baf A1 blocks virus-cell fusion

Baf A1 is thought to prevent endosome acidification, thereby preventing viral fusion and protein activation. Therefore, we tracked viral capsid and envelope proteins separately to visualize their fate during cell entry. To do this, we examined co-localization of these two viral components with markers of different parts of the endosomal hub (Rab7, Rab11, and LAMP1) in Baf A1-treated cells at 5–20 min p.i. (Additional file 3: Figure S3 and Additional file 4: Figure S4).

As described above, in non-treated cells the ZIKV capsid and envelope proteins travelled together to late endosomes, where fusion occurs. While capsid proteins

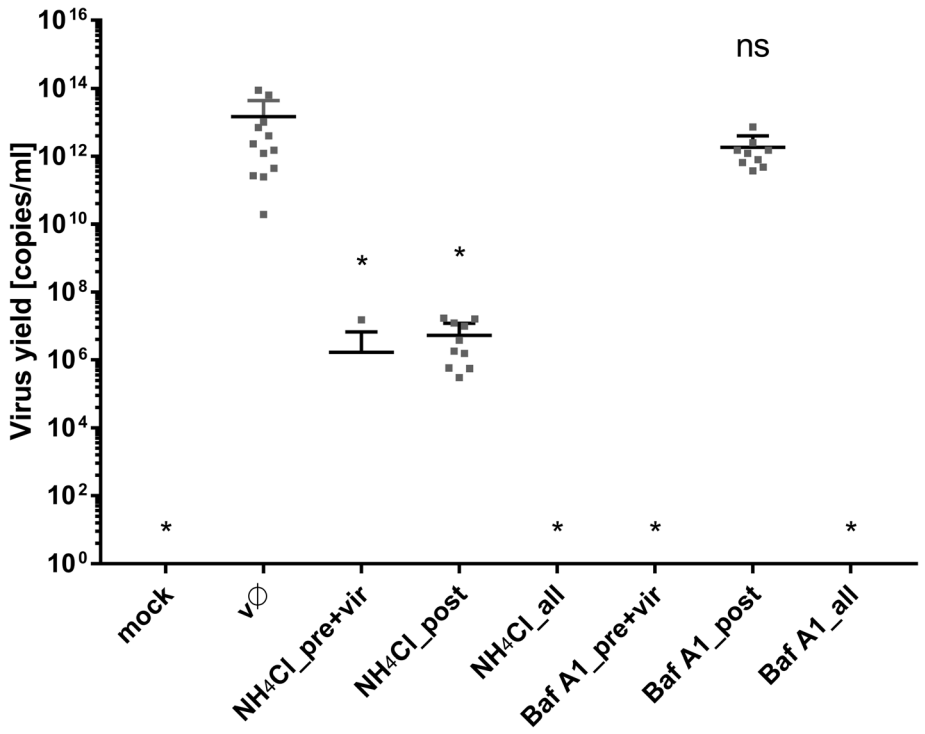

Fig. 14 NH_4Cl interfere with late stages of ZIKV infection. Vero cells were treated Baf A1 and NH_4Cl in 3 settings: (pre + vir) prior to + during ZIKV infection (t = 1 h + 2 h); (all) prior to, during and post-ZIKV infection (t = 1 h + 2 h + 72 h) or (post) post-ZIKV infection only (t = 72 h, starting from the time point 2 h p.i.). 3 days p.i. viral RNA was isolated from medium and quantified with RT-qPCR. mock – mock infected cells; vØ – ZIKV-infected cells; NH_4Cl – 50 mM NH_4Cl; BafA1–100 nM bafilomycin A1; control – inhibitor-untreated, non-infected cells. To determine the significance of differences between compared groups, single-factor analysis of variance (ANOVA) was applied. P values < 0.05 were considered significant. One asterisk (*) identifies adjusted P values between 0.01 and 0.05, two asterisks (**) identify adjusted P values between 0.01 and 0.001, three asterisks (***) identify adjusted P values between 0.001 and 0.0001

entered the cytoplasm, envelope proteins were slowly re-traffic to the cell surface. In the presence of Baf A1, fusion was blocked, and both components tended to co-localize with Rab11- and LAMP-1-positive structures at 15 min p.i. (Fig. 9), suggesting that in the presence of Baf A1 viral particles do not fuse with the membrane of the vesicle. Rather, they are destined to undergo degradation in lysosomes. However, some are transported back to the cell surface via the slow recycling pathway.

NH_4Cl hampers infection inducing fast recycling of virions back to the cell surface

A very different confocal image was observed when cells were treated with NH_4Cl. In this case, few virus particles were observed in the cytoplasm (in contrast to Baf A1-treated cells, in which the number of internalized virions was similar to that in control cells) (Fig. 10). First, we used flow cytometry analysis to test whether NH_4Cl affects binding of ZIKV to the cell surface, which would explain this phenomenon. As shown in Fig. 11, NH_4Cl had no significant impact on ZIKV adhesion to cells.

Next, despite the low number of internalized viral particles, we examined their co-localization with cellular markers (Additional file 5: Figure S5 and Additional file 6: Figure S6). In NH_4Cl-treated cells, both the capsid and envelope proteins co-localized with Rab7 (Fig. 12), suggesting that internalized virions follow their normal entry route. Moreover, slightly increased co-localization of Rab11 with the envelope protein, but not the capsid protein, at 20 min p.i. (Fig. 12), may suggest that, at least for these single virus particles, fusion actually occurs. We observed that, in the presence of NH_4Cl, although the virus may enter the cell, the number of internalized viruses was very small. Because the inhibitor did not affect the virus-cell interaction, we hypothesized that the observed phenomenon may result from extensive anterograde transport. We did not observe co-localization with Rab27; therefore, we excluded the role of exosomes in NH_4Cl-redirected virus trafficking (data not shown). To verify the role of fast recycling endosomes, we used a different approach. Because it was very difficult to visualize this rapid process, we examined subcellular localization of ZIKV upon NH_4Cl treatment of Vero cells in which expression of Rab35, a marker protein that guides endosomes to the fast recycling track, was transiently silenced. In the presence of NH_4Cl, the majority of virions localized to the cell surface of control and scrambled siRNA-transfected cells, whereas those in cells transfected with Rab35-specific siRNA were retained within the cell (trapped near the cell surface) until 1 h p.i. (Fig. 13). This observation led us to conclude that NH_4Cl impairs ZIKV infection at an early stage by redirecting virions back to the cell surface.

NH_4Cl-induced re-modelling of intracellular trafficking: effects on viral replication, assembly, and egress

Intracellular trafficking is important for virus replication, not only at the early stages but also during virus assembly and egress. The data regarding NH_4Cl-mediated remodeling of the endosomal hub led us to hypothesize that the compound may also interfere with the late stages of infection. To confirm this, Vero cells were infected for 2 h with ZIKV under normal conditions (i.e., in the absence of pH-modifying agents). Afterwards, cells were rinsed thrice with PBS and then incubated at 37 °C for 3 days in standard medium containing Baf A1 or NH_4Cl. Although Baf A1 did not affect the viral yield, NH_4Cl led to a 6.5 log reduction (Fig. 14), highlighting differences in the mode of action between these two agents and identifying a role for NH_4Cl during the late stages of infection.

Discussion

During infection, viruses hijack the inward transport machinery of the cell [42–45]. While some viruses are able to fuse with the cell membrane and initiate infection almost immediately after entry, others need to be ferried long distances, e.g., during infection of neural cells [46–49]. This study focused on events that occur after the initial interaction between ZIKV and its cellular receptor.

As observed for other flaviviruses and for ZIKV in different in vitro models [10, 12, 14], our findings demonstrate that ZIKV enters Vero cells by clathrin-dependent endocytosis. Co-localization of viral particles with clathrin was observed 2–10 min p.i., as expected for CME. However, synchronization of virus entry was not ideal due to the fact that the process was regulated by temperature; the numerical co-localization rates were significant but moderate (Fig. 1; Pearson's coefficient ranging from 0.103 to 0.216 and Manders' coefficients up to 0.384). To ensure that the observed co-localization is not an artifact, complementary studies, including clathrin silencing (Fig. 2) or CME-specific inhibitors (Fig. 3), were carried out and confirmed our initial observations.

Subsequent to clathrin-dependent internalization, the virus is encapsulated within the endosome prior to delivery to a precisely defined location. During transport, the microenvironment within the maturing endosome changes gradually; the falling pH, cellular proteases, alterations in the vesicle's membrane content, and fluctuations in redox potential affect the cargo. Viruses are fine-tuned to become active only under conditions that maximize the chances of a productive infection; therefore in most cases this event takes place at a precisely defined site within the endosomal hub [50–58]. Tracking single dengue virus particles revealed that they pass the early endosomes and fuse predominantly with vesicle membranes as they mature into late endosomes at 10–13

min p.i. [42]. Our observations of ZIKV trafficking are congruent with these findings; we noticed separation of the ZIKV envelope and capsid protein trafficking routes between 10 and 15 min p.i. These two viral proteins were seen together for the last time in Rab7-positive structures. These results are also consistent with the data obtained with a novel a novel surrogate-receptor approach described by Rawle et al. [59]. Later the ZIKV envelope appeared to be transported back to the cell surface via slow recycling endosomes. The latter observation is striking, because it is commonly believed that, after endocytosis, viruses avoid leaving evidence of their presence on the plasma membrane as this delays detection by immunosurveillance system [46].

Multiple studies on flaviviruses showed that to acquire fusion competence the envelope proteins need to be primed proteolytically at two sites [50, 60–62]. First cleavage occurs during transport through the *trans*--Golgi network, where a tight complex of prM and E proteins on the surface of newly formed immature virion undergoes a low pH-induced conformational change, followed by cleavage by furin or a furin-like protease [60, 61]. Consequently, mature infectious virions that carry the dimeric E protein in a metastable conformation are released from the cell [62]. The second event occurs during endocytosis into a permissive cell; when the E protein is exposed to low pH, it undergoes rearrangment and enters a fusion-competent state [50].

To identify the factors that activate the ZIKV fusion protein, we used two classes of protease inhibitors. Inactivation of cysteine proteases (e.g., cathepsins) and serine proteases did not affect the infection process. However, furin inhibitors hampered the replication cycle, especially when present during the late stages. This observation is consistent with a common belief that furin in essential for maturation of ZIKV, similarly as for other flaviviruses. Despite the fact that ZIKV E and M proteins structures have been resolved [63, 64] and furin-specific cleavage site in ZIKV sequences is present [65], no report showing the role of furin during ZIKV replication is available (Fig. 5) [60, 65–72].

One may conclude that furin or a furin-like enzyme activates progeny viruses, while no second protease is required during entry to susceptible cell (as reported for other members of *Flaviviridae* family) [60, 61]. By contrast, some results advocating a role for furin during virus maturation may be due to an artifact, linked to the low specificity of the protease inhibitors used [73].

Here, we show that entry of ZIKV depends on the endosomal pH, and that endosome acidification is a prerequisite for fusion. Because we wanted to map the entry of a single virion into the cell, we used two agents commonly used to assess virus dependence on acidic environments. NH_4Cl is a water-soluble salt of ammonia that diffuses into the endosome and acts as a proton sink, thereby inhibiting acidification of the endosome [74]. The second compound, Baf A1, is a vacuolar type H^+-ATPase inhibitor that binds to the V0 sector subunit c of the ATPase complex and inhibits H^+ translocation, thereby blocking endosome acidification [75]. Even though the outcome of both treatments was similar, the mechanism of action appeared to be very different.

In the presence of Baf A1, ZIKV particles were internalized and trafficked to the late endosomal compartment. However, due to altered pH in the vesicles, virions were not able to enter a fusogenic state and remained trapped in the endosomes, which seemed to progress slowly to lysosomes. Partial degradation and, to a lesser extent, slow recycling to the cell surface are probably responsible for removal of the degradation products, so that whole virions share the fate of the envelope protein. By contrast, in the presence of NH_4Cl the majority of virions are retained on the cell surface, which suggests limited virus attachment/entry. First, we confirmed that the virus–receptor interaction was not affected by the basic compound; no alterations were observed. Consequently, potential causes of such a phenomenon include limited internalization or re-trafficking to the cell surface. A limited number of virions localizing inside the cells meant the we could not obtain credible results from co-localization assays. Because no significant increase in co-localization with the slow recycling endosome marker Rab11 was observed in NH_4Cl-treated cells, we tried to inhibit the fast recycling machinery by transiently transfecting Vero cells with siRNAs targeting the fast recycling endosome marker Rab35. Depleting Rab35 resulted in retention of virions inside the cell, showing that the NH_4Cl-mediated inhibition results from rewiring of the endosomal hub rather than a simple increase in endosomal pH.

Conclusions

To summarize, we mapped the entry route of ZIKV using Vero cells as the research model. The results are consistent with data on ZIKV entry into other cell types including primary cells, suggesting that the virus uses a universal entry mechanism. First, the virus uses CME to enter the cell, and then travels through the endosomal compartment to reach the late endosomes prior to fusion. Subsequently, the viral envelope tends to recycle to the cell surface. While it is essential that progeny viruses are primed by furin-like enzymes during assembly, entry seems to be protease-independent. Interestingly, we noted that NH_4Cl (believed to simply buffer the endosomal microenvironment) is in fact re-directing the cargo and ejecting it into the extracellular space. In our previous study we reported

similar example of virus entry pathway redirection [76], showing that external factors may affect virus entry in an non-obvious way. We believe that the results presented herein not only increase our understanding of ZIKV biology, but also provide novel molecular targets for future therapies.

Additional files

Additional file 1: Confocal images of ZIKV-infected Vero cells presenting co localization between ZIKV structural proteins and Rab7, Rab11 and LAMP1 at indicated time points p.i.. Rab7 – late endosomes marker protein, Rab11 – slow recycling endosomes marker protein, LAMP1 – lysosomes marker protein. ZIKV capsid and envelope proteins are visualized in green, cellular proteins are shown in red and nuclei in blue. Co-localization coefficients indicated in the bottom left corners of the images are presented as mean ± SD of at least two independent experiments; r – Pearson's coefficient; M2 - Manders' coefficient M2 (ZIKV capsid/envelope protein overlapping with Rab7/Rab11/LAMP1). Scale bar = 10 μm. **Figure S1.** Co-localization profile for ZIKV capsid protein and subcellular marker proteins in Vero cells. (TIFF 2158 kb)

Additional file 2: Figure S2. Co-localization profile for ZIKV envelope protein and subcellular marker proteins in Vero cell. (TIFF 2315 kb)

Additional file 3: Figure S3. Co-localization profile for ZIKV capsid protein and subcellular marker proteins in Baf A1-treated Vero cells. (TIFF 2207 kb)

Additional file 4: Figure S4. Co-localization profile for ZIKV envelope protein and subcellular marker proteins in Baf A1-treated Vero cells. (TIFF 1894 kb)

Additional file 5: Figure S5. Co-localization profile for ZIKV capsid protein and subcellular marker proteins in NH4Cl-treated Vero cells. (TIFF 2103 kb)

Additional file 6: Figure S6. Co-localization profile for ZIKV envelope protein and subcellular marker proteins in NH4Cl-treated Vero cells. (TIFF 1722 kb)

Abbreviations

AMTD: Amantadine (1-adamantylaminean); Baf A1: Bafilomycin A1 [(3Z,5E,7R,8S,9S,11E,13E,15S,16R)-8-hydroxy-16-[(1S,2R,3S)-2-hydroxy-1-methyl-3-[(2R,4R,5S,6R)-tetrahydro-2,4-dihydroxy-5-methyl-6-(1-methylethyl)-2H-pyran-2-yl]butyl]-3,15-dimethoxy-5,7,9,11-tetramethyloxacyclohexadeca-3,5,11,13-tetraen-2-one); Cam: Camostat [4-[[4-[(aminoiminomethyl)amino]benzoyl]oxy] benzeneacetic acid 2-(dimethylamino)-2-oxoethyl ester methanesulfonate); CME: Clathrin-mediated endocytosis; CMK: Decanoyl-arg-val-lys-arg-chloromethylketone; Dyn: Dynasore [3-hydroxynaphthalene-2-carboxylic acid (3,4-dihydroxybenzylidene)hydrazide]; E64: Trans-epoxysuccinyl-L-leucylamido (4-guanidino) butane, L-trans-3-Carboxyoxiran-2-carbonyl-L-leucylagmatine, N-(trans-epoxysuccinyl)-L-leucine 4-guanidinobutylamide; EEA1: Early endosome antigen 1; MM: MitMAB (tetradecyltrimethylammonium bromide); PtS: PitStop 2 [N-[5-[4-bromobenzylidene]-4-oxo-4,5-dihydro-1,3-thiazol-2-yl] naphthalene-1-sulfonamide]; ZIKV: Zika virus

Acknowledgements

KP would like to acknowledge networking contribution by the COST Action CM1407 "Challenging organic syntheses inspired by nature - from natural products chemistry to drug discovery".

Funding

This work was supported by grants from the National Science Center (UMO-2017/25/N/NZ6/01310 (KO), UMO-2012/07/E/NZ6/01712 and UMO-2016/21/B/NZ6/01307 and UMO-2017/27/B/NZ6/02488) (KP).
The Faculty of Biochemistry, Biophysics and Biotechnology of the Jagiellonian University is a beneficiary of the structural funds from the European Union (grant No: POIG.02.01.00–12-064/08 – "Molecular biotechnology for health").
Faculty of Biochemistry, Biophysics and Biotechnology of the Jagiellonian University is a partner of the Leading National Research Center supported by the Ministry of Science and Higher Education of the Republic of Poland.
The funders had no role in study design, data collection and analysis, decision to publish, or preparation of the manuscript.

Availability of data and materials

All data generated or analysed during this study are included in this published article [and its Additional files.

Authors' contributions

KO and KP designed research, analysed data and wrote the paper; KO and YC performed research; CJ, BM and ZR contributed new reagents or analytic tools. All authors read and approved the final manuscript.

Authors' information

KO and YC are PhD students at the Jagiellonian University; KO is the main researcher and the current manuscript is based mainly on her work, while YC supported the research with methodology and data analysis. KO was further responsible for investigation, methodology, visualization of data, funding acquisition and writing of the original draft of the manuscript. CJ was an external advisor on confocal microscopy and data analysis. BM provided us with technical support, while ZR is an expert on confocal microscopy working at the Jagiellonian University, who helped us with imaging and took part in interpretation of the results. KP is appointed as a professor at the Jagiellonian University and he was responsible for conceptualization, data analysis, funding acquisition, manuscript writing and review. He also serves as a promotor for KO and YC.

Ethics approval and consent to participate

Not applicable.

Consent for publication

Not applicable.

Competing interests

The authors declare that they have no competing interests.

Publisher's Note

Author details

[1]Virogenetics Laboratory of Virology, Malopolska Centre of Biotechnology, Jagiellonian University, Gronostajowa,7a 2.25, 30–387 Krakow, Poland. [2]Microbiology Department, Faculty of Biochemistry, Biophysics and Biotechnology, Jagiellonian University, Gronostajowa 7, 30-387 Krakow, Poland. [3]Institute for Virology, University Clinics and Medical Faculty, University of Leipzig, Leipzig, Germany. [4]Department of Pharmacology, School of Medicine with the Division of Dentistry in Zabrze, Medical University of Silesia in Katowice, Zabrze, Poland. [5]Institute of Physics, Faculty of Physics, Astronomy and Applied Computer Sciences, Jagiellonian University, Lojasiewicza 11, 30-348 Krakow, Poland.

Received: 17 January 2019 Accepted: 3 April 2019
Published online: 03 May 2019

References

1. DICK GW, KITCHEN SF, HADDOW AJ. Zika virus. I. Isolations and serological specificity. Trans R Soc Trop Med Hyg. 1952;46(5):509–20.
2. Duffy MR, Chen TH, Hancock WT, Powers AM, Kool JL, Lanciotti RS, et al. Zika virus outbreak on Yap Island, Federated States of Micronesia. N Engl J Med. 2009;360(24):2536–43.
3. Hayes EB. Zika virus outside Africa. Emerg Infect Dis. 2009;15(9):1347–50.
4. Musso D, Nilles EJ, Cao-Lormeau VM. Rapid spread of emerging Zika virus in the Pacific area. Clin Microbiol Infect. 2014;20(10):O595–6.
5. Zanluca C, Melo VC, Mosimann AL, Santos GI, Santos CN, Luz K. First report of autochthonous transmission of Zika virus in Brazil. Mem Inst Oswaldo Cruz. 2015;110(4):569–72.
6. Rapid risk assessment. Zika virus epidemic in the Americas: potential association with microcephaly and Guillain-Barré syndrome. Stockholm: European Centre for Disease Prevention and Control; 2015.
7. Parra B, Lizarazo J, Jiménez-Arango JA, Zea-Vera AF, González-Manrique G, Vargas J, et al. Guillain-Barré syndrome associated with Zika virus infection in Colombia. N Engl J Med. 2016;375(16):1513–23.

8. Mlakar J, Korva M, Tul N, Popović M, Poljšak-Prijatelj M, Mraz J, et al. Zika virus associated with microcephaly. N Engl J Med. 2016;374(10):951–8.
9. Calvet G, Aguiar RS, Melo AS, Sampaio SA, de Filippis I, Fabri A, et al. Detection and sequencing of Zika virus from amniotic fluid of fetuses with microcephaly in Brazil: a case study. Lancet Infect Dis. 2016;16(6):653–60.
10. Meertens L, Labeau A, Dejarnac O, Cipriani S, Sinigaglia L, Bonnet-Madin L, et al. Axl mediates ZIKA virus entry in human glial cells and modulates innate immune responses. Cell Rep. 2017;18(2):324–33.
11. Hamel R, Dejarnac O, Wichit S, Ekchariyawat P, Neyret A, Luplertlop N, et al. Biology of Zika virus infection in human skin cells. J Virol. 2015;89(17):8880–96.
12. Savidis G, McDougall WM, Meraner P, Perreira JM, Portmann JM, Trincucci G, et al. Identification of Zika virus and dengue virus dependency factors using functional genomics. Cell Rep. 2016;16(1):232–46.
13. Hackett BA, Cherry S. Flavivirus internalization is regulated by a size-dependent endocytic pathway. Proc Natl Acad Sci U S A. 2018;115(16):4246–51.
14. Rinkenberger N, Schoggins JW. Mucolipin-2 Cation Channel increases trafficking efficiency of endocytosed viruses. MBio. 2018;9(1).
15. Delvecchio R, Higa LM, Pezzuto P, Valadão AL, Garcez PP, Monteiro FL, et al. Chloroquine, an endocytosis blocking agent, inhibits Zika virus infection in different cell models. Viruses. 2016;8(12).
16. Traub LM. Regarding the amazing choreography of clathrin coats. PLoS Biol. 2011;9(3):e1001037.
17. Cocucci E, Gaudin R, Kirchhausen T. Dynamin recruitment and membrane scission at the neck of a clathrin-coated pit. Mol Biol Cell. 2014;25(22):3595–609.
18. Boulant S, Kural C, Zeeh JC, Ubelmann F, Kirchhausen T. Actin dynamics counteract membrane tension during clathrin-mediated endocytosis. Nat Cell Biol. 2011;13(9):1124–31.
19. Aschenbrenner L, Lee T, Hasson T. Myo6 facilitates the translocation of endocytic vesicles from cell peripheries. Mol Biol Cell. 2003;14(7):2728–43.
20. Novick P, Brennwald P. Friends and family: the role of the Rab GTPases in vesicular traffic. Cell. 1993;75(4):597–601.
21. Jovic M, Sharma M, Rahajeng J, Caplan S. The early endosome: a busy sorting station for proteins at the crossroads. Histol Histopathol. 2010;25(1):99–112.
22. Huotari J, Helenius A. Endosome maturation. EMBO J. 2011;30(17):3481–500.
23. Maxfield FR, McGraw TE. Endocytic recycling. Nat Rev Mol Cell Biol. 2004; 5(2):121–32.
24. Maxfield FR, Yamashiro DJ. Endosome acidification and the pathways of receptor-mediated endocytosis. Adv Exp Med Biol. 1987;225:189–98.
25. Ostrowski M, Carmo NB, Krumeich S, Fanget I, Raposo G, Savina A, et al. Rab27a and Rab27b control different steps of the exosome secretion pathway. Nat Cell Biol. 2010;12(1):19–30; sup pp 1–13.
26. Fraile-Ramos A, Cepeda V, Elstak E, van der Sluijs P. Rab27a is required for human cytomegalovirus assembly. PLoS One. 2010;5(12):e15318.
27. Gerber PP, Cabrini M, Jancic C, Paoletti L, Banchio C, von Bilderling C, et al. Rab27a controls HIV-1 assembly by regulating plasma membrane levels of phosphatidylinositol 4,5-bisphosphate. J Cell Biol. 2015;209(3):435–52.
28. Lombardi D, Soldati T, Riederer MA, Goda Y, Zerial M, Pfeffer SR. Rab9 functions in transport between late endosomes and the trans Golgi network. EMBO J. 1993;12(2):677–82.
29. Gould EA, de Lamballerie X, Coutard B, Fooks AR, Outlaw M, Drosten C, et al. The European virus archive: a new resource for virology research. Antivir Res. 2012;95(2):167–71.
30. Reed LJ, Muench H. A Simple Method Of Estimating Fifty Per Cent Endpoints12. Am J Epidemiol. 1938;27(3):493–7.
31. Phonphok Y, Rosenthal KS. Stabilization of clathrin coated vesicles by amantadine, tromantadine and other hydrophobic amines. FEBS Lett. 1991; 281(1–2):188–90.
32. Crider BP, Xie XS, Stone DK. Bafilomycin inhibits proton flow through the H+ channel of vacuolar proton pumps. J Biol Chem. 1994;269(26): 17379–81.
33. Kawase M, Shirato K, van der Hoek L, Taguchi F, Matsuyama S. Simultaneous treatment of human bronchial epithelial cells with serine and cysteine protease inhibitors prevents severe acute respiratory syndrome coronavirus entry. J Virol. 2012;86(12):6537–45.
34. Angliker H. Synthesis of tight binding inhibitors and their action on the proprotein-processing enzyme furin. J Med Chem. 1995;38(20):4014–8.
35. Macia E, Ehrlich M, Massol R, Boucrot E, Brunner C, Kirchhausen T. Dynasore, a cell-permeable inhibitor of dynamin. Dev Cell. 2006;10(6):839–50.
36. Ares GR, Ortiz PA. Dynamin2, clathrin, and lipid rafts mediate endocytosis of the apical Na/K/2Cl cotransporter NKCC2 in thick ascending limbs. J Biol Chem. 2012;287(45):37824–34.
37. Fujita F, Uchida K, Moriyama T, Shima A, Shibasaki K, Inada H, et al. Intracellular alkalization causes pain sensation through activation of TRPA1 in mice. J Clin Invest. 2008;118(12):4049–57.
38. Boron WF. De Weer P. intracellular pH transients in squid giant axons caused by CO2, NH3, and metabolic inhibitors. J Gen Physiol. 1976;67(1):91–112.
39. Dutta D, Williamson CD, Cole NB, Donaldson JG. Pitstop 2 is a potent inhibitor of clathrin-independent endocytosis. PLoS One. 2012;7(9):e45799.
40. Bolte S, Cordelières FP. A guided tour into subcellular colocalization analysis in light microscopy. J Microsc. 2006;224(Pt 3:213–32.
41. Earp LJ, Delos SE, Park HE, White JM. The many mechanisms of viral membrane fusion proteins. Curr Top Microbiol Immunol. 2005;285:25–66.
42. van der Schaar HM, Rust MJ, Chen C. Van der Ende-Metselaar H, Wilschut J, Zhuang X, et al. dissecting the cell entry pathway of dengue virus by single-particle tracking in living cells. PLoS Pathog. 2008;4(12):e1000244.
43. Yang S, He M, Liu X, Li X, Fan B, Zhao S. Japanese encephalitis virus infects porcine kidney epithelial PK15 cells via clathrin- and cholesterol-dependent endocytosis. Virol J. 2013;10:258.
44. Chu JJ, Ng ML. Infectious entry of West Nile virus occurs through a clathrin-mediated endocytic pathway. J Virol. 2004;78(19):10543–55.
45. Blanchard E, Belouzard S, Goueslain L, Wakita T, Dubuisson J, Wychowski C, et al. Hepatitis C virus entry depends on clathrin-mediated endocytosis. J Virol. 2006;80(14):6964–72.
46. Mercer J, Schelhaas M, Helenius A. Virus entry by endocytosis. Annu Rev Biochem. 2010;79:803–33.
47. Oh Y, Zhang F, Wang Y, Lee EM, Choi IY, Lim H, et al. Zika virus directly infects peripheral neurons and induces cell death. Nat Neurosci. 2017;20(9):1209–12.
48. Velandia-Romero ML, Acosta-Losada O, Castellanos JE. In vivo infection by a neuroinvasive neurovirulent dengue virus. J Neuro-Oncol. 2012;18(5):374–87.
49. Shrestha B, Gottlieb D, Diamond MS. Infection and injury of neurons by West Nile encephalitis virus. J Virol. 2003;77(24):13203–13.
50. Stiasny K, Fritz R, Pangerl K, Heinz FX. Molecular mechanisms of flavivirus membrane fusion. Amino Acids. 2011;41(5):1159–63.
51. Krishnan MN, Sukumaran B, Pal U, Agaisse H, Murray JL, Hodge TW, et al. Rab 5 is required for the cellular entry of dengue and West Nile viruses. J Virol. 2007;81(9):4881–5.
52. Kimura T, Gollins SW, Porterfield JS. The effect of pH on the early interaction of West Nile virus with P388D1 cells. J Gen Virol. 1986;67 (Pt 11:2423–33.
53. Gollins SW, Porterfield JS. pH-dependent fusion between the flavivirus West Nile and liposomal model membranes. J Gen Virol. 1986;67 (Pt 1:157–66.
54. Espósito DL, Nguyen JB, DeWitt DC, Rhoades E, Modis Y. Physico-chemical requirements and kinetics of membrane fusion of flavivirus-like particles. J Gen Virol. 2015;96(Pt 7:1702–11.
55. Zaitseva E, Yang ST, Melikov K, Pourmal S, Chernomordik LV. Dengue virus ensures its fusion in late endosomes using compartment-specific lipids. PLoS Pathog. 2010;6(10):e1001131.
56. Corver J, Ortiz A, Allison SL, Schalich J, Heinz FX, Wilschut J. Membrane fusion activity of tick-borne encephalitis virus and recombinant subviral particles in a liposomal model system. Virology. 2000;269(1):37–46.
57. Liu CC, Zhang YN, Li ZY, Hou JX, Zhou J, Kan L, et al. Rab5 and Rab11 are required for Clathrin-dependent endocytosis of Japanese encephalitis virus in BHK-21 cells. J Virol. 2017;91(19).
58. Zhang YN, Liu YY, Xiao FC, Liu CC, Liang XD, Chen J, et al. Rab5, Rab7, and Rab11 are required for Caveola-dependent endocytosis of classical swine fever virus in porcine alveolar macrophages. J Virol. 2018;92(15).
59. Rawle RJ, Webster ER, Jelen M, Kasson PM, Boxer SG. pH dependence of Zika membrane fusion kinetics reveals an off-pathway state. ACS Cent Sci. 2018;4(11):1503–10.
60. Stadler K, Allison SL, Schalich J, Heinz FX. Proteolytic activation of tick-borne encephalitis virus by furin. J Virol. 1997;71(11):8475–81.
61. Elshuber S, Allison SL, Heinz FX, Mandl CW. Cleavage of protein prM is necessary for infection of BHK-21 cells by tick-borne encephalitis virus. J Gen Virol. 2003;84(Pt 1):183–91.
62. Stiasny K, Allison SL, Mandl CW, Heinz FX. Role of metastability and acidic pH in membrane fusion by tick-borne encephalitis virus. J Virol. 2001;75(16): 7392–8.
63. Sirohi D, Chen Z, Sun L, Klose T, Pierson TC, Rossmann MG, et al. The 3.8 Å resolution cryo-EM structure of Zika virus. Science. 2016;352(6284): 467–70.
64. Kostyuchenko VA, Lim EX, Zhang S, Fibriansah G, Ng TS, Ooi JS, et al. Structure of the thermally stable Zika virus. Nature. 2016;533(7603): 425–8.

65. Dai L, Song J, Lu X, Deng YQ, Musyoki AM, Cheng H, et al. Structures of the Zika virus envelope protein and its complex with a Flavivirus broadly protective antibody. Cell Host Microbe. 2016;19(5):696–704.
66. Nambala P, Su WC. Role of Zika virus prM protein in viral pathogenicity and use in vaccine development. Front Microbiol. 2018;9:1797.
67. Lin HH, Yip BS, Huang LM, Wu SC. Zika virus structural biology and progress in vaccine development. Biotechnol Adv. 2018;36(1):47–53.
68. Pierson TC, Diamond MS. Degrees of maturity: the complex structure and biology of flaviviruses. Curr Opin Virol. 2012;2(2):168–75.
69. Zybert IA. Van der Ende-Metselaar H, Wilschut J, Smit JM. Functional importance of dengue virus maturation: infectious properties of immature virions. J Gen Virol. 2008;89(Pt 12):3047–51.
70. Yu IM, Zhang W, Holdaway HA, Li L, Kostyuchenko VA, Chipman PR, et al. Structure of the immature dengue virus at low pH primes proteolytic maturation. Science. 2008;319(5871):1834–7.
71. Mukherjee S, Sirohi D, Dowd KA, Chen Z, Diamond MS, Kuhn RJ, et al. Enhancing dengue virus maturation using a stable furin over-expressing cell line. Virology. 2016;497:33–40.
72. Colpitts TM, Rodenhuis-Zybert I, Moesker B, Wang P, Fikrig E, Smit JM. prM-antibody renders immature West Nile virus infectious in vivo. J Gen Virol. 2011;92(Pt 10:2281–5.
73. Matsuyama S, Shirato K, Kawase M, Terada Y, Kawachi K, Fukushi S, et al. Middle East respiratory syndrome coronavirus spike protein is not activated directly by cellular furin during viral entry into target cells. J Virol. 2018.
74. Brindley MA, Maury W. Endocytosis and a low-pH step are required for productive entry of equine infectious anemia virus. J Virol. 2005;79(23):14482–8.
75. Bowman EJ, Graham LA, Stevens TH, Bowman BJ. The bafilomycin/concanamycin binding site in subunit c of the V-ATPases from Neurospora crassa and Saccharomyces cerevisiae. J Biol Chem. 2004;279(32):33131–8.
76. Owczarek K, Szczepanski A, Milewska A, Baster Z, Rajfur Z, Sarna M, et al. Early events during human coronavirus OC43 entry to the cell. Sci Rep. 2018;8(1):7124.

mgr Artur Szczepański

Wydział Biochemii, Biofizyki i Biotechnologii
Uniwersytet Jagielloński
ul. Gronostajowa 7
30-387 Kraków

Kraków, 8.05.2019 r.

Oświadczenie

Oświadczam, że w pracy:
Owczarek K, Szczepanski A, Milewska A, Baster Z, Rajfur Z, Sarna M, Pyrc K, Early events during human coronavirus OC43 entry to the cell. Sci Rep. 2018;8(1):7124
mój udział polegał na wykonaniu optymalizacji immunofluorescencyjnego znakowania białek komórkowych linii HCT-8. Wyrażam zgodę na zaliczenie wyżej wymienionej publikacji do rozprawy doktorskiej mgr Katarzyny Owczarek.

Podpis

Artur Szczepański

dr Aleksandra Milewska

Wydział Biochemii, Biofizyki i Biotechnologii
Uniwersytet Jagielloński
ul. Gronostajowa 7
30-387 Kraków

Kraków, 8.05.2019 r.

Oświadczenie

Oświadczam, że w pracy:
Owczarek K, Szczepanski A, Milewska A, Baster Z, Rajfur Z, Sarna M, Pyrc K, Early events during human coronavirus OC43 entry to the cell. Sci Rep. 2018;8(1):7124
mój udział polegał na opiece mentorskiej w zakresie cytometrii przepływowej. Wyrażam zgodę na zaliczenie wyżej wymienionej publikacji do rozprawy doktorskiej mgr Katarzyny Owczarek.

Podpis

A. Milewska

mgr inż. Zbigniew Baster

Wydział Fizyki, Astronomii i Informatyki Stosowanej
Uniwersytet Jagielloński
ul. Łojasiewicza 11,
30-348 Kraków

Kraków, 8.05.2019 r.

Oświadczenie

Oświadczam, że w pracy:
Owczarek K, Szczepanski A, Milewska A, Baster Z, Rajfur Z, Sarna M, Pyrc K, Early events during human coronavirus OC43 entry to the cell. Sci Rep. 2018;8(1):7124
mój udział polegał na wsparciu w zakresie mikroskopii konfokalnej. Wyrażam zgodę na zaliczenie wyżej wymienionej publikacji do rozprawy doktorskiej mgr Katarzyny Owczarek.

Podpis

Baster Zbigniew

dr hab. Zenon Rajfur

Wydział Fizyki, Astronomii i Informatyki Stosowanej
Uniwersytet Jagielloński
ul. Łojasiewicza 11,
30-348 Kraków

Kraków, 8.05.2019 r.

Oświadczenie

Oświadczam, że w pracy:
Owczarek K, Szczepanski A, Milewska A, Baster Z, Rajfur Z, Sarna M, Pyrc K, Early events during human coronavirus OC43 entry to the cell. Sci Rep. 2018;8(1):7124
mój udział polegał na opiece mentorskiej w zakresie mikroskopii konfokalnej. Wyrażam zgodę na zaliczenie wyżej wymienionej publikacji do rozprawy doktorskiej mgr Katarzyny Owczarek.

Podpis

dr Michał Sarna

Wydział Biochemii, Biofizyki i Biotechnologii
Uniwersytet Jagielloński
ul. Gronostajowa 7
30-387 Kraków

Kraków, 8.05.2019 r.

Oświadczenie

Oświadczam, że w pracy:
Owczarek K, Szczepanski A, Milewska A, Baster Z, Rajfur Z, Sarna M, Pyrc K, Early events during human coronavirus OC43 entry to the cell. Sci Rep. 2018;8(1):7124
mój udział polegał na opiece mentorskiej w zakresie mikroskopii konfokalnej. Wyrażam zgodę na zaliczenie wyżej wymienionej publikacji do rozprawy doktorskiej mgr Katarzyny Owczarek.

Michał Sarna

Podpis

prof. dr hab. Krzysztof Pyrć

Małopolskie Centrum Biotechnologii
Uniwersytet Jagielloński
ul. Gronostajowa 7A
30-387 Kraków

Kraków, 8.05.2019 r.

Oświadczenie

Oświadczam, że w pracy:
Owczarek K, Szczepanski A, Milewska A, Baster Z, Rajfur Z, Sarna M, Pyrc K, Early events during human coronavirus OC43 entry to the cell. Sci Rep. 2018;8(1):7124
mój udział polegał na opiece mentorskiej i merytorycznej w czasie planowania badań, prac doświadczalnych oraz przygotowania manuskryptu. Wyrażam zgodę na zaliczenie wyżej wymienionej publikacji do rozprawy doktorskiej mgr Katarzyny Owczarek.

Podpis

mgr Yuliya Chykunova

Kraków, 7.05.2019 r.

Wydział Biochemii, Biofizyki i Biotechnologii
Uniwersytet Jagielloński
ul. Gronostajowa 7
30-387 Kraków

Oświadczenie

Oświadczam, że w pracy:
Owczarek K, Chykunova Y, Jassoy C, Maksym B, Rajfur Z, Pyrc K, Zika virus: mapping and reprogramming the entry. Cell Commun Signal. 2019;17(1):41
mój udział polegał na wykonaniu analizy Western blot mającej na celu określenie wydajności procesu tymczasowego wyciszania wyrażania białek Rab35 oraz klatryny. Wyrażam zgodę na zaliczenie wyżej wymienionej publikacji do rozprawy doktorskiej mgr Katarzyny Owczarek.

Podpis

Yuliya Chykunova

prof. dr. Christian Jassoy

Institut für Virologie
Universitätsklinikum Leipzig AöR
Johannisallee 30
04103 Leipzig

Kraków, 7.05.2019 r.

Contribution statement

I declare that my contribution to the article entitled:
Owczarek K, Chykunova Y, Jassoy C, Maksym B, Rajfur Z, Pyrc K, Zika virus: mapping and reprogramming the entry. Cell Commun Signal. 2019;17(1):41
consisted of preparation of Zika capsid-specific antibodies. Hereby, I agree for encompassing the above mentioned article in the doctoral thesis of mgr Katarzyna Owczarek.

Signature

Prof. Dr. med. C. Jassoy
Institut für Virologie
UNIVERSITÄTSKLINIKUM LEIPZIG AöR
Johannisallee 30 · 04103 Leipzig
☎ (0341) 97-1 43 14 · Fax 97-1 43 09
e-mail: christian.jassoy@medizin.uni-leipzig.de

Dr n. med. Beata Maksym

Katedra i Zakład Farmakologii w Zabrzu
Śląskiego Uniwersytetu Medycznego w Katowicach
ul. Jordana 38,
41-808 Zabrze

Kraków, 7.05.2019 r.

Oświadczenie

Oświadczam, że w pracy:
Owczarek K, Chykunova Y, Jassoy C, Maksym B, Rajfur Z, Pyrc K, Zika virus: mapping and reprogramming the entry. Cell Commun Signal. 2019;17(1):41
mój udział polegał na opiece merytorycznej w trakcie prac doświadczalnych oraz przygotowania manuskryptu. Wyrażam zgodę na zaliczenie wyżej wymienionej publikacji do rozprawy doktorskiej mgr Katarzyny Owczarek.

Maksym Beata
Podpis

dr hab. Zenon Rajfur

Wydział Fizyki, Astronomii i Informatyki Stosowanej
Uniwersytet Jagielloński
ul. Łojasiewicza 11,
30-348 Kraków

Kraków, 8.05.2019 r.

Oświadczenie

Oświadczam, że w pracy:
Owczarek K, Chykunova Y, Jassoy C, Maksym B, Rajfur Z, Pyrc K, Zika virus: mapping and reprogramming the entry. Cell Commun Signal. 2019;17(1):41
mój udział polegał na opiece mentorskiej w zakresie mikroskopii konfokalnej. Wyrażam zgodę na zaliczenie wyżej wymienionej publikacji do rozprawy doktorskiej mgr Katarzyny Owczarek.

Podpis

prof. dr hab. Krzysztof Pyrć

Małopolskie Centrum Biotechnologii
Uniwersytet Jagielloński
ul. Gronostajowa 7A
30-387 Kraków

Kraków, 8.05.2019 r.

Oświadczenie

Oświadczam, że w pracy:
Owczarek K, Chykunova Y, Jassoy C, Maksym B, Rajfur Z, Pyrc K, Zika virus: mapping and reprogramming the entry. Cell Commun Signal. 2019;17(1):41
mój udział polegał na opiece mentorskiej i merytorycznej w czasie planowania badań, prac doświadczalnych oraz przygotowania manuskryptu. Wyrażam zgodę na zaliczenie wyżej wymienionej publikacji do rozprawy doktorskiej mgr Katarzyny Owczarek.

Podpis